THE EFFECT OF APICOPLAST PROTEINS AND TRICLOSAN ANALOGS ON THE GROWTH OF *PLASMODIUM FALCIPARUM*

by
Hans B. Liu

A thesis submitted to Johns Hopkins University in conformity with the requirements for the degree of Master of Science (Sc.M.)

Baltimore, Maryland
June 2018

ABSTRACT

Each year, malaria claims approximately half a million lives while infecting hundreds of millions of people worldwide. *Plasmodium falciparum* (*Pf*), the primary causative agent of human malaria, harbors an essential organelle known as the apicoplast. While the putative metabolic pathways within this organelle have been largely elucidated, proteins required for its maintenance remain to be determined. To address this, we have genetically engineered the *Pf*Mev parasite line, to which exogenous supplementation of Mevalonate, a precursor metabolite for mammalian isoprenoid biosynthesis, enables the survival of parasites that have lost the apicoplast. Using this metabolic bypass line, we have knocked out various proteins related to the SUF pathway, and determined that SufS and MnmA, two sulfur-utilizing proteins, are required for maintaining the apicoplast. To further explore proteins involved in apicoplast maintenance, we have demonstrated the capability of both the CLD system and TetR-DOZI system to conditionally knock down PyrKII, a protein that we have shown to be required for maintaining the apicoplast. These results on PyrKII pave the way for our plan of probing the resultant changes within the nuclear and plastidial transcriptome.

In addition, due to the sustained recurrence of drug resistance in *Plasmodium* parasites, there is a constant need for the search and development of novel effective antimalarials. One promising candidate, triclosan, exhibits anti-plasmodial activity at the micro-molar range. With the goal of discovering a triclosan analog with substantially amplified antiparasitic activity, we have screened seven triclosan analogs for their antiparasitic activity against blood stage *Pf*. Through conducting this screen, we have confirmed the potency of a compound, designated herein as djm-11-03A, and seek to identify its molecular targets in order to uncover clues towards its potency optimization.

Advisor: Dr. Sean T. Prigge
Secondary reader: Dr. Philip Jordan

ACKNOWLEDGMENT

A number of people contributed to the work presented herein. Due to the constraint of space, only the major ones are mentioned below.

Dr. Aleah D. Roberts taught me the basics of malaria culture, including culture maintenance, making growth medium, and magnetic purification. What's more, the CLD system employed in **CHAPTER 4** would not be the full-fledged molecular tool that it is without her dedicated hard work towards its design and optimization.

Dr. David J. Meyers synthesized the triclosan analogs that were used in **CHAPTER 3** (the "djm" in front of the designations of each triclosan analog are his initials). Given the need to design synthesis route for, and validate, each analog, this is by no means a small feat.

Dr. Hugo Jhun prepared the working stocks of triclosan analogs and showed me how to set up the drug assays used in **CHAPTER 3**. In addition, he provided great help with respect to trouble shooting as well as optimization of the drug assay, and shares the responsibility with me for the drug resistance induction experiment.

Dr. Krithika Rajaram taught me how to do single cloning via limiting dilution. Given the large number of knock-out lines, presented in **CHAPTER 2**, that needed to be single cloned, being able to share the burden with her on this task was of great help to me.

Russell P. Swift was responsible for the genetics work in both **CHAPTER 2** and **CHAPTER 4**, including plasmid design, PCR primer design, and transfections for the parasite lines. Without his tremendous amount of dedicated hard work, none of the work in these two chapters would be possible.

Lastly, Dr. Sean T. Prigge played a major role for the experimental design, assay optimization, and troubleshooting for all of the work presented herein. Not only this, Dr. Prigge fosters a productive and enjoyable work environment for the lab as a whole. Being able to work for, and learn from, him is a tremendous pleasure to me, and I very much look forward to continuing my work with him.

TABLE OF CONTENTS

LIST OF TABLES

LIST OF FIGURES

LIST OF ABBREVIATIONS

AACT	acetoacetyl CoA thiolase
ABS	asexual blood stage
Acetyl CoA	acetyl-coenzyme A
ACP	acyl carrier protein
ADP	adenosine diphosphate
ALS	asexual liver stage
AP	atovaquone-proguanil
aTc	anhydrotetracycline
ATP	adenosine triphosphate
ATPase	adenosine triphosphatase
B. subtilis	*Bacillus subtilis*
CLD	conditional localization domain
CMA	Complete Medium with AlbuMAX
CR	cold room
DD	destabilization domain
DHFR	dihydrofolate reductase
DMAPP	dimethylallyl pyrophosphate
DMSO	dimethyl sulfoxide
Dox	doxycycline
DOZI	development of zygote inhibited
DXPR	DXP reductoisomerase
DXS	1-deoxy-D-xylulose-5-phosphate (DXP) synthase
EDTA	ethylenediaminetetraacetic acid

ER	endoplasmic reticulum
E. coli	*Escherichia coli*
FAS-II	Type II fatty acid synthesis
Fdx	ferredoxin
FKBP	FK506 binding protein
FNR	ferredoxin $NADP^+$ reductase
FSC-A	forward scatter-area
FSC-H	forward scatter-height
GA3P	glyceraldehyde 3-phosphate
GcpE/IspG	(*E*)-4-hydroxy-3-methyl-but-2-enyl diphosphate synthase
GDP	guanosine diphosphate
GFP	green florescent protein
Gln	glutamine
Glu	glutamate
HMGR	3-hydroxy-3-methylglutaryl-CoA reductase
HMGS	3-hydroxy-3-methylglutaryl-CoA synthase
Hs	*Homo sapiens*
IC	incubator
IC_{50}	half maximal inhibitory concentration
IDI	isopentenyl pyrophosphate delta isomerase
IPP	isopentenyl pyrophosphate
IPPI	isopentenyl pyrophosphate isomerase
iRBC	infected RBC
ISC	iron-sulfur cluster

IspD	4-diphosphocytidyl-2*C*-methyl-D-erythritol synthetase
IspE	4-diphosphocytidyl-2*C*-methyl-D-erythritol kinase
IspF	2*C*-methyl-D-erythritol 2,4-cyclodiphosphate synthase
IspG/GcpE	(*E*)-4-hydroxy-3-methyl-but-2-enyl diphosphate synthase
IspH/LytB	(*E*)-4-hydroxy-3-methyl-but-2-enyl diphosphate reductase
iTPT	inner triose phosphate transporter
LC	liver cell
LDH	lactate dehydrogenase
LipA	lipoic acid synthase
Lys	lysine
LytB/IspH	(*E*)-4-hydroxy-3-methyl-but-2-enyl diphosphate reductase
MEP	2*C*-methyl-D-erythritol 4-phosphate
MiaB	tRNA methylthiotransferase
MPD	mevalonate phosphate decarboxylase
MVA	mevalonate
MVK	mevalonate kinase
NAD^+	nicotinamide adenine dinucleotide
oTPT	outer triose phosphate transporter
Pb	*Plasmodium berghei*
PBS	phosphate-buffered saline
PCR	polymerase chain reaction
PDH	pyruvate dehydrogenase
PEP	phosphoenolpyruvate
Pf	*Plasmodium falciparum*

PlasmoAP	*Plasmodium falciparum* apicoplast-targeted proteins
PMK	phosphomevalonate kinase
MPD	mevalonate phosphate decarboxylase
Pv	*Plasmodium vivax*
PyrKI	pyruvate kinase I
PyrKII	pyruvate kinase II
RBC	red blood cell
s^2U	2-thio-uridine
Sc	*Saccharomyces cerevisiae*
SgPP	signal processing peptidase
SP	sulfadoxine-pyrimethamine
SPP	stromal processing peptidase
SSC-A	side scatter-area
SUF	sulfur utilization factors
TetR	Tet repressor
TFA	trifluoroacetic acid
Tg	*Toxoplasma gondii*

CHAPTER 1: Introduction to malaria

Malaria as a public health burden

Malaria is an ancient disease that has plagued mankind for over 4,000 years. Each year, the deadly disease infects hundreds of millions of people worldwide, endangering nearly half of the world's population [1]. In 2016, globally, there were approximately 216 million reported cases of malaria infections and 445,000 deaths. Among the reported cases, 90% of the infections and 91% of the deaths occurred in Africa, while the rest of the incidences were scattered throughout Southeast Asia, Europe, and the Americas [1]. In addition to the considerable death toll incurred, the disease constitutes a significant source of financial strain on the government of the endemic countries and those who pledge to help eradicate the disease, collectively. In fact, in 2016 alone, about 2.7 billion dollars were spent on the global control/elimination of malaria [1], which included measures such as vector control, diagnosis, and treatment [1]. As such, malaria is not only a life-threatening disease, but also a significant economic burden.

Human malaria is caused by five species of *Plasmodium* parasites. In particular, *Plasmodium falciparum* (*Pf*), the most deadly among the five, is most prevalent in West Africa and accounts for the majority of the malaria cases [1], while *Plasmodium vivax* (*Pv*), the runner-up, primarily affects other countries outside of Sub-Saharan Africa [1].

The *Plasmodium* mosquito stage

The *Plasmodium* parasite has a complex life cycle (reviewed in [2], [3], and [4]) that involves two hosts, the human and the female *Anopheles* mosquito, and three developmental stages – the mosquito stage, the asexual liver stage (ALS), and the asexual blood stage (ABS). Shown below is a summary of the general characteristics of the parasite throughout the various stages of its complete life cycle (**Table 1.1**). When a mosquito takes a blood meal from a human who is infected with malaria, it can ingest

the parasitized RBCs from that individual, thereby initiating the 17-day sporogonic cycle. Importantly, actual successful infection of the mosquito by the parasite requires the sexual reproduction of the parasites within the mosquito. Specifically, upon arrival inside the midgut of the mosquito, the male and female gametocytes (the sexual form of the parasite) exit the RBCs and differentiate into gametes of the respective sex. A male gamete penetrates and fuses with a female gamete, generating a fertilized female gamete, also known as a zygote, the only diploid form of the *Plasmodium* parasite (during all other stages of its life cycle, the parasite is haploid). These zygotes, through physical elongation and the acquisition of motility, develop into what are called ookinetes, which then invade and lodge under the basal lamina of the mosquito midgut, where they subsequently develop into oocysts. In the final phase of the *Plasmodium* life cycle within the mosquito, the oocysts rupture and release sporozoites in a process known as sporogony. These free sporozoites then make their way from the midgut to the salivary glands of the mosquito.

The *Plasmodium* asexual liver stage (ALS)

Plasmodium asexual reproduction during the ALS is largely analogous to that of the ABS. In addition, since the work presented herein focuses on the ABS, the ALS is described only in brief. When taking a blood meal from a human, a malaria-infected mosquito inoculates sporozoites from its salivary glands into the bitten human, thereby initiating the ALS, which in *Pf* takes approximately 10 days to complete. After their injection through the human dermis, the sporozoites travel within the bloodstream to reach the liver, where they infect liver cells (LCs) and mature into the form of the parasite known as a schizont, each of which contains multiple daughter merozoites. Upon sufficient parasitic development, the LC ruptures to release 1,000s of daughter merozoites, which enter the bloodstream once again to invade RBCs. Upon successful invasion of a RBC, an encapsulating membrane, known as the parasitophorous vacuole, forms around the parasite, and it is within this

vacuole that subsequent parasite growth and development during the ABS occurs.

The *Plasmodium* asexual blood stage (ABS)

The ABS, which is responsible for the clinical manifestations of malaria, consists of four developmental stages. During a mere 2-minute window of this 2-day life cycle, free parasites, i.e., merozoites, are in the process of invading RBCs (**Figure 1.1A**). The successful invasion of a RBC followed by the establishment of the merozoite(s) therein launches the ring-stage, during which the parasite body takes on a characteristic ring shape (**Figure 1.1B**) that gradually enlarges during growth. Throughout this stage of its life cycle, the parasite starts to ingest the host cell hemoglobin, which gets hydrolyzed to its protein component (amino acids) and its non-protein component (iron-containing heme). The amino acids are taken up as nutrition, while the heme can produce reactive oxygen species that are toxic to the parasite. As the parasite grows, it morphologically transitions from the ring shape to an ameboid shape, which marks the start of the trophozoite-stage (**Figure 1.1C**). At the trophozoite-stage, the reactive oxygen species derived from hemoglobin ingestion have accumulated enough to constitute a substantial source of oxidative stress. In order to overcome this toxicity, the parasite generates a hemozoin crystal consisting of heme organized in order to limit exposure of the iron atoms. Continuing on the developmental cycle, division of parasite organelles and genomic replication occurs. Now, although each *Pf* parasite harbors numerous organelles, only three contain their own genomes – the nucleus, apicoplast, and mitochondrion, which are collectively referred to as the "organellar trio" hereafter. Notably, each *Pf* parasite carries a single apicoplast and mitochondrion, and these two organelles remain in close proximity to each other throughout the ABS [5]. Upon sufficient development under the trophozoite-stage, the parasite undergoes a process known as schizogony. During this intricately orchestrated process, each member of the parental cell organellar trio first gets partitioned [5]. This organellar division is then followed by the partitioning of the cytosol

such that each resulting daughter cell, i.e., merozoite, is able to acquire its own organellar trio [5], yielding a schizont-stage parasite that contains 16 – 32 daughter merozoites (**Figure 1.1D**). Notably, at the schizont-stage, sufficient amount of heme has been incorporated into the hemozoin crystal so as to confer a paramagnetic property that is particularly strong at this stage of the parasite life cycle. From an experimental standpoint, such a distinguishing feature conveniently enables the isolation of schizont-stage parasites from a mixed-stage culture via purification under a strong magnetic field (see the **MATERIALS AND METHODS** section of **CHAPTER 3** for more details). During the final phase of schizogony, the daughter merozoites within an individual schizont can undergo one of two fates. As the first option, the merozoites rupture the RBC membrane and thereupon get released into the bloodstream to invade new RBCs, thus launching another cycle of the ABS within the same human host. As an alternative to perpetuating the ABS, the merozoites can differentiate into gametocytes, which can be ingested by a mosquito during a blood meal, thereby initiating a new round of transmission to a potentially different human host.

Table 1.1. Summary of general characteristics of *Plasmodium falciparum*. The six characteristics shown are: (1) physical location, (2) mode of reproduction, (3) ploidy, (4) associated physical form(s), (5) whether the parasites are pathologic to the infected human host, and (6) the approximate duration to achieve completion of the particular life cycle within *Pf*. The asexual and sexual forms of the parasite, as well as the cycle duration are color-coded in blue and red, respectively. N/A = not applicable.

Physical Location	Mode of reproduction	Ploidy	Associated physical forms		Pathologic	time
Mosquito (saliva)	Asexual	Haploid	• Sporozoite		No	N/A
Mosquito (midgut)	Sexual	Haploid*	• Gametocyte • Gamete • Zygote • Ookinete • Oocyst • Sporozoite		No	17 d
Human (LC)	Asexual	Haploid	• Merozoite • Ring • Trophozoite • Schizont		No	10 d
Human (RBC)	Asexual Sexual	Haploid	• Merozoite • Ring • Trophozoite • Schizont	• Gametocyte	Yes	48 h 15 d

*The *Plasmodium* parasite remains haploid throughout all stages of its life cycle, with one exception: the zygote form of the parasite is diploid.

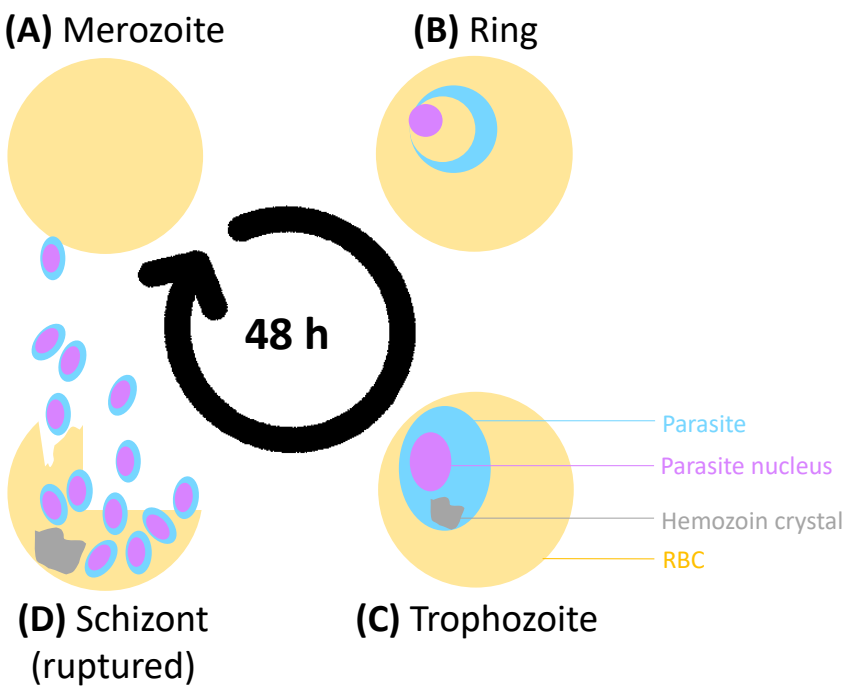

Figure 1.1. A simplified depiction of the *Pf* ABS life cycle. (A) A merozoite is a free parasite attempting to invade a RBC. **(B)** Once established within a RBC, the merozoite develops and enlarges into a ring, which has a characteristic ring shape. **(C)** A ring further develops into a trophozoite, which is ameboid and has a hemozoin crystal resulting from the ingestion of RBC hemoglobin. **(D)** A trophozoite undergoes a division known as schizogony, giving rise to a single schizont that contains 16 – 32 daughter merozoites. Eventually, the parasitized RBC ruptures, releasing the daughter merozoites into the bloodstream and starting the ABS anew. The various color-coded components are indicated for the trophozoite-stage.

The *Plasmodium* apicoplast

Plasmodium spp. are among the ~5,000 species of parasites that belong to the phylum Apicomplexa. Although these obligate intracellular parasites are minute in size, they pose a formidable threat to human health as well as the agricultural industry. For instance, *Babesia* spp. and *Theileria* spp. are

responsible for babesiosis and theileriosis, respectively, both common diseases of livestock, while *Toxoplasma gondii* (*Tg*) and *Plasmodium* spp. are the respective causative agents of the human diseases toxoplasmosis and malaria. Now, despite the variety of genera and associated diseases attributed to this phylum, apicomplexans have been thought to possess two common defining physical features – (1) the apical complex, an anterior structure comprised of individual secretory organelles (micronemes, rhoptries, and dense granules) that collectively enable the parasite to invade the host cell and establish itself therein, and (2) the apicoplast, a relict plastid containing a well-conserved 35 k.b. circular genome. That being said, the apparent absence of the apicoplast has been demonstrated in certain genera within the phylum, including *Cryptosporidium* spp. [6] and the related *Gregarina* spp. [7], and could be potentially attributed to the early evolutionary divergence of these species from other members of the phylum and loss of the organelle. Notwithstanding these exceptions, however, the apicoplast is not only present within *Plasmodium* spp. but also houses metabolic pathways requisite to the development and/or survival of the parasite during both the ABS [8] and the ALS [9, 10].

The apoplast is thought to be evolutionarily derived from two sequential endosymbiotic events (reviewed in [11] and [12]) (**Figure 1.2**). In the first, i.e., primary endosymbiosis, a photosynthetic cyanobacterium was engulfed and retained by a eukaryote, giving rise to a red alga circa 1.3 Gya. At this stage, the endosymbiont would have functioned as a two-membrane chloroplast. Thereafter, around 800 Mya, the red alga was presumably engulfed and retained by another heterotrophic eukaryote, giving rise to a group of organisms collectively termed Chromalveolates, to which apicomplexans belong. The plasma membrane of the algal cell collapsed onto its chloroplast, adding a third membrane to the organelle, while a fourth vacuolar membrane was added during the engulfment of the algal cell by the second heterotrophic eukaryote. Over the course of evolutionary time, this remnant chloroplast retained its organellar genome, but lost redundant genes and those responsible for photosynthesis. Importantly, the endosymbiotic origin of the apicoplast poses

substantial implications for the parasite in terms of the targeting of nuclear-encoded apicoplast-localized proteins (discussed below) and their traversal across the quadruple plastidial membrane (not covered herein).

As mentioned above, each member of the organellar trio has its individual genome. More specifically, *Pf* contains a nuclear genome, which contains 14 chromosomes and 5,268 protein-encoding genes [13], as well as two extra-chromosomal DNA elements – a 6 k.b. mitochondrial genome and a 35 k.b. apicoplast genome, both of which are maternally inherited based on evidence from *Plasmodium gallinaceum* [14]. The *Pf* apicoplast genome, in particular, consists of a circular sequence of 38,682 nucleotides that almost exclusively encode biomolecules involved in gene expression [15], such as rRNAs, tRNAs, and ribosomal proteins [15]. Such diminutive size and streamlined proteome of this plastid genome are presumably evolutionary consequences of the transfer of genes from the endosymbiont to the host cell nucleus, as a means to minimize the chances of accumulating deleterious genetic mutations. Now, because the apicoplast genome has a limited repertoire of encoded proteins, specific nuclear-encoded proteins must be imported into the apicoplast to fulfill their metabolic functions therein. In that regard, as there are several organelles within the parasite, such proteins must be specifically targeted to the plastid, a cardinal task accredited to the N-terminal bipartite pre-sequence present on these nuclear-encoded proteins [16] (for a more detailed discussion of apicoplast-targeting of nuclear-encoded proteins, see the **INTRODUCTION** section of **CHAPTER 4**). Importantly, the *Pf* bipartite pre-sequence consists of a signal peptide and a transit peptide [16], and *Pf* transit peptides can be distinguished from the mature proteins with respect to the prevalence of particular amino acids [17]. As such, these distinguishing features conveniently enabled the creation of a bioinformatic tool known as *Plasmodium falciparum* apicoplast-targeted proteins (PlasmoAP), which utilizes a set of criteria based on amino acid sequence to identify putative bipartite pre-sequences, and hence, apicoplast-targeted proteins [17]. In particular, among the 5,268 nuclear-encoded *Pf* proteins

[13], 466 were predicted to be targeted to the apicoplast by PlasmoAP [17]. This finding not only supported the notion that the organelle is reliant on specific nuclear-encoded proteins to carry out its function, but also facilitated the construction of the putative metabolic pathways within the organelle. All told, four major metabolic pathways are known to be present within the apicoplast – (1) the sulfur utilization factors (SUF) pathway of [Fe-S] cluster biosynthesis, (2) the methyl-erythritol phosphate (MEP) pathway of isoprenoid biosynthesis, (3) the type II fatty acid synthesis (FAS-II) pathway, and (4) the heme biosynthesis pathway.

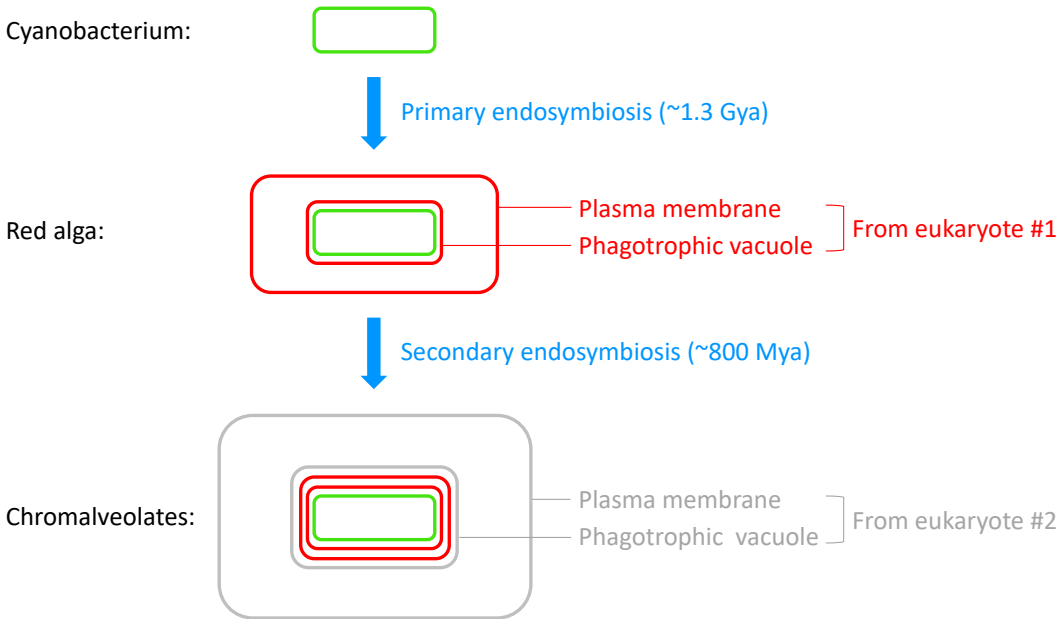

Figure 1.2. Secondary endosymbiotic origin of the apicoplast. During primary endosymbiosis circa 1.3 Gya, a cyanobacterium was engulfed and retained by a heterotrophic eukaryote, giving rise to a red alga cell containing a two-membrane chloroplast. During secondary endosymbiosis circa 800 Mya, the red alga was engulfed and retained in a phagotrophic vacuole of a second heterotrophic eukaryote, giving rise to the group of organisms called Chromalveolates, to which apicomplexans belong. From inside out, the three innermost membranes of the apicoplast were derived from the two membranes of the chloroplast surrounded by the red algal plasma membrane, and the fourth membrane of the apicoplast was derived from the phagotrophic vacuole of the second eukaryote.

Thesis rationale

Although the putative metabolic pathways within the *Pf* apicoplast have been largely elucidated, the identity of specific apicoplast proteins that are required for maintaining this organelle, as well as the means by which these proteins do so, remain to be determined. As one would surmise, the reasonable method of unveiling the function of a protein is to alter its expression and subsequently investigate the aftermath of such tweaking at the genomic, transcriptomic, proteomic, or cellular/phenotypic level. However, because the apicoplast is an organelle that is essential to the survival of *Pf*, direct genetic deletion or knock-down of any protein that is required for maintaining this organelle would automatically result in the death of the parasite, necessitating the development of novel molecular tools that keep the parasite alive despite the loss of essential parasitic proteins. To that end, **CHAPTER 2** showcases our genetically engineered *Pf*Mev line, which allows us to study essential parasite proteins under Mevalonate supplementation. Using this metabolic bypass line, we have examined proteins involved in the SUF pathway of [Fe-S] cluster biosynthesis with respect to their requirement for parasite survival as well as apicoplast maintenance during the ABS. To further explore proteins involved in apicoplast maintenance, we demonstrate, in **CHAPTER 4**, the capability of both the CLD system and TetR-DOZI system to conditionally knock down PyrKII, a protein that we have shown to be required for maintaining the apicoplast. Importantly, these results on PyrKII pave the way for our subsequent experimental approach to probe the resultant changes within the nuclear and plastidial transcriptome.

Finally, since quinine ushered in the era of synthetic antimalarial drugs in the 1630s, there has been a sustained recurrence of drug resistance in *Plasmodium* parasites. As one would expect, these resistant parasite strains necessitate the search and development of novel effective antimalarials. Among the wide range of chemicals screened by various studies, one promising candidate is triclosan, a compound exhibiting anti-plasmodial activity at the micro-molar range. Heretofore, in fact,

numerous studies have examined a variety of triclosan analogs, with the hope of discovering an analog with substantially amplified antiparasitic activity. With the same goal in mind, we have, in **CHAPTER 3**, screened seven triclosan analogs for their antiparasitic activity against ABS *Pf*. Among the examined analogs, we have confirmed the potency of a compound designated herein as djm-11-03A, which was found to be the most potent among the seven. Our next step is to induce drug resistance in ABS *Pf* using this analog in order to uncover the genetic determinants of resistance against this compound. This approach should identify the molecular targets of the compound within the parasite, and thus, shed light on how to optimize the compound to better inhibit these targets.

REFERENCES

[1] World Health Organization, "World Malaria Report 2017," *World Health Organization*, Nov. 2017. [Online]. Available: http://www.who.int/malaria/publications/world-malaria-report-2017/en/ [Accessed Apr. 30, 2018].

[2] A. F. Cowman, J. Healer, D. Marapana, and K. Marsh, "Malaria: Biology and Disease," *Cell*, vol. 167, no. 3. pp. 610–624, 2016.

[3] S. Toler, "The plasmodial apicoplast was retained under evolutionary selective pressure to assuage blood stage oxidative stress," *Med. Hypotheses*, vol. 65, no. 4, pp. 683–690, 2005.

[4] X. Su, K. Hayton, and T. E. Wellems, "Genetic linkage and association analyses for trait mapping in Plasmodium falciparum," *Nature Reviews Genetics*, vol. 8, no. 7. pp. 497–506, 2007.

[5] G. G. van Dooren, M. Marti, C. J. Tonkin, L. M. Stimmler, A. F. Cowman, and G. I. McFadden, "Development of the endoplasmic reticulum, mitochondrion and apicoplast during the asexual life cycle of *Plasmodium falciparum*," *Mol. Microbiol.*, vol. 57, no. 2, pp. 405–419, Jul. 2005.

[6] G. Zhu, M. J. Marchewka, and J. S. Keithly, "Cryptosporidium parvum appears to lack a plastid genome," *Microbiology*, vol. 1700, no. 146, pp. 53–315, 2018.

[7] M. A. Tosco and C. K. Omoto, "Gregarina niphandrodes may Lack Both a Plastid Genome and Organelle," *J. Eukaryot. Microbiol.*, vol. 54, no. 1, pp. 66–72, Jan. 2007.

[8] E. Yeh and J. L. DeRisi, "Chemical Rescue of Malaria Parasites Lacking an Apicoplast Defines Organelle Function in Blood-Stage Plasmodium falciparum," *PLoS Biol.*, vol. 9, no. 8, p. e1001138, Aug. 2011.

[9] A. M. Vaughan *et al.*, "Type II fatty acid synthesis is essential only for malaria parasite late liver stage development," *Cell. Microbiol.*, vol. 11, no. 3, pp. 506–520, Mar. 2009.

[10] M. Yu *et al.*, "The Fatty Acid Biosynthesis Enzyme FabI Plays a Key Role in the Development of Liver-Stage Malarial Parasites," *Cell Host Microbe*, vol. 4, no. 6, pp. 567–578, 2008.

[11] G. G. van Dooren and B. Striepen, "The algal past and parasite present of the apicoplast," *Annu. Rev. Microbiol.*, vol. 67, no. 1, pp. 271–89, Sep. 2013.

[12] M. Kalanon and G. I. McFadden, "Malaria, Plasmodium falciparum and its apicoplast," *Biochem. Soc. Trans.*, vol. 38, no. 3, pp. 775–82, Jun. 2010.

[13] M. J. Gardner *et al.*, "Genome sequence of the human malaria parasite Plasmodium falciparum," *Nature*, vol. 419, no. 6906, pp. 498–511, 2002.

[14] A. Creasey, K. Mendis, J. Carlton, D. Williamson, L. Wilson, and R. Carter, "Maternal inheritance of extrachromosomal DNA in malaria parasites," *Mol. Biochem. Parasitol.*, vol. 65, pp.

95–98, 1994.

[15] I. Wilson *et al.*, "Complete Gene Map of the Plastid-like DNA of the Malaria Parasite Plasmodium falciparum," *J. Mol. Biol.*, vol. 261, pp. 155–172, 1996.

[16] R. F. Waller, M. B. Reed, A. F. Cowman, and G. I. McFadden, "Protein trafficking to the plastid of Plasmodium falciparum is via the secretory pathway," *EMBO J.*, vol. 19, no. 8, pp. 1794–802, Apr. 2000.

[17] B. J. Foth *et al.*, "Dissecting apicoplast targeting in the malaria parasite Plasmodium falciparum," *Science*, vol. 299, no. 5607, pp. 705–8, Jan. 2003.

CHAPTER 2: Iron-sulfur cluster proteins and apicoplast maintenance

ABSTRACT

The apicoplast is an organelle that is essential for the survival of *Pf*, the deadliest species among the five which cause human malaria. Although the protozoan parasite falls under the domain Eukarya, its plastid houses several pathways of bacterial origin, including the SUF pathway of [Fe-S] cluster biosynthesis, which has been shown to be required for the maintenance of the organelle. While prior studies have helped elucidate the organellar localization of, as well interactions between, specific proteins that utilize and/or help assemble [Fe-S] clusters in *Plasmodium* spp., a systematic examination of the essentiality of each individual protein for ABS *Pf* survival and apicoplast maintenance is wanting. To help address this, we employed a genetically engineered *Pf* bypass line (*Pf*Mev), to which exogenous supplementation of Mevalonate, a precursor metabolite of mammalian isoprenoid biosynthesis, enables the survival of parasites that have lost the organelle. From this parental line, we generated genetic knock-outs of individual, or pairs of, apicoplast-localized proteins that are involved with the utilization and/or assembly of [Fe-S] clusters. Among the thirteen proteins examined, we show that the one(s) involved with sulfur mobilization (SufS and SufE), cluster assembly (SufC and SufD), cluster transfer (NifU and SufA together but not individually), isoprenoid biosynthesis (DXPR, IspG, and IspH), and redox (Fdx) are indispensable for ABS *Pf* survival, while those involved with tRNA thio/methylation (MiaB) and lipoic acid metabolism (LipA) are dispensable. Furthermore, among the proteins examined, only MnmA and SufS, both of which utilize sulfur to carry out their respective functions, were found to be essential for the maintenance of the apicoplast.

INTRODUCTION

[Fe-S] clusters in *Plasmodium* spp.

Iron-sulfur clusters are inorganic prosthetic groups attached to specific proteins. These clusters are thought to serve as cofactors required for the proper functioning of the associated proteins, and can come in various forms, among which the most common are binuclear [2Fe-2S], cuboidal [3Fe-4S], and cubane [4Fe-4S] clusters. *Plasmodium* spp. harbor two functional [Fe-S] cluster biosynthesis pathways – the mitochondrion-localized iron-sulfur cluster (ISC) pathway and the apicoplast-localized sulfur utilization factors (SUF) pathway. As shown in the putative model for [Fe-S] cluster biosynthesis within the apicoplast (**Figure 2.1**), this pathway is thought to involve a total of seven SUF proteins (SufS, E, B, C, D, A, and U), most of which have been localized to the apicoplast – SufC was localized to the apicoplast in *Pf* [1]; SufS, E, and D were localized to the apicoplast in *Plasmodium berghei* (*Pb*) [2]; SufS and E were exclusively localized to the apicoplast in ABS *Pf* [3]; and NifU (a.k.a. SufU) was localized to the apicoplast in *Pb* [4]. Among these seven proteins, only SufB is specifically encoded by the apicoplast genome. As SufS, E, C, D, A, and U are encoded by the nuclear genome, these six proteins must be targeted specifically to the apicoplast (for a more detailed discussion of apicoplast-targeting of nuclear-encoded proteins, see the **INTRODUCTION** section of **CHAPTER 4**).

[Fe-S] cluster biosynthesis within the apicoplast is thought to be initiated by SufS, which, together with its interacting partner SufE, mobilizes sulfur from L-cysteine. Furthermore, SufE is thought to form a complex with SufS and enhance the cysteine desulfurase activity of SufS [5]. Although L-cysteine has been identified as a source of sulfur for assembling [Fe-S] clusters, the source of iron is unidentified as of yet. Nonetheless, the mobilization of iron and sulfur is thought to be followed by cluster assembly on a scaffold protein complex that takes the form of SufB-C_2-D [6]. Evidence for this comes from the *in vitro* demonstration of the complex formation between SufB and SufC [1, 6], SufC and SufD [6], and SuB and SufD [6], as well as [4Fe-4S] cluster generation in the

presence of the scaffold complex [6]. Lastly, the assembled [Fe-S] clusters are transferred via NifU and/or SufA to specific [Fe-S] cluster-utilizing proteins. Evidence for this comes from the *in vitro* demonstration of the preference of both cluster transfer proteins to bind [4Fe-4S] clusters and their capability of transferring the bound cluster onto *E. coli* aconitase B, a known [4Fe-4S] cluster-utilizing protein [6].

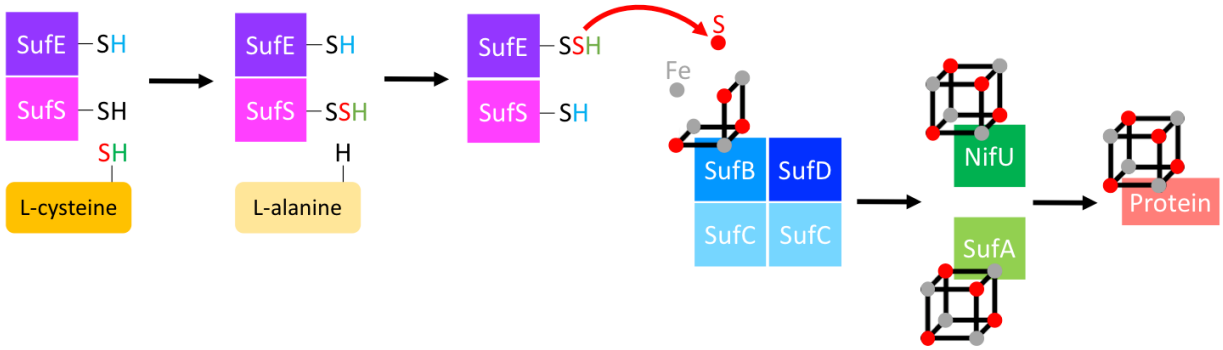

Figure 2.1. A model for the SUF pathway in the apicoplast of *Plasmodium* spp. SufS and SufE together initiate sulfur mobilization from L-cysteine. SufS acquires a sulfur from L-cysteine, thereby forming a persulfide group. Thereafter, this sulfur from the persulfide group of SufS is passed along to SufE, which then transfers it to the SufB-C_2-D scaffold complex, on which cluster assembly takes place. The iron used for assembling [Fe-S] clusters is derived from an unidentified source. Finally, NifU and/or SufA transfers the assembled clusters to specific [Fe-S] cluster-utilizing proteins. Note, for simplicity, only a [4Fe-4S] type cluster is depicted (for a comprehensive list of apicoplast-localized [Fe-S] cluster-utilizing proteins and their associated cluster type, see **Figure 2.3** below).

Now, although components of the SUF pathway have been identified, and steps to the cluster assembly process have been largely elucidated, the potential role of this pathway in the maintenance of the apicoplast has yet to be determined. From an experimental perspective, this is a particularly intractable question to tackle for two major reasons: (1) since the apicoplast is essential to the survival

of *Plasmodium* spp., direct genetic deletion of any protein that is required for maintaining this organelle would automatically result in the death of the parasite; (2) as evidenced from *in vitro* [Fe-S] cluster reconstitution experiments, the clusters are oxygen-sensitive and rapidly degrade under aerobic conditions. To circumvent these issues, we have genetically engineered a Mevalonate bypass *Pf* line, *Pf*Mev, to which exogenous supplementation of Mevalonate, a precursor metabolite of mammalian isoprenoid biosynthesis, enables the survival of parasites that have lost the organelle.

The design of the Mevalonate bypass line *Pf*Mev

Isoprenoids are polymers of either IPP or its isomer DMAPP, and can serve at least three purposes in *Pf*: (1) prenyl transferases can catalyze the prenylation of specific proteins using polymers of IPP or DMAPP [8]; (2) isoprenoids can be incorporated into dolichols [9], which are a group of organic compounds involved in the formation of glycoproteins; and (3) isoprenoids are needed for the synthesis of quinones (ubiquinone and menaquinone), which are a part of the electron transfer system within the mitochondrion. Two functional pathways exist for the biosynthesis of isoprenoids: (1) the Mevalonate-dependent pathway, or MVA pathway (**Figure 2.2A**), utilized by mammalian cells, and (2) the Mevalonate-independent pathway, or MEP pathway (**Figure 2.2B**), located within the apicoplast. Although both pathways result in the synthesis of isoprenoid precursors IPP and DMAPP, the two routes differ with respect to their starting materials, intermediates, as well as enzymes. More specifically, the Mevalonate-dependent pathway starts with two molecules of acetyl CoA, which are converted to Mevalonate via a series of reactions catalyzed by three enzymes. This Mevalonate then gets converted to IPP/DMAPP by four enzymes – MVK, PMK, MPD, and IDI. The Mevalonate-independent pathway, on the other hand, does not generate Mevalonate as an intermediate. Rather, the starting materials pyruvate and GA3P are converted to IPP and DMAPP through the action of seven enzymes – DXS, DXPR, IspD, IspE, IspF, IspG, and IspH.

Fosmidomycin, an antimalarial which targets the Mevalonate-independent pathway by inhibiting DXPR [10], induces growth arrest in *Pf* [10, 11]. However, supplementation with IPP alone rescues the parasites from this drug-induced phenotype [11], thereby indicating that, as long as IPP is available to ABS *Pf*, precursor molecules to IPP biosynthesis and enzymes lying upstream of IPP are dispensable for the survival of the parasite. Moreover, IPP supplementation enables the survival of ABS *Pf* parasites which have lost the apicoplast [11], indicating that it is not the apicoplast *per se*, but rather, the presence of specific isoprenoids generated within this organelle, that is required for the survival of ABS *Pf*. In that regard, IPP supplementation offers a metabolic bypass that enables the survival of parasites in which proteins that are needed for maintaining the apicoplast are somehow lost. Unfortunately, however, such a bypass system is rendered infeasible via the prohibitive cost of directly purchasing the molecule as well as the impracticality of its chemical synthesis. To overcome this hurdle, we have genetically engineered the *Pf*Mev line, which cytosolically expresses four enzymes of the Mevalonate-dependent pathway – MVK, PMK, MPD, and IDI. As outlined in the pathway (**Figure 2.2A**), these four enzymes convert Mevalonate to IPP/DMAPP. Therefore, as long as Mevalonate is provided in the growth medium for this bypass line, the parasites that have lost the apicoplast will be able to survive. Given this, the *Pf*Mev line allows us to delete any gene from the parasite, irrespective of whether the corresponding encoded protein is required for the survival of the parasite, and examine the aftermath of the deletion. With this bypass system in hand, therefore, we are able to address our initial question – how are [Fe-S] cluster proteins important to the maintenance of the apicoplast? To that end, we have generated thirteen *Pf*Mev-based genetic knock-out lines, each of which is either a single or double deletion mutant. The overall schematic illustrating the bypass system as well as pathways involving the proteins of interest to this study are shown below (**Figure 2.3**). With the exception of MnmA and DXPR, each protein targeted by our knock-out approach has a role in [Fe-S] cluster assembly and/or utilization.

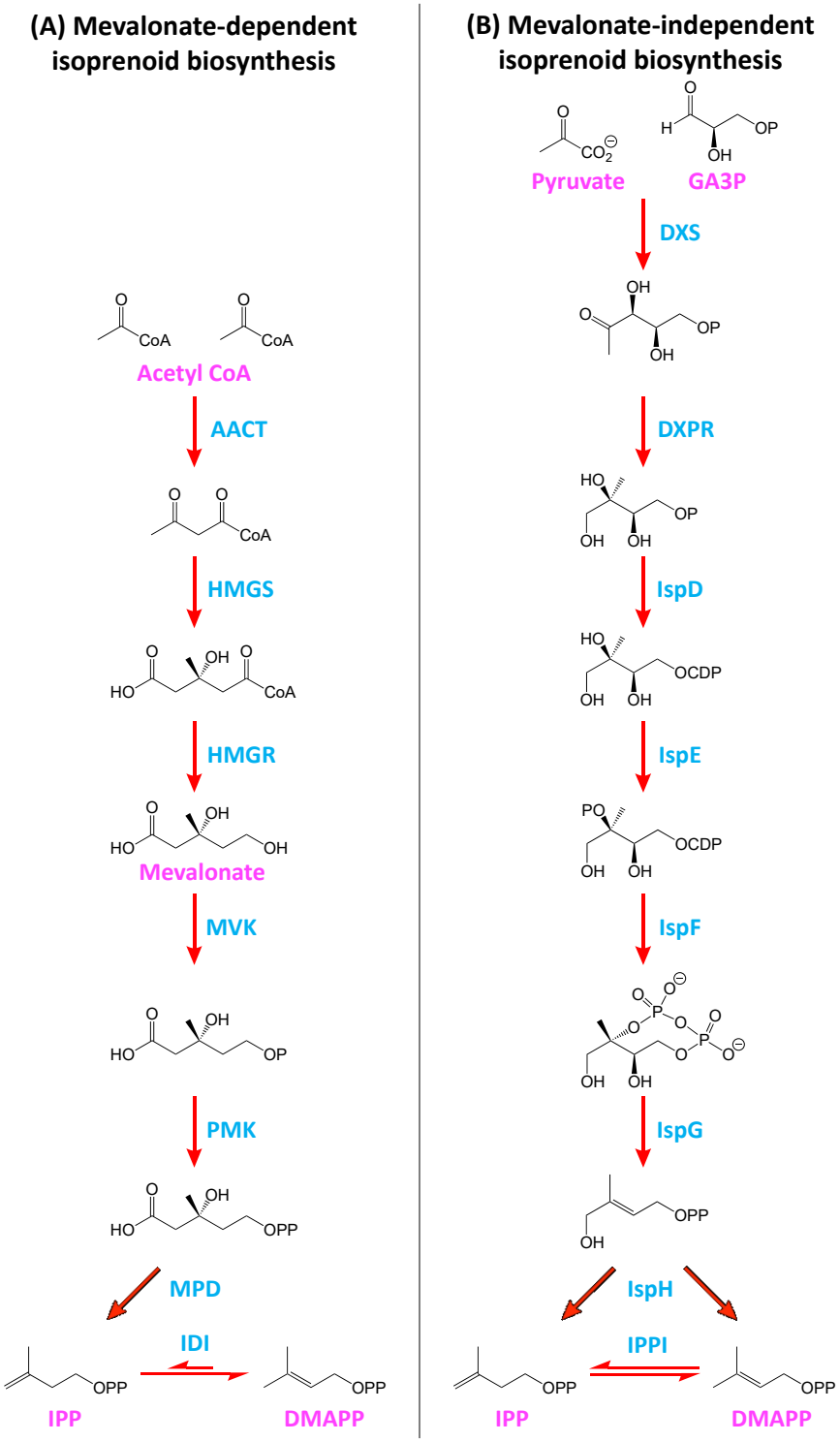

Figure 2.2. The two pathways of isoprenoid biosynthesis. (A) The Mevalonate-dependent pathway and **(B)** the Mevalonate-independent pathway of isoprenoid biosynthesis are shown. The names of enzymes are shown in blue; the names of key metabolites are shown in pink.

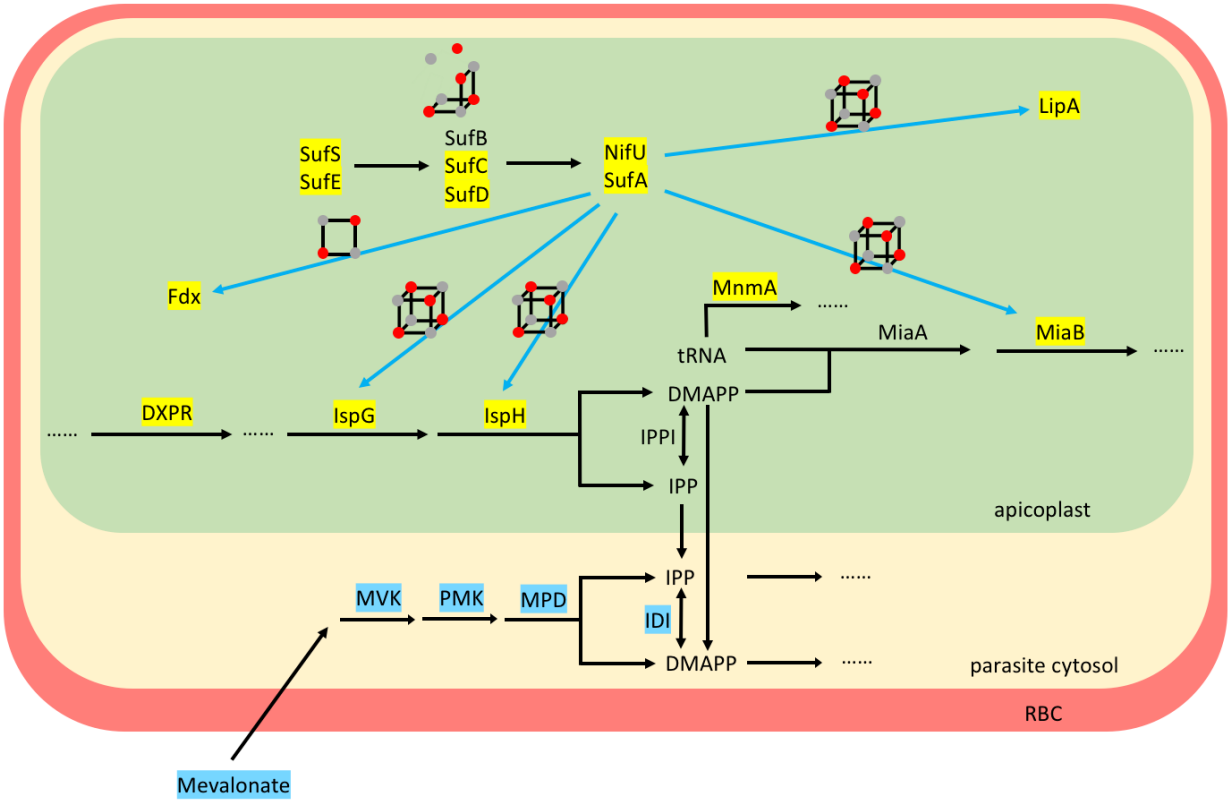

Figure 2.3. The *Pf*Mev bypass pathway. Mevalonate provided in the growth medium will enter the parasite cytosol, where it gets converted to IPP/DMAPP by four cytosolically expressed enzymes of the Mevalonate-dependent pathway. Given that isoprenoid biosynthesis is essential for the survival of ABS *Pf*, this supplementation enables the survival of parasites in which endogenous IPP biosynthesis is disrupted. Components of the bypass system are highlighted in blue; the thirteen *Pf* proteins targeted by our genetic knock-out strategy are highlighted in yellow. Among the five [Fe-S] cluster-utilizing proteins, IspG, IspH, LipA, and MiaB each has a [4Fe-4S] cluster, while Fdx has a [2Fe-2S] cluster. Among the thirteen targeted proteins, DXPR and MnmA are the only ones that are not known to be involved with [Fe-S] cluster assembly/utilization.

MATERIALS AND METHODS

Parasite culture maintenance

Each parasite culture was maintained at 1% hematocrit (using human blood) in 10 mL total volume in a 75 cm^2 sealed cell culture flask (Corning, cat. #430168) at 37°C. Each flask contained Complete Medium with AlbuMAX (CMA): RPMI 1640 medium (USBiological Life Sciences, cat. #R8999) supplemented with 25 mM HEPES (Sigma-Aldrich, cat. #H4034), 0.375% Sodium Bicarbonate (gibco, cat. #25080-094), 12.5 μg/mL Hypoxanthine (Sigma-Aldrich, cat. #H9377), 5 g/L AlbuMAX II (gibco, cat. #11021-037), and 25 μg/mL Gentamicin (Sigma-Aldrich, cat. #G3632), with or without 50 μM Mevalonate (Sigma-Aldrich, cat. #M4667). Prior to sealing the flask for incubation at 37°C, the flask was gassed with 94% N_2, 3% O_2, 3% CO_2 for 40 seconds.

The present study examined thirteen *Pf*Mev-based knock-out lines, among which only ΔLipA and ΔMiaB are not dependent on Mevalonate for survival based on our experiments. For these two lines specifically, therefore, the parasites were cultured in pure CMA medium for approximately 2 weeks prior to taking samples for the subsequent growth curve experiments. This eliminates any parasites that have spontaneously lost the apicoplast from the culture.

Genotyping PCR

For each knock-out line, a corresponding set of four PCR reactions was performed to ascertain the genotype of the knock-out. The four reactions were designed to detect either the 5' and 3' regions of the WT gene (5' and 3') or the 5' and 3' regions consistent with gene deletion (Δ5' and Δ3') (**Figure 2.4**). For each knock-out line, the same set of four PCR reactions performed on the knock-out line was performed on the parental *Pf*Mev line, which served as a WT control (**Figure 2.4**). Briefly, when the parasitemia for a culture was sufficiently high (about 5 – 8%) as determined via Giemsa staining, a sample from the culture was taken, heated at 90°C for 5 minutes on a digital heat block, and then

centrifuged at 6,500 rpm for 5 minutes. The supernatant was collected and stored at -20°C until the time of use. All PCR reactions were carried out with an ABI GeneAmp PCR system 9700 using the Phusion High-Fidelity DNA polymerase (Thermo Fisher Scientific, cat. #F530L), and the products were visualized on a 1.5% agarose gel. The reaction setup, thermal cycling conditions, and primer sequences are as follows:

sample	1	µL
5X HF buffer	10	µL
F primer (10 µM)	1.5	µL
R primer (10 µM)	1.5	µL
dNTP (10 mM)	1	µL
phusion	0.5	µL
Milli-Q water	34.5	µL
total vol.	50	µL

temperature	time	
95°C	3'50''	
95°C	0'30''	35 cycles
62°C	1'00''	
62°C	4'00''	
4°C	∞	

Primer name	Primer sequence
pl8insHA1F	GCTATTTAGGTGACACTATAGAATACTCAAGC
pl8insHA2R	AATCTAGAATTCGACAGACGCCGG
MnmA 5'F	CTACTTTGATGTTTTTTTATTTTTGCACATTTTATG
MnmA 3'R	GGTATTTTTTATTTGCTCATGTTTAAATCATTTATCTG
MnmA 5'WT R	CTTTATACTATTGTTTCTTTGTTCGTCTTCATCAATTTG
MnmA 3' WT F	CTTACTAAAAATTATGACCAAGATTTATTTACACATATACG
SufS 5'F	CAGAAAATGAGTGAGTTTTATAAAAAGGAAAACTC
SufS 3'R	CAATTTGCTGTGCCAAATATTTGATTTC
SufS 5'WT R	CCATATAACAATGGTTTTAAATTTATATTTTGATG
SufS 3' WT F	CCAGATATATTAATAACATCTGGTCATAAATTTTG
SufE 5'F	CATTTCATTCATTTTGGTAGTTAAAAAGAAAAGG
SufE 3'R	TCATTTTTATTAAAAACATATTTCATTTAATTTGTAAGA
SufE 5'WT R	CATGAGCATATTATATATAAAACAAAGAAATGTGC
SufE 3' WT F	CCTGATAAACATAAAATTAGACAAAATCAAGTTTTGG
SufC 5'F	GGGATTTGTCATACATATAAATATGTATAAAAAGGTCC
SufC 3'R	TAAGTACAAAATAATATCATATGTACATTATAAAATCCAC
SufC 5'WT R	CTTCTTCTAAATTTTTTAATAAAGATAATCTATCCATATC
SufC 3' WT F	GAGATAAGTGTAAGTGAATTTAATTTAATGATGATAGAAG
SufD 5'F	GTGTATATAATTTTTTGAAAAAAATGATTTAGCTAACACA
SufD 3'R	CAGATATTCCTCTTGTCATTAATGAGAAGATTGG
SufD 5'WT R	GTGTTTTCTCTTCATTTTGATGTCTATAGTTTTTTATAC
SufD 3' WT F	CCAATAACAAATCCTAGATTAGTTGTATATGTAAAAGG
NifU 5'F	ATACGAAATGAAATTAGTTTTTTAATAATATATTTATACC

NifU 3'R	CGTTAATGTGGAGAAAATTCAAAGACCTAC
NifU 5' WTR	CGAAATTATTTTGTATAAATAACACCTTTGC
NifU 3' WTF	CACACAACGTTAAAAATGAAATAACAGAAAG
SufA 5'F	CTTTTTTCTCCTTTTAATATTAAAAAGAAAAAAG
SufA 3'R	CCTAAAGATATATATTTATGTGTTATCTTATATATTTTTG
SufA 5' WTR	GCTCTTATTGTTATATAAAAATGTTTTTGGAG
SufA 3' WTF	GATATAGAACGAAATTGAAGAAGATGATTATATAC
DOXP 5' F	CTATTAATGATTTAGTAATAAATAATACATCAAAATGTG
DOXP 3'R	GTATTTTATTTTTTTTTTGTACTATGAAGAATTATGTTTG
DOXP 5' WT R	CCTTGAAAAGAATCAATACCAATAACTATTTTATC
DOXP 3' WT F	GGAAAATGGGTAAGAAAATAACTATAGATTCTG
IspG 5' F	CTAAATGAAGAAGGGAATTCTTCAAAAAAG
IspG 3' R	CATATTCAATTTATGGATCTTTCCATTTG
IspG 5' WT R	CAATACATAAATCAGAAAACTCAAAAGCC
IspG 3' WT F	GTATTAATAACCAGAAGAATTAATGAACTTTTACAATC
IspH 5' F	CCAGTAAGCAAAATATATCCATTCTGTATAC
IspH 3' R	TGTGATTTCATTTTTTCTCTTTCTTTTATCA
IspH 5' WT R	GGGTACATATATATTTTTCGATTCCCATC
IspH 3' WT F	CCATTAAATAAAAAGTTATTCTATGTTACACAAACC
Fdx 5'F	CTGGTATATTATAGTTTTATATTTAATAAGAAAAGGGC
Fdx 3'R	GGTAGCGAAGTTAATACATACACATATATATATGTG
Fdx 5' WT R	CGAATGTAATGAAGATGAATATATATTAGATGCTAG
Fdx 3' WT F	GGTAGCGAAGTTAATACATACACATATATATATGTG
LipA 5' F	CCTACATAAACTGTAATGTTTCAATATGACC
LipA 3' R	GGTTAACTAAATTTTTTTATAAAATATTCACCTGC
LipA 5' WT R	GTGCTTCTTCACATACGGTATGTAAG
LipA 3' WT F	CTTTCAATACAGCTAAAGCTATATGTGAATG
MiaB 5'F	GATATTAAATGGGAAAGCAAAACTTATAAGTTTTTTATTC
MiaB 3'R	GTGATACATTTTTCAAATATCTCCATATCTTTTTCTG
MiaB 5' WT R	GATGTTGATAAGCATTCCAAGTCATATTCTC
MiaB 3' WT F	GGATGTGCTCATAATAGTTCAGATTCTG

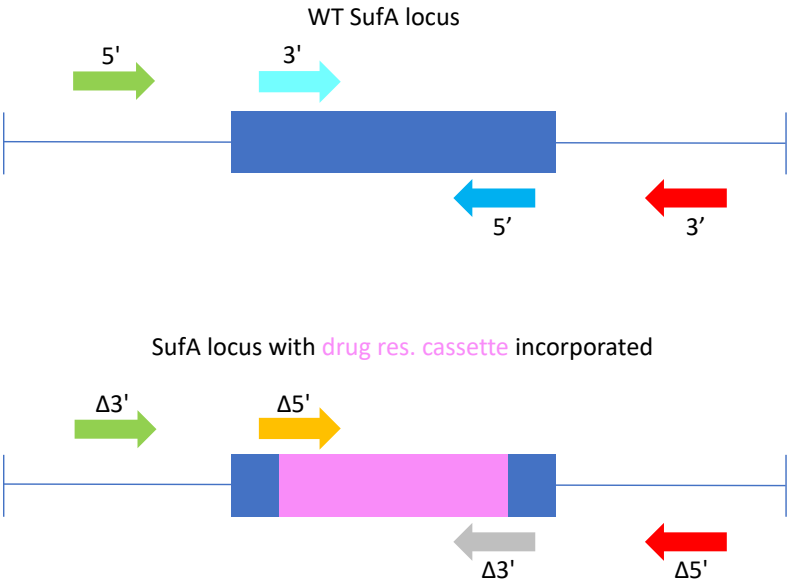

primer combo	F primer	R primer
Δ5'	PL8 HA2 F II	SufA 3' R
Δ3'	SufA 5' F II	PL8 HA1 R
5'	SufA 5' F II	SufA 5' WTR
3'	SufA 3' WTF	SufA 3' R

Figure 2.4. General genotyping PCR scheme. The SufA genomic locus is shown as an example. For each knock-out line, a set of four genotyping PCR reactions was performed. These reactions, designated as Δ5', Δ3', 5', and 3', along with the identity of forward and reverse primer per reaction, are indicated. For the WT genomic locus, amplicons are only expected for the reactions 5' and 3'; for the disrupted locus, amplicons are only expected for the reactions Δ5'and Δ3'.

Organellar genome PCR

For each knock-out line, the status (presence or absence) of the nuclear and organellar genomes was determined by amplifying the *LDH* (nuclear genome), *SufB* (apicoplast genome), and *Cox1* (mitochondrial genome) genes. Samples were collected in the same fashion as mentioned above for genotyping PCR. For each knock-out line, the same set of three PCR reactions performed on the knock-out line was performed on the parental *Pf*Mev line, which served as a WT control. The reaction setup, thermal cycling conditions, and primer sequences are as follows:

sample	1	µL
5X HF buffer	10	µL
F primer (10 µM)	1.5	µL
R primer (10 µM)	1.5	µL
dNTP (10 mM)	1	µL
phusion	0.5	µL
Milli-Q water	34.5	µL
total vol.	50	µL

temperature	time	
95°C	3'30''	
95°C	0'30''	35 cycles
63°C	0'30''	
72°C	0'45''	
72°C	4'00''	
4°C	∞	

Primer name	Primer sequence
LDH F	GGAGATGTAGATTTGTTCGATATTG
LDH R	CTTGTAAAGGGATACCACCTACAG
SufB FII	CATGTAGCTATAGTAGAAATAATAGTA
SufB R	GACTCTGAAATACTTAAACCACGTTGC
Cox1 F	CTTCATCTTTAAGAATAATTGCACAAGAAAATGTAAATC
Cox1 R	GTACATATGATGTACCCATACTAAGCTTCC

Generation of growth curves

Growth curves were generated using a plate-based SYBR Green assay. As illustrated in the overall plan (per IC plate) used to generate growth curves for the thirteen *Pf*Mev-based knock-out parasite lines (**Table 2.1**), each growth curve spans 4 days (from day 0 to day 4), and the parasitemia from each day was measured using flow cytometry. The following subsections detail each step of the overall plan.

Table 2.1. The overall plan (per incubator [IC] plate) for growth curve generation. This overall plan was used to generate growth curves for the thirteen *Pf*Mev-based knock-out parasite lines.

day	0	1	2	3	4
pt (if doubles / day)	0.5%	1%	2%	4%	8%
IC plate	seed @: • 0.5% pt • 2% hc • 250 µL / well • quadruplicate wells / sample	• change 150 µL media • shaker mix	• change 150 µL media • shaker mix	• change 150 µL media • shaker mix	• shaker mix
CR plate	• add 90 µL CMA	• add 10 µL sample	• add 10 µL sample	• add 10 µL sample	
flow	run using: • 1 µL / IC plate sample				run using: • 1 µL / IC plate sample • 10 µL / CR plate sample

Flow cytometry

Seeding

The parasitemia of each parasite line was determined using Giemsa staining. Based on this parasitemia, quadruplicate samples were seeded in a 96-well flat-bottom cell culture plate (Corning, cat. #3595) at 0.5% parasitemia (pt), 2% hematocrit (hc), and 250 μL total volume per well.

For each parasite line, a master mix containing the appropriate amount of culture content, 50% hematocrit blood, and enough CMA media to bring the total volume to 10 mL was prepared and centrifuged at 1,600 rcf at room temperature (~25°C) for 5 minutes. After removal of the media via aspiration, the cell pellet was resuspended in CMA medium, and spun again under the same centrifuge settings. Post media removal after the second spin, the cell pellet was resuspended in the appropriate amount of CMA medium, and equally split into two tubes. To one of the two tubes, the appropriate amount of 10 mM Mevalonate stock solution (in sterile water) was added to yield a final concentration of 50 μM Mevalonate. Thereafter, each sample was seeded at 250 μL per well. In order to prevent any evaporation from the edge wells, a moat consisting of 1 mM EDTA was prepared around the sample wells at 250 μL per well. The prepared plate was placed into a Modular Incubator Chamber (Billups-Rothenberg Inc., MIC-101), and gassed with 94% N_2, 3% O_2, 3% CO_2 for 1 minute and 15 seconds prior to incubation at 37°C. Immediately post seeding, the parasitemia for each seeded well was measured by flow cytometry (see below for details) to confirm the accuracy of the seeded parasitemia.

Sample collection and storage

Samples were collected at the approximate 24, 48, and 72 hour time points (on days 1, 2, and 3, respectively) post seeding (**Table 2.1**). Each sample that was collected from days 1 – 3 was diluted 1:10 by the type of media within the well from which the sample was derived, and stored in a 96-well round-bottom plate (Corning, cat. #3359) at 4°C until SYBR Green staining on day 4. Based on our

observations, this storage protocol preserves the sample parasitemia for at least three overnights (see the **RESULTS AND DISCUSSION** section for details).

SYBR Green staining

SYBR Green staining was carried out in a 96-well round-bottom cell culture plate (Corning, cat. #3359) under protection from light. 100 μL of 1X SYBR Green (Invitrogen, cat. #S7563) in 1X phosphate-buffered saline (PBS) (pre-warmed to 37°C) was deposited into each well, followed by 1 μL of a 2% (or 10 μL of 0.2%) hematocrit sample. Then, the plate was incubated for 30 minutes under protection from light on a vibrating platform shaker at 950 rpm. After incubation, 150 μL of 1X PBS (pre-warmed to 37°C) was added to each well in order to dilute the excess unbound SYBR Green. When empty wells were available on the plate, an uninfected control (2% hematocrit in CMA) was prepared on the day of staining and treated in parallel with the rest of the samples on the plate.

Cytometer gates and settings

The day 4 samples, along with day 1 – 3 samples, were analyzed with an Attune Nxt Flow Cytometer (Thermo Fisher Scientific) on day 4. Parameters under the settings panel were set as follows: 50 μL for the Acquisition Volume; 250 μL for the Total Sample Volume; 25 μL/minute for the running speed; and 10,000 events within the R2 gate as the sample acquisition stopping point. The flow cytometer gates are illustrated below (**Figure 2.5**).

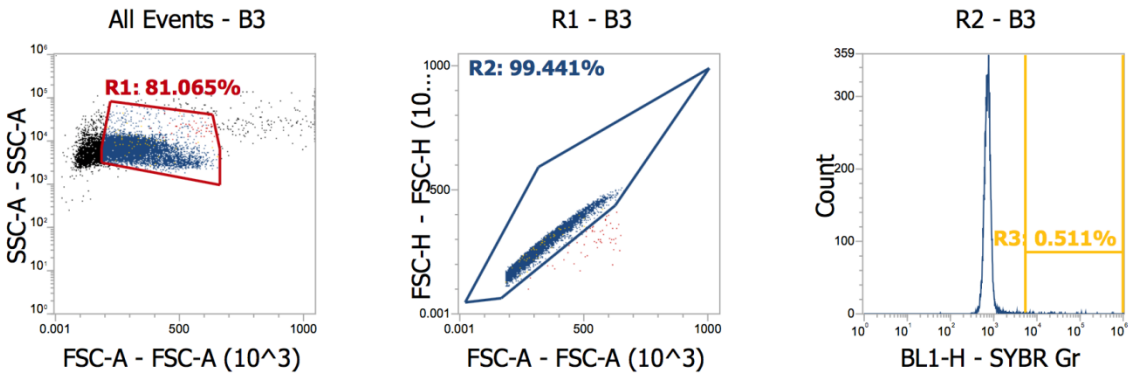

Figure 2.5. Flow cytometer gates. The R1 gate within the Forward Scatter-Area (FSC-A) by Side Scatter-Area (SSC-A) analysis (left panel) was used to identify total RBCs from each sample; the R2 gate within the FSC-A by Forward Scatter-Height (FSC-H) analysis (middle panel) was drawn to isolate single cells from the total cells; the R3 gate within the SYBR Green fluorescence by Count analysis (right panel) was drawn to give the parasitemia (the percent of SYBR Green-positive single RBCs out of all single RBCs).

Limiting dilution

Seeding

Single cloning of each knock-out parasite line was carried out via limiting dilution. For each parasite line, the type of medium used for the initial dilution and subsequent media changes is the same as that within the flask from which the sample was derived. The parasitemia for each culture was determined using Giemsa staining, and used to calculate the number of infected RBCs (iRBCs) per µL of culture. Based on this iRBC concentration, a sample consisting of 1,000 iRBCs/µL was prepared. This sample was then diluted 1:10 thrice sequentially, yielding a parasite sample with a final concentration of 1 iRBC/µL. Each well of a 96-well flat bottom cell culture plate (Corning, cat. #3595) was filled with 200 µL of growth medium with 2% hematocrit RBCs. 100 µL of the 1 iRBC/µL parasite solution was then added to each well of row A on the plate. Finally, a 1:3 serial dilution was carried out from row

to row, starting from row A and all the way down to row H. The prepared plate was placed into a Modular Incubator Chamber (Billups-Rothenberg Inc., MIC-101), and gassed with 94% N_2, 3% O_2, 3% CO_2 for 1 minute and 15 seconds prior to incubation at 37°C.

Media change and culture maintenance

After seeding on day 0, the media was changed on days 5, 7, 9, 12, and 14. On days 5 and 12, a 0.5% hematocrit medium was used to replace lost RBCs; on days 7, 9, and 14, pure medium (without any blood) was used; on day 16, selected iRBC-positive wells that were the farthest down in the dilution series (i.e., closest to row H) were picked and transferred into a 24-well flat bottom cell culture plate (Corning, cat. #S3524) at 2% hematocrit and 1 mL total volume per well. The 24-well plate was then maintained and routinely monitored. Upon reaching a high enough parasitemia (~8%), the content within the well was transferred into a 75 cm^2 sealed cell culture flask (Corning, cat. #430168) and further maintained under normal culture conditions. For each cloned parasite line, the genotype and the status of the organellar (nuclear, apicoplast, and mitochondrial) genomes were confirmed by PCR.

RESULTS AND DISCUSSION

Confirmation of the knock-out genotype

After generating the thirteen *Pf*Mev-based knock-out lines, we first confirmed the genotype of each knock-out. As shown in the general genotyping scheme (**Figure 2.4**), amplicons are expected for the reactions Δ5' and Δ3' only for each knock-out line, while amplicons are expected for the reactions 5' and 3' only for the WT control. In this fashion, our genotyping PCR results confirmed the genotype of each knock-out and indicated an absence of any contamination by WT parasites for each knock-out line (**Figure 2.6A' – M'**).

Optimization of the flow assay

Having ascertained the genotype of each knock-out line, we proceeded to validate the essentiality of each protein examined herein with respect to the survival of ABS *Pf*. To that end, we sought to compare the growth of each knock-out line in the presence of Mevalonate *vs.* its growth without such supplementation, over a span of 4 days (from day 0 to day 4). For all growth curves generated herein, the parasitemia for the seeded samples were measured on day 0 in order to confirm the accuracy of the seeding. As for the days 1 – 3 samples, we wanted to avoid measuring the parasitemia on a daily basis, and thus tested whether sample storage under 4°C (without using a fixative) is able to preserve the parasitemia. As shown in our results (**Table 2.2**), storage of samples under 4°C is able to preserve the parasitemia for at least three days. Thus, for all the growth curves, the days 1 – 3 samples were stored under 4°C, and measured, along with the day 4 sample, on day 4.

Table 2.2. Validation of the cold room storage method. A comparison of the parasitemia derived from the same sample with or without storage at 4°C is shown. CR (cold room) denotes samples that were stored at 4°C and analyzed on day 4; IC (incubator) denotes samples that were analyzed on the day of sample collection, without undergoing any prior storage at 4°C. Results are shown for three different starting parasitemia – 0.3%, 0.5%, and 1%.

	0.3% starting parasitemia		0.5% starting parasitemia		1% starting parasitemia	
day	IC	CR	IC	CR	IC	CR
1	0.69%	0.71%	1.36%	1.39%	2.10%	1.65%
2	1.24%	1.72%	1.52%	1.22%	3.76%	4.55%
3	2.02%	1.83%	4.01%	3.79%	5.16%	5.87%

Figure 2.6. Organellar genome/genotyping PCR for thirteen *Pf*Mev-based knock-out lines. Results for organellar genome PCR amplifying the *LDH*, *SufB*, and *Cox1* gene from the nuclear (N), apicoplast (A), and mitochondrial (M) genome, respectively, are shown for the knock-out lines **(A)** ΔMnmA, **(B)** ΔSufS, **(C)** ΔSufE, **(D)** SufC, **(E)** SufD, **(F)** ΔSufC ΔSufD, **(G)** ΔNifU ΔSufA, **(H)** ΔDXPR, **(I)** ΔIspG, **(J)** ΔIspH, **(K)** ΔFdx, **(L)** ΔLipA, and **(M)** ΔMiaB. Results for genotyping PCR are shown for the knock-out lines **(A')** ΔMnmA, **(B')** ΔSufS, **(C')** ΔSufE, **(D')** SufC, **(E')** SufD, **(F')** ΔSufC ΔSufD (for the SufC genomic locus), **(F")** ΔSufC ΔSufD (for the SufD genomic locus), **(G')** ΔNifU ΔSufA (for the NifU genomic locus), **(G")** ΔNifU ΔSufA (for the SufA genomic locus), **(H')** ΔDXPR, **(I')** ΔIspG, **(J')** ΔIspH, **(K')** ΔFdx, **(L')** ΔLipA, and **(M')** ΔMiaB. The genotyping PCR reactions designated Δ5', Δ3', 5', and 3' correspond to those shown in **Figure 2.4**. For each PCR reaction for both types of PCR, the *Pf*Mev line was included as a WT control. The results shown for ΔMnmA and ΔSufS are from polyclonal parasites, while the results shown for the remaining knock-out lines are from monoclonal parasites.

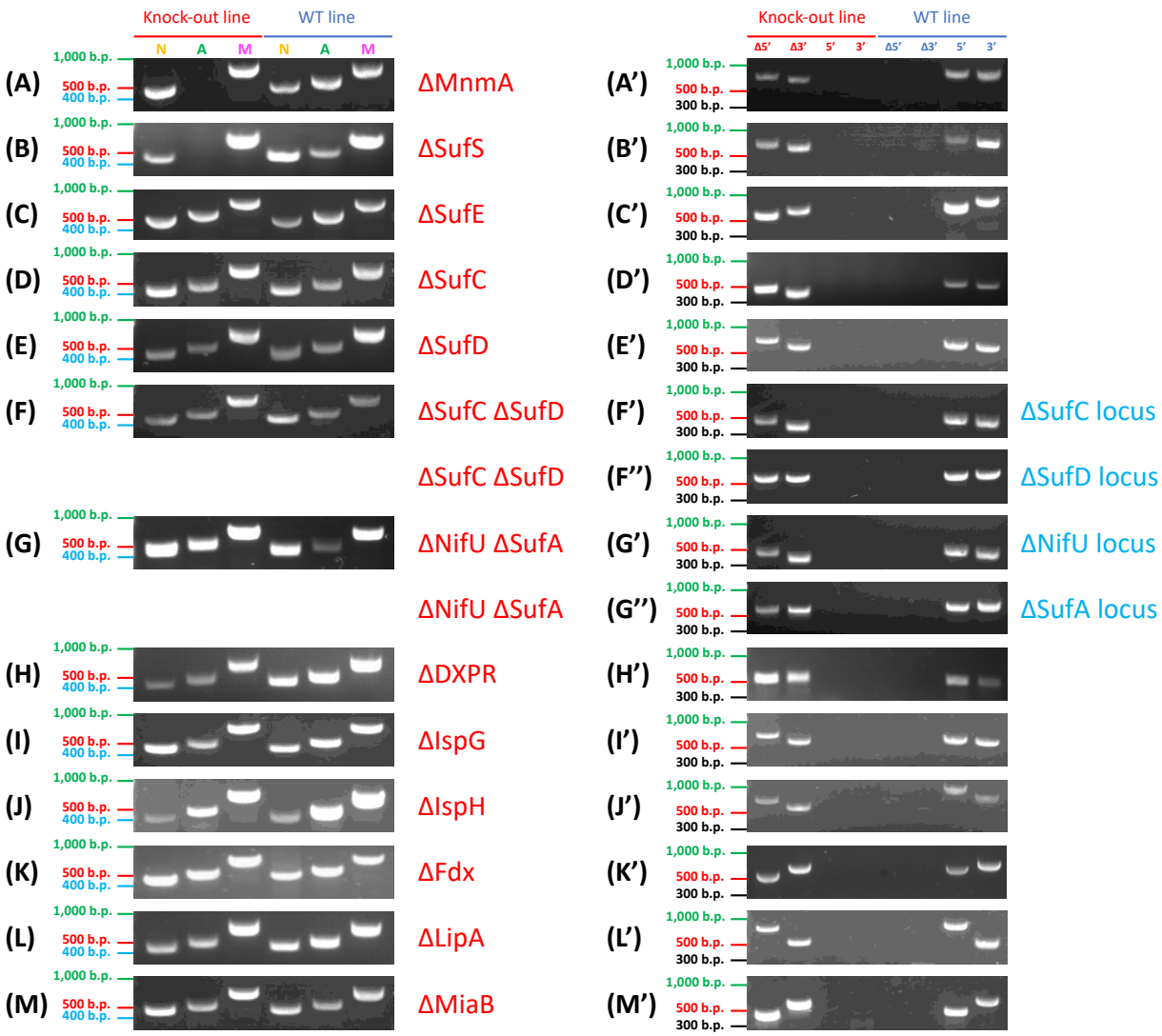
Knock-out line
WT line
N A M N A M
(A) ΔMnmA
(B) ΔSufS
(C) ΔSufE
(D) ΔSufC
(E) ΔSufD
(F) ΔSufC ΔSufD
ΔSufC ΔSufD
(G) ΔNifU ΔSufA
ΔNifU ΔSufA
(H) ΔDXPR
(I) ΔIspG
(J) ΔIspH
(K) ΔFdx
(L) ΔLipA
(M) ΔMiaB
1,000 b.p.
500 b.p.
400 b.p.
300 b.p.
Knock-out line
WT line
Δ5′ Δ3′ 5′ 3′ Δ5′ Δ3′ 5′ 3′
(A′)
(B′)
(C′)
(D′)
(E′)
(F′) ΔSufC locus
(F″) ΔSufD locus
(G′) ΔNifU locus
(G″) ΔSufA locus
(H′)
(I′)
(J′)
(K′)
(L′)
(M′)

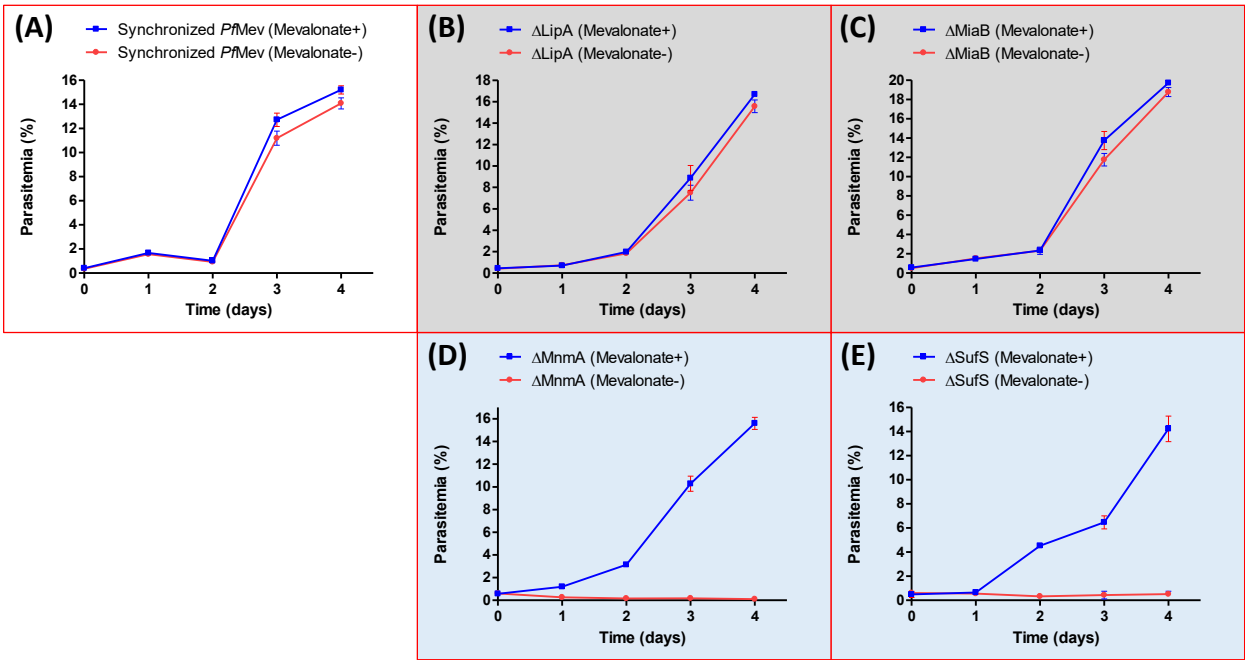

Figure 2.7. Growth curves for *Pf*Mev and four *Pf*Mev-based knock-out lines. Parasites were seeded at 0.5% parasitemia on day 0 and allowed to grow up to day 4. As indicated, two different media conditions were used for each line: CMA with or without 50 μM Mevalonate. Each data point (error bar) represents the mean (standard deviation) derived from four technical replicates. For any data point, the apparent absence of an error bar is due to its small size. **(A)** The *Pf*Mev line (synchronized) served as a control demonstrating Mevalonate-independence. **(B)** ΔLipA and **(C)** ΔMiaB show Mevalonate-independence. **(D)** ΔMnmA and **(E)** ΔSufS show Mevalonate-dependence. Growth curves for proteins that are required for the maintenance of the apicoplast in ABS *Pf* are shown in the blue panels; growth curves for proteins that are dispensable for ABS *Pf* are shown in the grey panels (see text under the **RESULTS AND DISCUSSION** section for details).

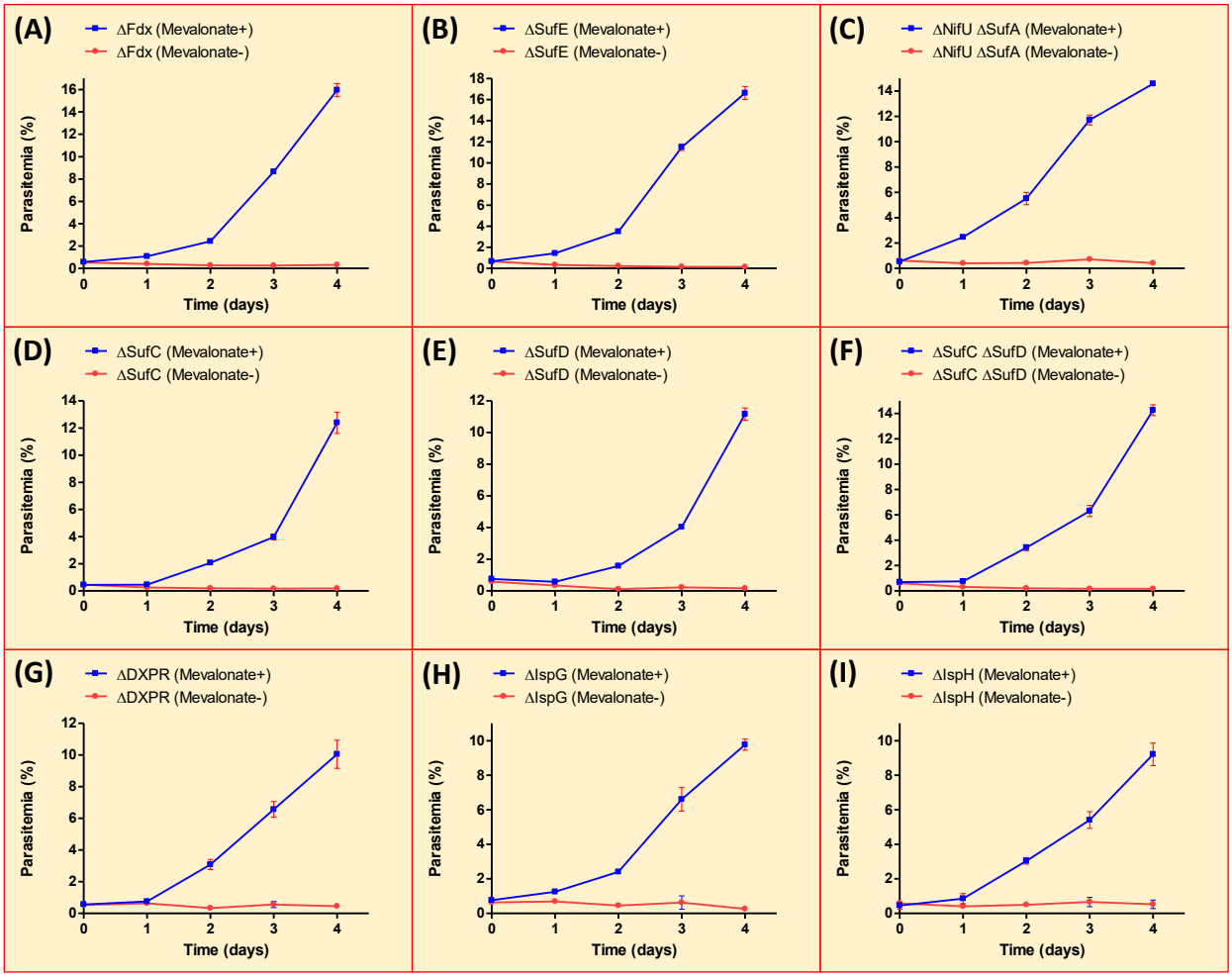

Figure 2.8. Growth curves for nine *Pf*Mev-based knock-out lines. Non-synchronous parasites were seeded at 0.5% parasitemia on day 0 and allowed to grow up to day 4. As indicated, two different media conditions were used for each line: CMA with or without 50 μM Mevalonate. Each data point (error bar) represents the mean (standard deviation) derived from four technical replicates. For any data point, the apparent absence of an error bar is due to its small size. Each of the nine lines shown exhibits Mevalonate-independence: **(A)** ΔFdx, **(B)** ΔSufE, **(C)** ΔNifU ΔSufA, **(D)** SufC, **(E)** SufD, **(F)** ΔSufC ΔSufD, **(G)** ΔDXPR, **(H)** ΔIspG, and **(I)** ΔIspH. All of the lines shown are essential for the survival of ABS *Pf*, but are not required for the maintenance of the apicoplast (see text under the **RESULTS AND DISCUSSION** section for details).

A recent study done on *Pb* attempted to delete all SUF genes except for SufB (SufS, E, C, D, and A) but was only successful in generating viable SufA mutants, suggesting that SufS, E, C, and D are required for the propagation of blood stage infection, while SufA is dispensable for that purpose [2]. Herein, we have examined thirteen *Pf*Mev-based knock-out lines using flow cytometry and organellar genome PCR. Among the proteins that were knocked out, MnmA, SufS, SufE, SufC, SufD, NifU and SufA (together but not individually), DXPR, IspG, IspH, and Fdx were shown to be indispensable for the survival of ABS *Pf*, while LipA and MiB were shown to be dispensable for the survival of ABS *Pf*. Furthermore, among these proteins, only SufS and MnmA were shown to be required for the maintenance of the apicoplast in addition to parasite survival (**Table 2.3**). Taken together at face value, these data suggest the three following conclusions:

(1) MnmA and SufS are required for the survival of ABS *Pf* in that these proteins are required for the maintenance of the apicoplast.

(2) SufC, SufD, NifU and SufA (together but not individually), DXPR, IspG, IspH, and Fdx are required for the survival of ABS *Pf* due to reasons other than being required for maintaining the apicoplast.

(3) LipA and MiaB are dispensable for ABS *Pf*.

Table 2.3. Summary of organellar genome PCR and flow cytometry results. Results are shown for *Pf*Mev and thirteen *Pf*Mev-based knock-out lines. Indicated for each parasite line are Mevalonate-(in)dependence and organellar genome status (presence *vs.* absence). The various proteins examined can be classified into three categories according to the same color-coding for the panels of **Figure 2.7** and **Figure 2.8**: those that are essential by being required for apicoplast maintenance (blue), essential due to reasons other than being required for apicoplast maintenance (yellow), and non-essential (grey).

	Line	Mev-dependent	Nuclear genome	Apicoplast genome	Mito. genome
(1)	ΔMnmA	+	+	-	+
(2)	ΔSufS	+	+	-	+
(3)	ΔSufE	+	+	+	+
(4)	ΔSufC	+	+	+	+
(5)	ΔSufD	+	+	+	+
(6)	ΔSufC ΔSufD	+	+	+	+
(7)	ΔNifU ΔSufA	+	+	+	+
(8)	ΔDXPR	+	+	+	+
(9)	ΔIspG	+	+	+	+
(10)	ΔIspH	+	+	+	+
(11)	ΔFdx	+	+	+	+
(12)	ΔLipA	-	+	+	+
(13)	ΔMiaB	-	+	+	+
(14)	*Pf* Mev	-	+	+	+

SufS and SufE

In *Pb*, SufS has been shown to be important for the development of sporozoites present within the oocysts in the mosquito vector, suggesting that the protein is essential for *Plasmodium* development during the mosquito stage, and possibly other developmental stages of the parasite as well [6]. Consistent with this, our results show that SufS is needed for the survival of ABS *Pf* (**Figure 2.7E**), and that this essentiality can be attributed, at least in part, to the requirement of the protein for the maintenance of the apicoplast (**Figure 2.6B**). In addition, we have shown herein that SufE, the

interacting partner of SufS, is required for the survival of ABS *Pf* (**Figure 2.8B**) but is not required for maintaining the apicoplast (**Figure 2.6C**). From a mechanistic perspective, SufS functions as a cysteine desulfurase that mobilizes sulfur from L-cysteine and subsequently transfers the liberated persulfide sulfur to SufE (**Figure 2.1**). Although *Pf* SufE by itself possesses no cysteine desulfurase activity, its ability to enhance the cysteine desulfurase activity of both *E. coli* and *Pf* SufS has been demonstrated *in vitro* [5]. In addition, the capability to complement the loss of *E. coli* SufS by *Pf* SufS has been shown [3]. Consistent with both proteins having a role in [Fe-S] cluster biosynthesis, we find that both SufS and SufE are essential for the survival of ABS *Pf*. In particular, the essentiality of SufE indicates that this protein is necessary for transferring sulfur to the SufB-C_2-D scaffold complex and that SufS alone is not able to deliver sulfur to this complex. Taken together, these results suggest that SufS has an additional role in supporting apicoplast maintenance that is not shared by SufE (see below).

MnmA

Having demonstrated that SufS is required for the maintenance of the apicoplast, we sought to generate genetic knock-outs of sulfur-utilizing proteins from our *Pf*Mev line in order to understand why SufS is required for apicoplast maintenance. To that end, we chose to knock out MnmA, a thio-uridylase involved in the post transcriptional modification of $tRNA^{Glu}$, $tRNA^{Gln}$, and $tRNA^{Lys}$ [12], the tRNAs for the amino acids glutamate (Glu), glutamine (Gln), and lysine (Lys), respectively. Each of these three amino acids is encoded by two degenerate codons, each of which has a purine in the third, or wobble, position, thereby enabling the non-canonical base pairing between the first base of the tRNA anti-codon and the third base of the cognate mRNA codon. For these three tRNAs, the 2-thio-uridine (s^2U) modification of the wobble position is conserved in all three domains of life. The cysteine desulfurase IscS and MnmA from *E. coli* have been shown to be essential for s^2U synthesis *in vitro* [12, 13]. Moreover, YrvO, one of four cysteine desulfurases from the Gram-positive bacterium *B. subtilis*,

is functionally analogous to *E. coli* SufS, and the co-expression of *B. subtilis* YrvO and *B. subtilis* MnmA in an *E. coli* IscS deletion strain was able to restore s^2U synthesis [14]. From a mechanistic perspective, *E. coli* IscS serves as a cysteine desulfurase which catalyzes the reductive elimination of sulfur from L-cysteine. This liberated sulfur is then relayed among five proteins and ultimately ends up with MnmA, which utilizes it in the s^2U thiolation reaction [15]. Herein, we have shown that MnmA is required for the survival of ABS *Pf* (**Figure 2.7D**) and that it is also required for maintaining the apicoplast (**Figure 2.6A**). This is the same phenotype that we observed for SufS (**Figures 2.7E and 2.6B**), suggesting that SufS might function in conjunction with MnmA in tRNA thiolation reactions that are essential for maintaining the apicoplast. More specifically, in *E. coli*, the absence of MnmA has been linked to an increase in the frequency of frameshift mutations during the translation process [16]. In addition, mutation of the gene encoding MnmA for both *E. coli* and *Salmonella enterica* was phenotypically linked to a reduction in growth in these bacteria, and such a defect was attributed to an inability of the mutants to synthesize mnm^5s^2U [17], an s^2U derivative. Unfortunately, information on MnmA in *Plasmodium* spp. is nonexistent. However, if *Pf* MnmA fulfills a role analogous to that of its bacteria homologue, it is possible that, in ABS *Pf*, MnmA is required for ensuring the accuracy of translation for the nuclear and/or apicoplast genome. In that regard, ascertaining the organellar localization of MnmA via fluorescence microscopy should help narrow down whether the protein is required for successful translation within the apicoplast, the nucleus, or both.

SufB, SufC, and SufD

During [Fe-S] cluster assembly in the apicoplast of *Pf*, SufB, SufC, and SufD together form a so-called scaffold complex, on which cluster assembly then takes place. In *Pf*, the complex formation between SufB and SufD [6], SufC and SufD [6], as well as SufB and SufC [1, 6] have been demonstrated *in vitro*, and the complex was found to likely exist with a SufB : SufC : SufD stoichiometry of 1 : 2 : 1 [6].

Herein, our data indicate that SufC and SufD are both indispensable for ABS *Pf* survival (**Figure 2.8D, E, and F**), but are not required for apicoplast maintenance (**Figure 2.6D, E, and F**). Taken together, these data suggest that the [Fe-S] cluster scaffold complex is somehow required for the survival of ABS *Pf*, which is expected for two reasons based on the results presented herein. First, given that certain [Fe-S] cluster-dependent proteins (i.e., Fdx, IspG, and IspH) are required for ABS *Pf* survival (**Figure 2.8A, H, and I**), it is likely that the successful assembly of the complex is necessary to ensure that the [Fe-S] cluster-dependent proteins would successfully acquire the clusters, and thus be able to carry out their essential functions. Second, NifU and/or SufA serve to transfer the assembled [Fe-S] cluster to the aforementioned essential [Fe-S] cluster-dependent proteins. Given this, that the absence of cluster transfer led to the death of the parasites (**Figure 2.8C**) indicates that cluster assembly, transfer, and utilization are required for ABS *Pf* survival.

As noted above, the ΔSufC parasites are dependent on Mevalonate for survival (**Figure 2.8D**), consistent with the IPP-dependence of the SufC dominant negative parasites shown in our earlier study [3]. In contrast with that previous study, however, the ΔSufC line presented herein has an intact apicoplast (**Figure 2.6D**). Such a discrepancy could be attributed, at least in part, to certain differences between the methods by which the two lines were generated. Specifically, generation of the SufC(K104A) dominant negative mutant involved the over-expression of an inactive mutant of the protein in which an active site lysine was substituted with an alanine [3]. Since the endogenous genomic locus remained unperturbed, endogenous SufC was presumably still expressed at a normal level. By contrast, generation of the ΔSufC line involved a disruption of the endogenous genomic locus (**Figure 2.4**), thus yielding a complete cessation of SufC protein production from the parasite. Now, although the over-expression of SufC(K104A) with the strong calmodulin [PF14_0323] promoter could have generated additional stress that led to the loss of the apicoplast in the dominant negative study [3], a control parasite line generated with WT SufC driven by the same promoter did not lead to apicoplast

loss [3]. An alternative explanation is that the 200 μM IPP used as a chemical bypass in the dominant negative study, combined with the protein over-expression, created additional stress that was not mimicked by the Mevalonate bypass system used for the knock-out lines presented herein.

In *E. coli*, the ATPase activity of SufC and the presence of SufD have both been demonstrated to be important for the acquisition of iron during [Fe-S] cluster assembly [18], and the same could hold true for the *Pf* orthologs of these proteins. Herein, we have shown that SufC is required for the survival of ABS *Pf* (**Figures 2.8D and 2.6D**), an observation that could be explained if the ATPase activity of *Pf* SufC, like that of its *E. coli* ortholog, is required for successful cluster assembly. In addition, the enhancement of the basal ATPase activity of SufC by SufD has been demonstrated in *Pf in vitro* [6]. Given that both SufC and SufD are individually required for ABS *Pf* survival (**Figure 2.8D, E, and F**), it is possible that this enhancement of the ATPase activity of SufC by SufD is required in order for SufC to attain sufficient activity to ensure successful scaffold assembly.

NifU and SufA

With respect to the propagation of blood stage infection, both NifU [4] and SufA [2] have been proven to be individually dispensable. Consistent with these results, we found that the deletion of either individual cluster transfer proteins confers no growth defect (**data not shown**), whereas the deletion of both proteins together results in the death of the parasite (**Figure 2.8C**). Analysis using UV/visible spectroscopy has shown that both NifU and SufA bind to [4Fe-4S] clusters, and the ability of both proteins to transfer the cluster has been demonstrated *in vitro* [6]. Presumably, the [2Fe-2S] cluster found on *Pf* ferredoxin (Fdx) [PMID: 17251200] is also transferred by these proteins. Herein, our gene deletion data show that NifU and SufA carry out redundant functions in cluster transfer, indicating that either protein is capable of transferring [4Fe-4S] or [2Fe-2S] clusters. The synthetic lethal

phenotype of the NifU/SufA double deletion suggests that no other protein can fulfill the role of transferring [Fe-S] clusters in the apicoplast of malaria parasites.

Fdx

The apicoplast of *Pf* harbors a redox system comprised of Fdx and its redox partner ferredoxin NADP$^+$ reductase (FNR). In photosynthetic plastids (i.e., chloroplasts of plants), FNR catalyzes the following light-dependent reaction: $2Fdx_{reduced}$ (i.e., Fe^{2+}) + $NADP^+$ + H^+ → $2Fdx_{oxidized}$ (i.e., Fe^{3+}) + NADPH. Specifically, electrons from photosystem I are first transferred to $Fdx_{oxidized}$ to generate $Fdx_{reduced}$. Thereafter, FNR catalyzes the transfer of these electrons from $Fdx_{reduced}$ to $NADP^+$, thereby generating $Fdx_{oxidized}$ and NADPH, which is either fed into the Calvin cycle to generate ATP or employed as a cofactor in anabolic reactions. In non-photosynthetic plastids such as the apicoplast and those of plant roots, however, the reaction is thought to proceed in the reverse direction to generate $Fdx_{reduced}$, which can then act as a reductant for various metabolic reactions. Notably, a search of various *Plasmodium* genome databases identified the *Pf* homologue of plant Fdx proteins, along with an N-terminal bipartite pre-sequence characteristic of apicoplast-localized proteins [19] (for a more detailed discussion of apicoplast-targeting of nuclear-encoded proteins, see the **INTRODUCTION** section of **CHAPTER 4**). Furthermore, amino acid sequence alignment of the putative *Pf* Fdx with that of a subset of plant Fdx proteins revealed the presence, on the *Pf* Fdx, of the four well-conserved cysteine residues required for [2Fe-2S] cluster formation [19]. NMR chemical shift analysis identified three regions surrounding the [2Fe-2S] binding site within *Pf* Fdx that are responsible for the interaction of the protein with FNR, and specific acidic amino acid residues within these regions were confirmed, via site-directed mutagenesis, to be important for the physical as well as electron transfer interactions between Fdx and FNR [20]. Herein, we have shown that both Fdx (**Figure 2.8A**) and FNR (**data not shown**) are required for the survival of ABS *Pf*, but neither is required for the

maintenance of the apicoplast (**Figure 2.6K; data not shown**). Taken together, these results indicate that the apicoplast redox system is required for the survival of ABS *Pf*, and that both Fdx and FNR are requisite components for a functional redox system.

DXPR

As the second step of isoprenoid precursor biosynthesis in the *Plasmodium* apicoplast, DXPR catalyzes the conversion of DOXP to MEP (**Figure 2.2B**). In the apicomplexan parasite *Tg*, the transit peptide of *Pf*DXPR is capable of trafficking GFP to the apicoplast, thus indicating the apicoplast localization, in *Pf*, for DXPR as well as other components of the isoprenoid precursor biosynthesis pathway [10]. Importantly, the antibacterial fosmidomycin has been shown to inhibit the growth of ABS *Pf in vitro* by targeting DXPR [10], in accordance with the essentiality of isoprenoid biosynthesis for the survival of *Pf* [11]. Consistent with this, our data show that DXPR is required for the survival of ABS *Pf*, as evidenced by the Mevalonate-dependence of the ΔDXPR line (**Figure 2.8G**). Given the essentiality of the isoprenoid precursor IPP for the survival of *Plasmodium* [11], it is expected that any protein required for IPP biosynthesis (e.g., DXPR, IspG, and IspH) would be likewise indispensable, in line with our observations (**Figure 2.8G, H, and I**). However, although the DXPR is required for the generation of IPP, it is not required for the maintenance of the apicoplast (**Figure 2.6H**).

IspG and IspH

IspG and IspH catalyze the penultimate and ultimate reactions, respectively, of IPP biosynthesis (**Figure 2.2B**). UV/visible spectroscopy has demonstrated *in vitro* the presence of [4Fe-4S] clusters as prosthetic groups on *E. coli* GcpE [21] and LytB [22], the orthologs of *Pf* IspG and IspH, respectively. In *Plasmodium*, IspH catalyzes the simultaneous generation of IPP and DMAPP from HMBPP (**Figure 2.2B**), a reaction that has been suggested to involve the transfer of two single electrons from the [4Fe-

4S] cluster of IspH. In line with this, the Fdx/FNR pair of *Pf* has been shown to be capable of transferring electrons from NADPH to IspH *in vitro* [23], resulting in the generation of the expected isoprenoid precursors IPP and DMAPP [23]. Now, although analogous experiments were not performed with IspG, this indicates that the apicoplast Fdx/FNR redox system could function as an electron donor to IspH, and possibly other enzymes of the isoprenoid precursor pathway or even other metabolic pathways within the apicoplast. Therefore, although Fdx is not required for the maintenance of the apicoplast (**Figure 2.6K**), its requirement for the survival of ABS *Pf* (**Figure 2.8A**) is consistent with the notion that the Fdx/FNR redox system serves as a requisite electron donor to power the reaction catalyzed by IspH and possibly IspG as well as other important metabolic reactions within the organelle.

LipA

LipA is a [4Fe-4S] cluster-containing protein [3] that has been localized to the apicoplast [24]. LipA catalyzes the second step of lipoic acid synthesis by introducing two sulfur atoms, presumably derived from one of its two [4Fe-4S] clusters, into an octanoyl group that is bound to pyruvate dehydrogenase (PDH), an enzyme complex comprised of four subunits – E1α, E1β, E2, and E3. In *Plasmodium yoelii*, although deletion of the genes encoding either the E1α or E3 subunit ablated the capability of the ALS parasites to transition into the ABS, ABS development itself was not affected [25]. Furthermore, the E2 subunit of the PDH complex is responsible for generating acetyl CoA, a precursor for the FAS-II pathway. That being said, no growth defect in the ABS was evident upon the deletion of two of the enzymes in the FAS-II pathway, FabI [26, 27] and FabB/F [26]. As such, the dispensability of both the PDH complex as well as the FAS-II pathway for ABS *Plasmodium* development suggests that LipA should be likewise nonessential for ABS *Pf*, which is in accordance with our observations (**Figures 2.7B and 2.6L**).

MiaB

While data on MiaB in *Plasmodium* spp. is wanting, certain information on the *Pf* protein can be gleaned from studies on its *E. coli* ortholog. In *E. coli*, MiaA is thought to transfer the isopentenyl group derived from DMAPP to modify select tRNAs. More specifically, the isopentenyl group is attached to the N^6 (Nitrogen at position 6) of an adenosine base located at a particular position within the anti-codon region of the tRNA. The resulting isopentenylated tRNAs are then further modified by MiaB, a methyl-thiolase. UV/visible spectroscopy has demonstrated that, under reducing as well as anaerobic conditions, *E. coli* MiaB contains [4Fe-4S] clusters, which were observed to degrade to either [3Fe-4S] or [2Fe-2S] clusters upon exposure to air [28]. In addition, the [Fe-S] cluster of *E. coli* MiaB was shown to be required for the ability of the protein to modify tRNAs, as evidenced by site-directed mutagenesis experiments whereby specific conserved cysteine residues required for iron chelation were substituted with alanine [28]. Now, if MiaB is required for the maintenance of the apicoplast, the disruption of any of the components lying upstream of the protein should result in the loss of the organelle. That being said, since treatment of ABS *Pf* with fosmidomycin, an antimalarial that disrupts isoprenoid biosynthesis [10], does not lead to the loss of the apicoplast [3], it is expected that MiaB is not required for the maintenance of the apicoplast, just as we observed (**Figure 2.6M**). In addition, we have shown herein that MiaB is not required for the survival of ABS *Pf* (**Figure 2.7C**), suggesting that either (1) the tRNA modification function performed by this enzyme is non-essential to the parasite, or (2) the modification is important but can be produced by another protein.

REFERENCES

[1] B. Kumar *et al.*, "Interaction between sulphur mobilisation proteins SufB and SufC: evidence for an iron-sulphur cluster biogenesis pathway in the apicoplast of Plasmodium falciparum," *Int. J. Parasitol.*, vol. 41, no. 9, pp. 991–9, Aug. 2011.

[2] J. M. Haussig, K. Matuschewski, and T. W. A. Kooij, "Identification of vital and dispensable sulfur utilization factors in the Plasmodium apicoplast," *PLoS One*, vol. 9, no. 2, p. e89718, Feb. 2014.

[3] J. E. Gisselberg, T. A. Dellibovi-Ragheb, K. A. Matthews, G. Bosch, and S. T. Prigge, "The Suf Iron-Sulfur Cluster Synthesis Pathway Is Required for Apicoplast Maintenance in Malaria Parasites," *PLoS Pathog.*, vol. 9, no. 9, p. e1003655, Sep. 2013.

[4] J. M. Haussig, K. Matuschewski, and T. W. A. Kooij, "Experimental Genetics of Plasmodium berghei NFU in the Apicoplast Iron-Sulfur Cluster Biogenesis Pathway," *PLoS One*, vol. 8, no. 6, p. e67269, Jun. 2013.

[5] M. Charan, N. Singh, B. Kumar, K. Srivastava, M. I. Siddiqi, and S. Habib, "Sulfur mobilization for Fe-S cluster assembly by the essential SUF pathway in the Plasmodium falciparum apicoplast and its inhibition," *Antimicrob. Agents Chemother.*, vol. 58, no. 6, pp. 3389–98, Jun. 2014.

[6] M. Charan *et al.*, "[Fe-S] cluster assembly in the apicoplast and its indispensability in mosquito stages of the malaria parasite," *FEBS J.*, vol. 284, no. 16, pp. 2629–2648, Aug. 2017.

[7] D. Chakrabarti *et al.*, "Protein prenyl transferase activities of Plasmodium falciparum," *Mol. Biochem. Parasitol.*, vol. 94, no. 94, pp. 175–184, 1998.

[8] A. S. Couto, E. A. Kimura, V. J. Peres, M. L. Uhrig, and A. M. Katzin, "Active isoprenoid pathway in the intra-erythrocytic stages of Plasmodium falciparum : presence of dolichols of 11 and 12 isoprene units," *Biochem. J.*, vol. 341, pp. 629–637, 1999.

[9] H. Jomaa *et al.*, "Inhibitors of the nonmevalonate pathway of isoprenoid biosynthesis as antimalarial drugs," *Science*, vol. 285, no. 5433, pp. 1573–6, Sep. 1999.

[10] E. Yeh and J. L. DeRisi, "Chemical Rescue of Malaria Parasites Lacking an Apicoplast Defines Organelle Function in Blood-Stage Plasmodium falciparum," *PLoS Biol.*, vol. 9, no. 8, p. e1001138, Aug. 2011.

[11] R. Kambampati and C. T. Lauhon, "Mnma and IscS are required for in vitro 2-thiouridine biosynthesis in Escherichia coli," *Biochemistry*, vol. 42, no. 4, pp. 1109–1117, 2003.

[12] Y. Ikeuchi, N. Shigi, J.-I. Kato, A. Nishimura, and T. Suzuki, "Mechanistic Insights into Sulfur Relay by Multiple Sulfur Mediators Involved in Thiouridine Biosynthesis at tRNA Wobble Positions," *Mol. Cell*, vol. 21, pp. 97–108, 2006.

[13] K. A. Black and P. C. Dos Santos, "Abbreviated Pathway for Biosynthesis of 2-Thiouridine in Bacillus subtilis," *J. Bacteriol.*, vol. 197, no. 11, pp. 1952–62, Jun. 2015.

[14] T. Numata, Y. Ikeuchi, S. Fukai, T. Suzuki, and O. Nureki, "Snapshots of tRNA sulphuration via an adenylated intermediate," *Nature*, vol. 442, no. 7101, pp. 419–424, Jul. 2006.

[15] J. Urbonavicius, Q. Qian, J. M. Durand, T. G. Hagervall, and G. R. Björk, "Improvement of reading frame maintenance is a common function for several tRNA modifications," *EMBO J.*, vol. 20, no. 17, pp. 4863–73, Sep. 2001.

[16] K. Nilsson, H. K. Lundgren, T. G. Hagervall, and G. R. Björk, "The cysteine desulfurase IscS is required for synthesis of all five thiolated nucleosides present in tRNA from Salmonella enterica serovar typhimurium," *J. Bacteriol.*, vol. 184, no. 24, pp. 6830–5, Dec. 2002.

[17] A. Saini, D. T. Mapolelo, H. K. Chahal, M. K. Johnson, and F. W. Outten, "SufD and SufC ATPase Activity Are Required for Iron Acquisition during in Vivo Fe-S Cluster Formation on SufB," *Biochemistry*, vol. 49, pp. 9402–9412, 2010.

[18] M. Vollmer, N. Thomsen, S. Wiek, and F. Seeber, "Apicomplexan parasites possess distinct nuclear-encoded, but apicoplast-localized, plant-type ferredoxin-NADP+ reductase and ferredoxin," *J. Biol. Chem.*, vol. 276, no. 8, pp. 5483–90, Feb. 2001.

[19] Y. Kimata-Ariga, T. Saitoh, T. Ikegami, T. Horii, and T. Hase, "Molecular interaction of ferredoxin and ferredoxin-NADP+ reductase from human malaria parasite," *J. Biochem.*, vol. 142, no. 6, pp. 715–720, Sep. 2007.

[20] M. Seemann *et al.*, "Isoprenoid Biosynthesis through the Methylerythritol Phosphate Pathway: The (E)-4-Hydroxy-3-methylbut-2-enyl Diphosphate Synthase (GcpE) is a [4Fe–4S] Protein," *Angew. Chemie Int. Ed.*, vol. 41, no. 22, pp. 4337–4339, Nov. 2002.

[21] M. Wolff *et al.*, "Isoprenoid biosynthesis via the methylerythritol phosphate pathway: The (E)-4-hydroxy-3-methylbut-2-enyl diphosphate reductase (LytB/IspH) from Escherichia coli is a [4Fe-4S] protein," *FEBS Lett.*, vol. 541, no. 1–3, pp. 115–120, 2003.

[22] R. C. Röhrich *et al.*, "Reconstitution of an apicoplast-localised electron transfer pathway involved in the isoprenoid biosynthesis of Plasmodium falciparum," *FEBS Lett.*, vol. 579, no. 28, pp. 6433–6438, 2005.

[23] C. Wrenger and S. Müller, "The human malaria parasite Plasmodium falciparum has distinct organelle-specific lipoylation pathways," *Mol. Microbiol.*, vol. 53, no. 1, pp. 103–113, May 2004.

[24] Y. Pei *et al.*, "*Plasmodium* pyruvate dehydrogenase activity is only essential for the parasite's progression from liver infection to blood infection," *Mol. Microbiol.*, vol. 75, no. 4, pp. 957–971, Feb. 2010.

[25] A. M. Vaughan *et al.*, "Type II fatty acid synthesis is essential only for malaria parasite late liver stage development," *Cell. Microbiol.*, vol. 11, no. 3, pp. 506–520, Mar. 2009.

[26] M. Yu *et al.*, "The Fatty Acid Biosynthesis Enzyme FabI Plays a Key Role in the Development of Liver-Stage Malarial Parasites," *Cell Host Microbe*, vol. 4, no. 6, pp. 567–578, 2008.

[27] F. Pierrel, G. R. Björk, M. Fontecave, and M. Atta, "Enzymatic modification of tRNAs: MiaB is an iron-sulfur protein," *J. Biol. Chem.*, vol. 277, no. 16, pp. 13367–70, Apr. 2002.

CHAPTER 3: Triclosan analogs as antimalarial drugs

ABSTRACT

Given the rapid rise of drug resistance in *Pf* parasites, there is a constant need for the discovery and development of novel effective antimalarials. Importantly, in order for a compound to be effective, it must not only exhibit potent antiparasitic activity but also possess parasitic molecular targets that are distinct from those of the previously employed drugs. That being said, one promising compound is triclosan. While an early study by Surolia and Surolia (2001) suggested that triclosan exerts its antimalarial effect by targeting *Pf* FabI, the FAS-II pathway has been later proven to be dispensable for the parasite during the ABS. Furthermore, a recent study has identified one of the *Plasmodium* targets of triclosan to be DHFR, which is one of the targets of the antimalarials sulfadoxine-pyrimethamine (SP) and atovaquone-proguanil (AP), both of which were quickly met with resistance since their introduction. However, because studies have demonstrated the improved potency, over triclosan, of select analogs against the Dd2 *Pf* strain, which is resistant to both SP and AP, triclosan likely possesses other molecular targets that are distinct from those of SP and AP. With the hope of discovering the real molecular targets of triclosan-based antimalarials, we have screened seven triclosan analogs for their antiparasitic activity in ABS *Pf*. Through this screen, we have identified a compound, designated herein as djm-11-03A, to have outstanding antimalarial activity, with an IC_{50} of 33 – 44 nM. Our next step is to induce drug resistance using this compound, which would help identify the molecular targets of this compound in *Pf*, and thus, shed light on how to further optimize its potency.

INTRODUCTION

Triclosan (**Figure 3.1A**), a compound found in common household items such as toothpaste, soap, and plastics, exhibits activity against a broad spectrum of bacteria. An early study by Surolia and Surolia (2001) on the antimalarial activity of triclosan reported that the compound was able to inhibit *Plasmodium* growth both *in vivo* and *in vitro*, and that such activity can be attributed, at least in part, to the inhibition of enoyl-acyl carrier protein reductase (FabI) of the *Plasmodium* FAS-II pathway [1]. Given that the FAS-II pathway is entirely absent from human cells and given that the FAS-II pathway in *Plasmodium* spp. is localized to the apicoplast (an organelle that is essential to the parasite but absent from human cells), these initial results implicated triclosan as a promising antimalarial therapeutic, and helped spearhead a cascade of studies focused primarily on the biochemical characterization of the binding between the drug (or its variants) and its putative target [2–8] and potency optimization through the design of triclosan analogs [3, 9–14]. However, a study published in 2008 showed that a FabI mutant *Pf* line did not differ from its WT counterpart with respect to sensitivity to triclosan, thus indicating that the inhibition of ABS *Pf* growth by the drug is not achieved through the inhibition of FabI [15]. Moreover, the same study showed that FabI knock-out parasites (both *Pb* and *Pf*) were not affected in their ability to elongate FA compared to WT, thus indicating that all FA elongation is catalyzed by an elongation pathway (ELO) rather than by the FAS-II *de novo* FA synthesis pathway [15]. As evidenced by the attenuated infectivity of sporozoites derived from *Pb* parasites lacking FabI, the protein was found to be important for the development of ALS merozoites instead [15], consistent with microarray data showing that a significant number of genes and proteins of the FAS-II pathway are specifically expressed during the ALS [16]. Further complicating matters, authors of a *Nature Correspondence* from 2011 examined the 2001 study by Surolia and Surolia and reported that, while they were able to confirm the *in vitro* activity of triclosan against ABS *Pf*, the drug did not seem to have an

effect *in vivo* [17]. Given such inconsistent findings among the various studies, it remains unclear as to what the actual drug targets of triclosan are in ABS malaria parasites.

Recently, a study identified dihydrofolate reductase (DHFR) of both *Pf* and *Pv* to be a target of the antimalarial action of triclosan [18]. To arrive at this conclusion, the authors generated strains of *Saccharomyces cerevisiae* (*Sc*) in which the gene encoding the essential *Sc*DHFR is replaced by that encoding either *Pf*DHFR or *Pv*DHFR, its ortholog in *Pf* and *Pv*, respectively [18–20]. Given that the deletion in *Sc* can be complemented by the presence of the *Plasmodium* ortholog, these mutant yeast strains enable one to screen for any drug that targets *Pf*DHFR [18–20]. Using this strategy, Bilsland *et al.* (2018) identified DHFR as a target of the antimalarial action of triclosan in *Pf* as well as *Pv*, and subsequently confirmed this *in vitro* [18]. While this study has helped shed light on the antimalarial action of triclosan, it also raises two important points of consideration regarding triclosan. First, DHFR is a target of the antifolates pyrimethamine and proguanil. The former is used in combination with sulfadoxine in the drug sulfadoxine-pyrimethamine (SP, trade name Fansidar), which was introduced around 1970 and was quickly met with resistant strains (reviewed in [21]); similarly, the latter is used in combination with atovaquone in the drug atovaquone-proguanil (AP, trade name Malarone), which was introduced around 2000 and was likewise quickly met with resistant strains (reviewed in [21]). As such, if DHFR is the sole target through which triclosan exerts its antimalarial effect, then the pursuit of triclosan analogs as an antimalarial should perhaps be forsaken. That being said, however, previous studies have tested various triclosan analogs containing B-ring-only modifications against the Dd2 strain and observed notably improved potency compared to that of the parental compound [9, 15]. Now, since this particular *Pf* strain contains mutations within the *dhfr* gene that are known to confer resistance to pyrimethamine and proguanil (N51I, C59R, and S108N) [22] and is resistant to SP, such inhibitory effect of the analog against the Dd2 strain suggests that the drug targets of triclosan and that of SP or AP are not totally overlapping. As for the second point of

consideration, the yeast screen employed by Bilsland *et al.* (2018) relies on the deliberate introduction of a candidate drug target gene from *Plasmodium*, or whatever other species of one's choosing, into yeast. For this reason, the screen is more useful for one to confirm, but not discover, drug targets for which there is existing literature already supporting the role of the gene as a drug target. Because of this limitation as well, it is possible that there are additional primary targets of triclosan, other than DHFR, that remain to be identified.

With all of this taken into consideration, we have taken a twofold approach with the goal of developing a novel potent triclosan-based antimalarial. First, we have screened a group of triclosan analogs against the growth of ABS *Pf in vitro* in order to identify the most potent compound among the group. Second, we seek to identify the specific drug targets of this analog within the parasite through the induction of drug resistance followed by genomic DNA sequencing. Importantly, this twofold approach enables the comprehensive identification of all drug targets of this analog, a piece of information that would be invaluable towards the potency optimization of this analog.

Now, the analogs examined herein contain various modifications of specific substituents around the diaryl ether scaffold of triclosan, based on the design of two notable triclosan analogs examined in previous studies – C25 from [9] (**Figure 3.1B**) and 39b from [23] (**Figure 3.1D**). In particular, Stec *et al.* (2013) screened for antiparasitic activity against ABS *Pf* using a wide variety of triclosan analogs, among which the most potent was the one designated 39b, which yielded an IC_{50} of 30 nM and 80 nM towards the D6 (CDC/Sierra Leone) and TM91C235 (WRAIR, Thailand) *Pf* strains, respectively [23]. Such remarkable activity makes this compound one of the most potent triclosan analogs reported to date, and thus, an excellent candidate for further potency optimization. Now, since the augmented activity of 39b is solely attributed to modifications of the A-ring, we sought to further optimize its potency through modifications of its B-ring. In that regard, among the various B-ring 2' substituted triclosan analogs examined by Freundlich *et al.* (2006), the compound designated C25

exhibited notable antiparasitic activity against ABS *Pf*, with an EC_{50} of 180 nM and 220 nM towards the 3D7 and Dd2 strains, respectively [9]. As such, our primary triclosan analog of interest, the compound designated djm-11-05 (**Figure 3.1C**), is comprised of the A-ring of 39b and the B-ring of C25. Using this compound as the basis, we have chemically synthesized six additional compounds, each of which contains a modified 2' substituent on the A- and/or B-ring of djm-11-05. Using this set of seven triclosan analogs, we first screened for antiparasitic activity against ABS *Pf* in order to identify the compound exhibiting the most potent activity, which was then used for resistance induction towards the goal of drug target identification.

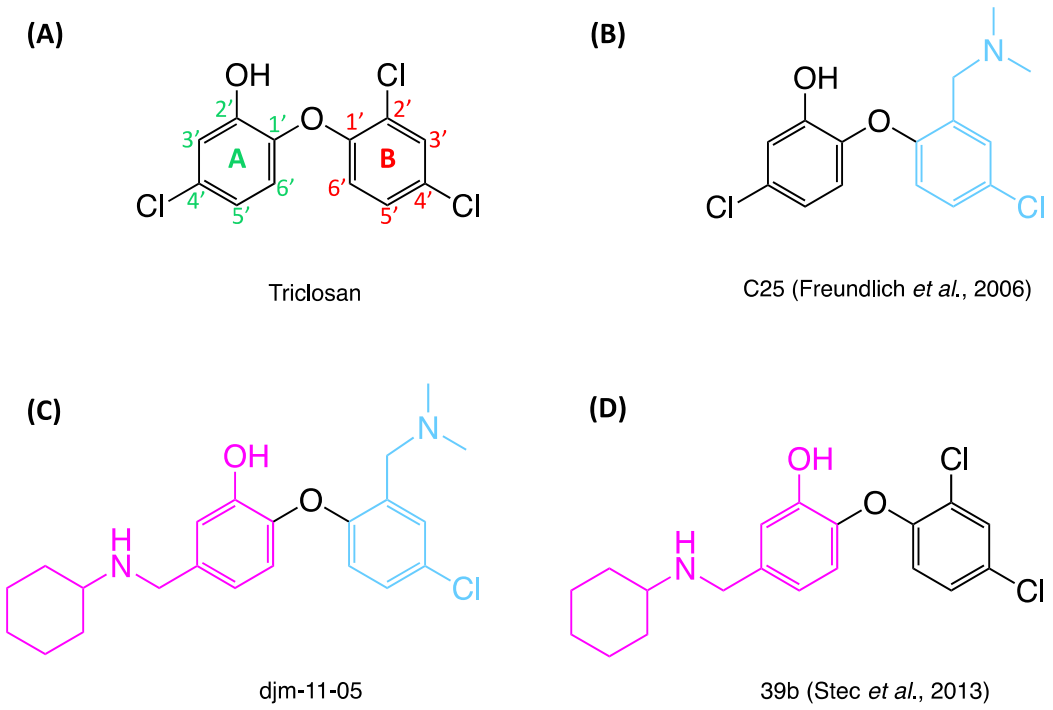

Figure 3.1. The chemical structure of triclosan and three of its analogs. Shown are the chemical structure of **(A)** triclosan, **(B)** C25, a notable compound from [9], **(C)** djm-11-05, the primary compound of interest in our study, and **(D)** 39b, a notable compound from [23]. As indicated by the color-coding, djm-11-05 is a triclosan analog comprised of the A-ring of 39b (pink) and the B-ring of C25 (blue). Using triclosan as an example, the A-ring and B-ring are indicated, and the numbering of the carbons on each ring is shown.

MATERIALS AND METHODS

Preparation of chemicals

Each chemically synthesized triclosan analog included 0, 1, or 2X trifluoroacetic acid (TFA) as counterions. For each compound, the chemical structure (not including TFA) was drawn in ChemDraw, and the pure molecular weight was determined via ChemDraw. The actual molecular weight was determined by adding the molecular weight for the appropriate amount of TFA to the pure molecular weight. Based on the actual molecular weight, each compound was dissolved in the appropriate amount of DMSO to yield a 50 mM working stock, which was used for the parasite growth inhibition assays.

Generation of growth curves used for IC_{50} determination

Growth curves used for IC_{50} determination were generated using a plate-based assay. Given that the sensitivity of the parasite to a particular drug may vary depending on the stage of its life cycle [1, 24, 25], all drug experiments were performed using synchronized parasites, following the same time scheme (**Table 3.1**) – 6 hours post synchronization, the IC plate was prepared; 48 hours post IC plate preparation, the parasitemia was measured using flow cytometry. The following subsections detail each step of this overall plan.

Table 3.1. The overall plan (per IC plate) for the drug assays. This overall plan was used to determine the IC_{50} value for each of the drug tested.

day	0	1	2
IC plate	MACS LS column (10:00 AM) seed @ (4:00 PM): • 0.5% pt • 1% hc • 0.1% DMSO • 250 µL / well • triplicate wells / sample		
parasite life cycle #	1	1	1
eluate parasite stage	• schizonts • early rings	• rings	late stage: • trophs • schizonts
flow			run (4:00 PM—10:00 PM)

Parasite culture maintenance

For all drug experiments, the $NF54^{attB}$ strain of *Pf* (the NF54 strain in which the attB recombination site is inserted into the cg6 genomic locus of the parasite) [26] was used. The culture was maintained in CMA medium using the same method as that detailed under the **MATERIALS AND METHODS** section from **CHAPTER 2**, with the exception that the hematocrit of the culture was kept at 5% (instead of 1%). This increases the parasite yield from the isolation of schizont-stage parasites via magnetic purification.

Magnetic purification

The isolation of schizont-stage parasites from the mixed-stage culture was done using the standard method of magnetic purification [27]. Briefly, a 75 cm^2 cell culture flask containing 2 mL of CMA medium and 200 µL of 50% hematocrit human blood was prepared and warmed to 37°C. A MACS LS column (Miltenyi BioTec, cat. #130-042-401) was inserted into a homemade magnet with a field strength of about 8,000 G. The column was washed with 400 µL of CMA medium, loaded with the 10 mL culture, and then washed with 3 mL of CMA medium. Finally, the column was removed from

the magnet, and schizont-stage parasites were eluted with 8 mL of CMA medium from the column into the pre-prepared flask, thus yielding a 10 mL schizont-stage culture at 1% hematocrit.

Flow cytometry

The measurement of parasitemia on day 2 of each experiment employed the same flow cytometry-based method as that detailed under the **MATERIALS AND METHODS** section from **CHAPTER 2**, with two exceptions: (1) each well was seeded at 1% hematocrit (instead of 2% hematocrit), and thus, 2 μL (instead of 1 μL) of sample per well was used for SYBR Green staining, and (2) each plate was stained with SYBR Green for 10 minutes (instead of 30 minutes).

Preparation of the IC plate

As illustrated in the layout of the IC plate below (**Figure 3.2**), each IC plate contains four different types of wells – drug, vehicle control, death control, and uninfected control. To prepare each IC plate, a total of three 96-well plates were used – the IC plate itself, the drug plate, and the DMSO plate (**Figure 3.3**). The following subsections detail the preparation of each of the three plates.

Preparation of the drug plate

As shown in **Figure 3.3**, the drug, typically with a stock concentration of 50 mM, is deposited into the A12 well of the drug plate. Then, across row A, the amount of drug is diluted from well to well by 100% DMSO, from A12 all the way down to A1. For each experiment, the specific dilution factor used for each well-to-well dilution was flexible and depended on two factors: (1) in general, we aimed to have a decent spread of drug concentrations – four wells for the "kill zone" (wells having drug concentrations that are sufficiently high to kill off all parasites), four wells for the "no-kill zone" (wells having drug concentrations that are sufficiently low such that no parasites would be killed), and four

wells for the "transition zone" (wells having drug concentrations that lie somewhere between that of the no-kill zone and the kill zone, and would thus contain the IC_{50} value for the drug). The final resulting range of drug concentration typically spans about 4 – 5 logs; (2) for each of the compound tested within our study, the IC_{50} curve has been generated at least twice. In the case when the IC_{50} value was available (either from our first trial of measurement or from prior studies), we have adjusted the well-to-well dilution factor such that the expected resulting IC_{50} value would end up somewhere in the middle of the transition zone.

In order to prevent a buildup of error that would result from a consecutive eleven-step serial dilution across row A, we first prepared, for each of the three zones, the well with the highest drug concentration (A12, A8, and A4 for the kill zone, transition zone, and no-kill zone, respectively), and then prepared, for each zone, the remaining three wells via serial dilution from the respective well with the highest drug concentration. More specifically, we first prepared the A12 well, and used the content within A12 to create the A8 well, from which the A4 well was then prepared. Finally, row B simply consists of a 1:40 dilution of row A. To prepare row B, therefore, 5 μL of row A was mixed with 195 μL of CMA medium.

Preparation of the DMSO plate

As shown in **Figure 3.3**, the DMSO plate was prepared in the exact same manner as the drug plate, with the exception that inhibitors were not included in any of the wells.

Preparation of the IC plate

The parasitemia for the culture was determined using Giemsa staining. Based on this parasitemia, we calculated the amount of culture content, 50% hematocrit blood, and CMA medium required for seeding samples at 0.5% parasitemia, 2% hematocrit, triplicate wells per sample, and 250 μL total

volume per well in a 96-well flat-bottom cell culture plate (Corning, cat. #3595). Each parasite-containing well was seeded as calculated, with the exception that 10 μL of CMA medium was first omitted, thus giving an initial total volume of 240 μL per well; each uninfected control well (IC plate D10 – D12) was prepared in the same manner as a parasite-containing well, with the exception that there were no parasites added. After preparation of the 240 μL for each well, 10 μL of specific content, depending on the well, was added to each well as follows: (1) for rows A, B, and C of the IC plate, 10 μL of drug plate row B was added. As illustrated in **Figure 3.3**, this addition constitutes a 1:25 dilution of both the drug and DMSO in drug plate row B, thus yielding a specific final drug concentration as well as 0.1% DMSO in CMA medium for each well; (2) for D1 – D6 (vehicle control) and D10 – D12 (uninfected control) of the IC plate, 10 μL of DMSO plate row B was added. As illustrated in **Figure 3.3**, this addition constitutes a 1:25 dilution of the DMSO in DMSO plate row B, thus yielding 0.1% DMSO in CMA medium for each of the nine wells; (3) the IC plate death control wells (D7 – D9) were prepared in the same fashion as the other drug wells, yielding 10 μM chloroquine in 0.1% DMSO in CMA medium for each of the three wells.

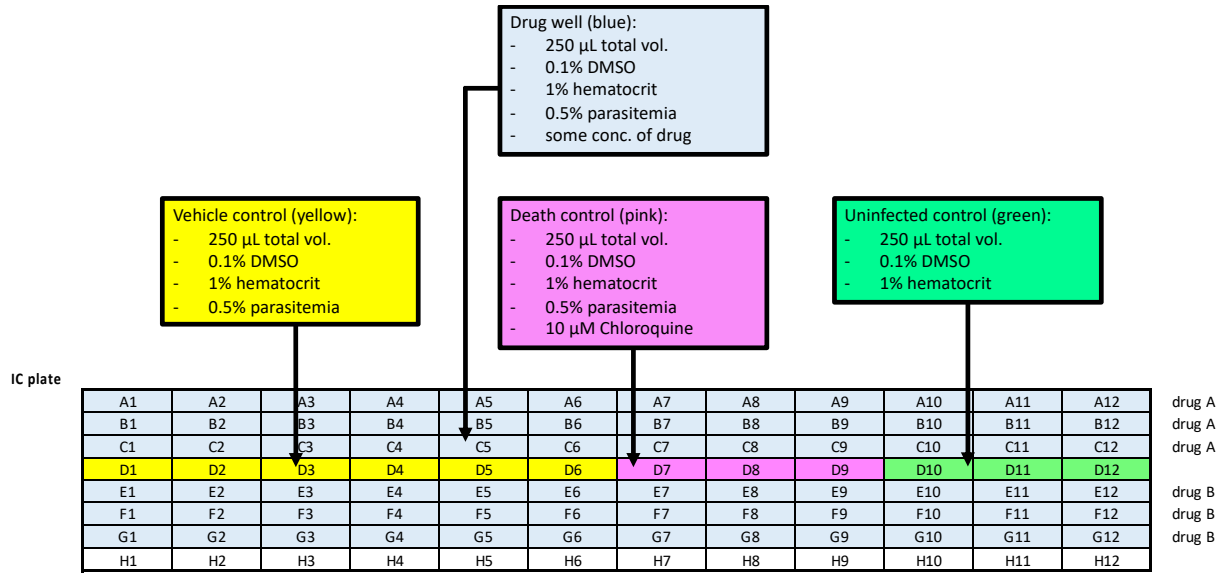

Figure 3.2. Layout of the IC plate. Each IC plate contains four different types of wells – drug (blue), including one set for drug A and another set for drug B, vehicle control (yellow), death control (pink), and uninfected control (green). For drug A, triplicate wells were seeded, with replicate 1, 2, and 3 occupying row A, B, and C, respectively; for drug B, triplicate wells were seeded, with replicate 1, 2, and 3 occupying row E, F, and G, respectively. Each well was seeded at 0.5% parasitemia (with the exception of the uninfected control wells, which contain no parasites), 1% hematocrit, 0.1% DMSO, and 250 µL total volume. Each drug well contains a specific concentration of a drug in 0.1% DMSO in CMA medium; each vehicle control well contains 0.1% DMSO in CMA; each death control well contains 10 µM chloroquine in 0.1% DMSO in CMA; each uninfected control well contains RBCs in 0.1% DMSO in CMA.

Figure 3.3. Preparation of the IC plate. Shown (from top to bottom) are the drug plate (rows A and B), IC plate (rows A to D), and DMSO plate (rows A and B). As indicated in this example IC plate preparation, drug plate A12 contains 50 mM drug, and the drug plate row A well-to-well dilution factor is indicated. The dilution scheme used to prepare drug plate column 12 is shown; the concentration of drug and DMSO for each well is indicated.

Determination of IC_{50} values

IC_{50} values were determined using the GraphPad Prism software (version 5.01). Briefly, for each well, the log [drug concentration (M)] (y-value) and the corresponding %parasitemia (x-value) were entered into the software. The data were analyzed with non-linear regression (curve fit) analysis, using the log [inhibitor] *vs.* response equation and the least squares (ordinary) fitting method.

RESULTS AND DISCUSSION

Validation of the drug assay

Our drug assay was validated by testing various drugs for which the IC_{50} value is already known based on previous studies – atovaquone, triclosan, and djm-11-03A, the same compound as 39b from [23]. The IC_{50} for atovaquone against *Pf* has been determined to be ~1 nM [28], and we have been able to reproduce this result consistently under our experimental conditions (**Figure 3.4A**). The IC_{50} for triclosan against *Pf* has been determined to be in the micro-molar range [1, 9], consistent with our measurements (**Figure 3.4B** and **Table 3.2**). As mentioned in the **INTRODUCTION** section of this chapter, the IC_{50} for 39b from the study by Stec *et al.* (2013) was determined to be 30 nM and 80 nM towards the D6 and TM91C235 *Pf* strains, respectively [23]. Although our assays were done using the $NF54^{attB}$ strain of *Pf*, the IC_{50} value for djm-11-03A was consistently determined to be in the same range (**Figure 3.4G** and **Table 3.2**).

Structure—activity relationship based on six triclosan analogs

The schematic illustrating the relationship between chemical structure and antiparasitic activity for six triclosan analogs is given below (**Figure 3.5**). Three notable observations can be made based on this schematic: (1) among these six triclosan analogs, djm-11-03A exhibited the strongest antiparasitic activity against ABS *Pf*, with an IC_{50} of 33 – 44 nM; (2) by comparing djm-10-25 to djm-10-44, a 2' amine, rather than a 2' chlorine, on the B-ring seems to work better with the 2' methoxy group on the A-ring; (3) by comparing djm-11-03A to either djm-10-25 or djm-11-05, the 2' hydroxyl and the 2' chlorine, on the A-ring and B-ring, respectively, seem to have an important synergistic effect.

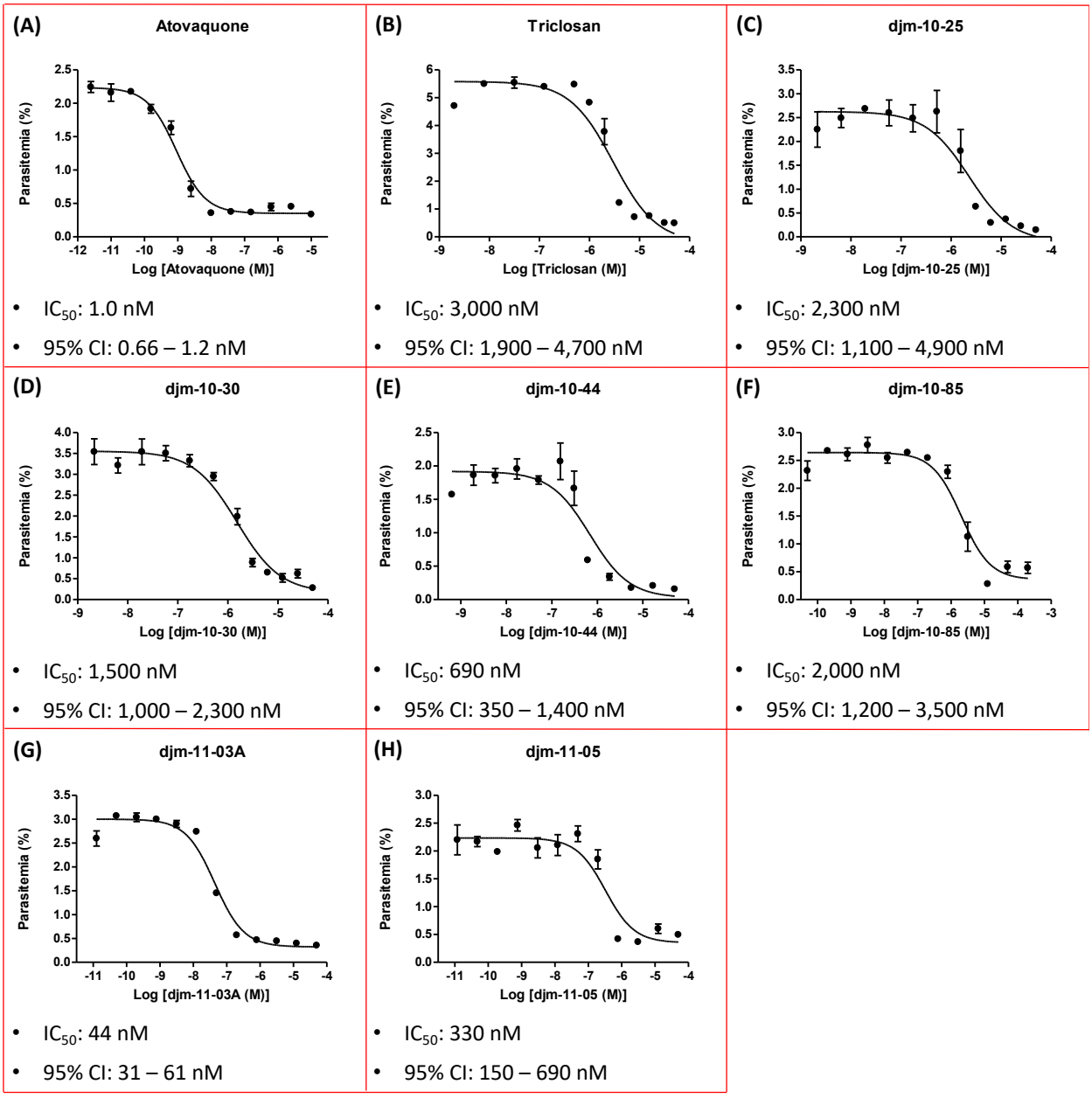

Figure 3.4. IC_{50} curves for various antimalarial drugs. Shown are the IC_{50} curves for **(A)** atovaquone, **(B)** triclosan, and six triclosan analogs – **(C)** djm-10-25, **(D)** djm-10-30, **(E)** djm-10-44, **(F)** djm-10-85, **(G)** djm-11-03A, and **(H)** djm-11-05. 6 hours post synchronization, $NF54^{attB}$ *Pf* parasites were seeded at 0.5% parasitemia, and allowed to grow for 48 hours in the presence or absence of a drug (see the **MATERIALS AND METHODS** section for details). The determined IC_{50} and 95% CI are indicated below each graph. Each data point (error bar) represents the mean (standard

deviation) derived from four technical replicates. For any data point, the apparent absence of an error bar is due to its small size. The IC_{50} curves for each drug was measured at least twice, and the curves shown are representative of each drug.

Table 3.2. General information on triclosan and seven of its analogs. Shown below are the name, exact mass (i.e., pure molecular weight), chemical structure, IC_{50}, and 95% CI for triclosan and seven of its analogs. With the exception of djm-10-56, which exhibited poor inhibitory activity against the growth of ABS *Pf*, values for IC_{50} and 95% CI from two biological replicates are shown for each drug. The average IC_{50} value is indicated in red. All numeric values for IC_{50} and 95% CI are shown with two significant digits.

Compound	Exact mass (g/mol)	Chemical structure	IC_{50} (nM)	95% CI (nM)
triclosan	287.95	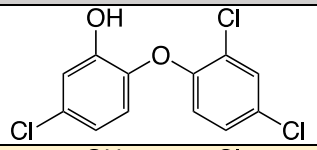	3,400 3,000 3,200	2,300 – 4,900 1,900 – 4,700
39b (Stec *et al.*, 2013)	365.09	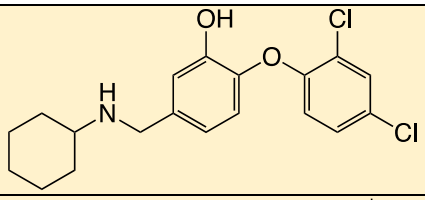	30 – 80	
C25 (Freundlich *et al.*, 2006)	311.05	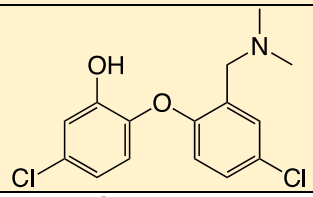	180 – 220	
djm-10-56	235.16	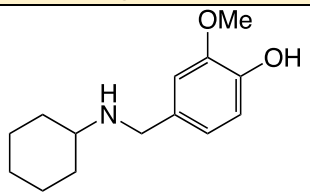	>11,000	
djm-10-25	379.11	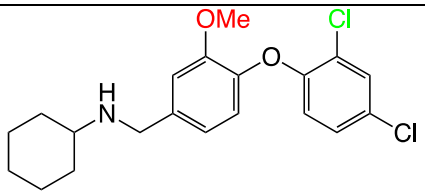	2,200 2,300 2,300	430 – 11,000 1,100 – 4,900

djm-10-30	373.14	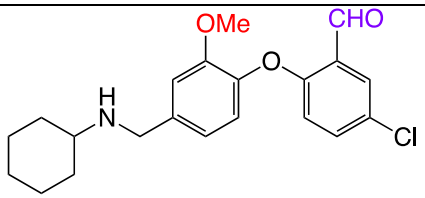	1,500 3,000 2,300	1,000 – 2,300 2,100 – 4,400
djm-10-44	402.21	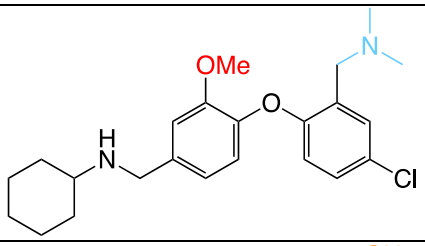	280 690 490	130 – 590 350 – 1,400
djm-10-85	375.16	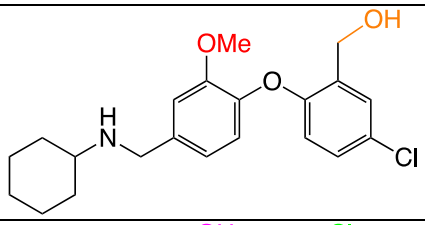	2,000 3,800 2,900	1,200 – 3,500 2,200 – 6,300
djm-11-03A	365.09	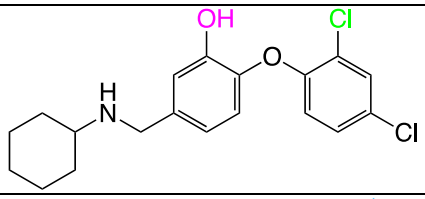	33 44 39	18 – 60 31 – 61
djm-11-05	388.19	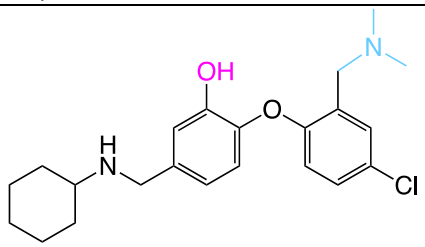	520 330 430	330 – 830 150 – 690

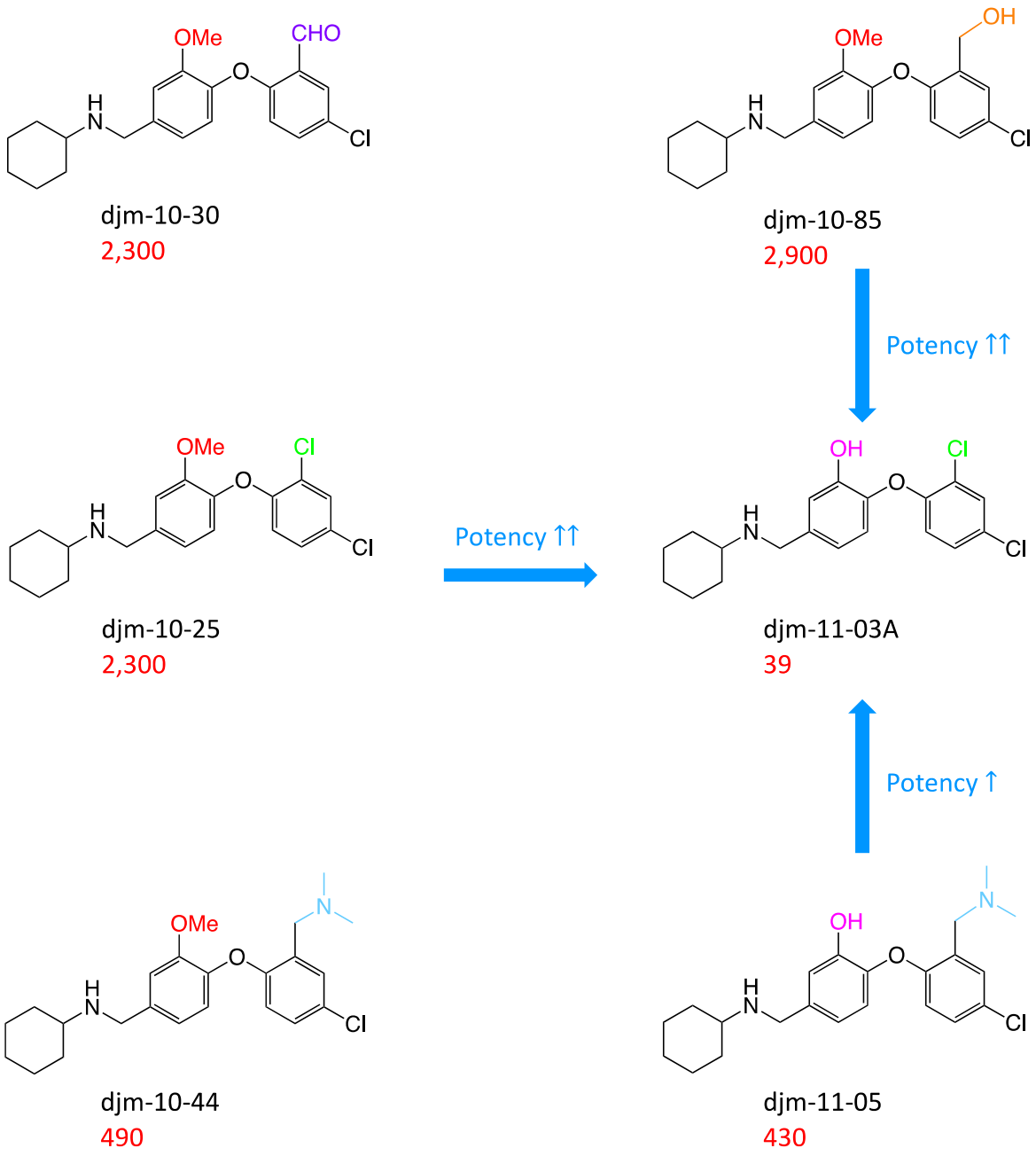

Figure 3.5. Structure—activity relationship based on six triclosan analogs. A schematic illustrating the relationship between chemical structure and antiparasitic activity for six triclosan analogs is depicted. For each compound, the average IC_{50} value (in nM) is indicated in red, and these values are the same as those given in **Table 3.2**. Notable shifts in antiparasitic activity are indicated in blue.

CONCLUDING REMARKS

Herein, we have examined seven triclosan analogs vis-à-vis their antiparasitic activity against ABS *Pf*. Among these analogs, djm-11-03A exhibited the strongest activity, with an average IC_{50} of 39 nM. Moreover, examination of the structure—activity relationship based on six of these analogs indicates that the outstanding activity of djm-11-03A could be attributed, at least in part, to the synergistic effect between its A-ring 2' hydroxyl and its B-ring 2' chlorine. However, as we were not able to improve the potency of this preexistent compound, future experiments may involve the screening for antiparasitic activity using additional novel triclosan analogs. Importantly, given that djm-11-03A exhibited excellent potency against ABS *Pf*, we have opted to carry out drug resistance induction experiments with this compound. Once resistant parasites are obtained, we plan to carry out genomic sequencing in order to uncover the genetic determinants of drug resistance. In particular, a clear answer may come in the form of either a mutation in a candidate drug target gene or a copy number variation for that gene. In any case, the results from the genomic sequencing should be confirmed by the mutation, knock-down, or over-expression of the candidate gene. All in all, such an approach should help uncover the specific drug targets of this compound, and thus, shed light on how to further optimize its potency.

REFERENCES

[1] N. Surolia and A. Surolia, "Triclosan offers protection against blood stages of malaria by inhibiting enoyl-ACP reductase of Plasmodium falciparum," *Nat. Med.*, vol. 7, no. 2, pp. 167–73, Feb. 2001.

[2] K. Maity, T. Banerjee, N. Prabakaran, N. Surolia, A. Surolia, and K. Suguna, "Effect of substrate binding loop mutations on the structure, kinetics, and inhibition of enoyl acyl carrier protein reductase from Plasmodium falciparum," *IUBMB Life*, vol. 63, no. 1, pp. 30–41, Jan. 2011.

[3] N. Kapoor, T. Banerjee, P. Babu, K. Maity, N. Surolia, and A. Surolia, "Design, development, synthesis, and docking analysis of 2'-substituted triclosan analogs as inhibitors for Plasmodium falciparum enoyl-ACP reductase," *IUBMB Life*, vol. 61, no. 11, pp. 1083–91, Nov. 2009.

[4] J. S. Freundlich *et al.*, "X-ray structural analysis of Plasmodium falciparum enoyl acyl carrier protein reductase as a pathway toward the optimization of triclosan antimalarial efficacy," *J. Biol. Chem.*, vol. 282, no. 35, pp. 25436–44, Aug. 2007.

[5] M. Kapoor, J. Gopalakrishnapai, N. Surolia, and A. Surolia, "Mutational analysis of the triclosan-binding region of enoyl-ACP (acyl-carrier protein) reductase from Plasmodium falciparum," *Biochem. J.*, vol. 381, no. Pt 3, pp. 735–41, Aug. 2004.

[6] M. Kapoor, M. J. Dar, A. Surolia, and N. Surolia, "Kinetic determinants of the interaction of enoyl-ACP reductase from Plasmodium falciparum with its substrates and inhibitors," *Biochem. Biophys. Res. Commun.*, vol. 289, no. 4, pp. 832–7, Dec. 2001.

[7] M. Kapoor, P. L. S. Mukhi, N. Surolia, K. Suguna, and A. Surolia, "Kinetic and structural analysis of the increased affinity of enoyl-ACP (acyl-carrier protein) reductase for triclosan in the presence of NAD+," *Biochem. J.*, vol. 381, no. Pt 3, pp. 725–33, Aug. 2004.

[8] M. Kapoor, C. C. Reddy, M. V Krishnasastry, N. Surolia, and A. Surolia, "Slow-tight-binding inhibition of enoyl-acyl carrier protein reductase from Plasmodium falciparum by triclosan," *Biochem. J.*, vol. 381, no. Pt 3, pp. 719–24, Aug. 2004.

[9] J. S. Freundlich *et al.*, "Synthesis and biological activity of diaryl ether inhibitors of malarial enoyl acyl carrier protein reductase. Part 2: 2'-substituted triclosan derivatives," *Bioorg. Med. Chem. Lett.*, vol. 16, no. 8, pp. 2163–9, Apr. 2006.

[10] J. S. Freundlich *et al.*, "Synthesis, biological activity, and X-ray crystal structural analysis of diaryl ether inhibitors of malarial enoyl acyl carrier protein reductase. Part 1: 4'-substituted triclosan derivatives," *Bioorg. Med. Chem. Lett.*, vol. 15, no. 23, pp. 5247–52, Dec. 2005.

[11] S. Mishra, K. Karmodiya, P. Parasuraman, A. Surolia, and N. Surolia, "Design, synthesis, and application of novel triclosan prodrugs as potential antimalarial and antibacterial agents," *Bioorg. Med. Chem.*, vol. 16, no. 10, pp. 5536–46, May 2008.

[12] V. Frecer, E. Megnassan, and S. Miertus, "Design and in silico screening of combinatorial library of antimalarial analogs of triclosan inhibiting Plasmodium falciparum enoyl-acyl carrier protein reductase," *Eur. J. Med. Chem.*, vol. 44, no. 7, pp. 3009–19, Jul. 2009.

[13] K. Maity, S. P. Bhargav, B. Sankaran, N. Surolia, A. Surolia, and K. Suguna, "X-ray crystallographic analysis of the complexes of enoyl acyl carrier protein reductase of Plasmodium falciparum with triclosan variants to elucidate the importance of different functional groups in enzyme inhibition," *IUBMB Life*, vol. 62, no. 6, pp. 467–76, Jun. 2010.

[14] S. P. Muench *et al.*, "Development of a triclosan scaffold which allows for adaptations on both the A- and B-ring for transport peptides," *Bioorg. Med. Chem. Lett.*, vol. 23, no. 12, pp. 3551–5, Jun. 2013.

[15] M. Yu *et al.*, "The Fatty Acid Biosynthesis Enzyme FabI Plays a Key Role in the Development of Liver-Stage Malarial Parasites," *Cell Host Microbe*, vol. 4, no. 6, pp. 567–578, 2008.

[16] A. S. Tarun *et al.*, "A combined transcriptome and proteome survey of malaria parasite liver stages," *Proc. Natl. Acad. Sci.*, vol. 105, no. 1, pp. 305–310, 2008.

[17] W. Baschong *et al.*, "Triclosan is minimally effective in rodent malaria models," *Nat. Med.*, vol. 17, no. 1, pp. 33-4; author reply 34-5, Jan. 2011.

[18] E. Bilsland *et al.*, "Plasmodium dihydrofolate reductase is a second enzyme target for the antimalarial action of triclosan," *Sci. Rep.*, vol. 8, no. 1, p. 1038, Dec. 2018.

[19] E. Bilsland, P. Pir, A. Gutteridge, A. Johns, R. D. King, and S. G. Oliver, "Functional Expression of Parasite Drug Targets and Their Human Orthologs in Yeast," *PLoS Negl. Trop. Dis.*, vol. 5, no. 10, p. e1320, Oct. 2011.

[20] E. Bilsland *et al.*, "Yeast-based automated high-throughput screens to identify anti-parasitic lead compounds," *Open Biol.*, vol. 3, no. 2, p. 120158, Feb. 2013.

[21] B. Blasco, D. Leroy, and D. A. Fidock, "Antimalarial drug resistance: linking Plasmodium falciparum parasite biology to the clinic," *Nat. Med.*, vol. 23, no. 8, pp. 917–928, Aug. 2017.

[22] M. Chugh *et al.*, "Identification and deconvolution of cross-resistance signals from antimalarial compounds using multidrug-resistant Plasmodium falciparum strains," *Antimicrob. Agents Chemother.*, vol. 59, no. 2, pp. 1110–8, Feb. 2015.

[23] J. Stec *et al.*, "Modification of Triclosan Scaffold in Search of Improved Inhibitors for Enoyl-Acyl Carrier Protein (ACP) Reductase in Toxoplasma gondii," *ChemMedChem*, vol. 8, no. 7, pp. 1138–1160, 2013.

[24] L. Y. Gluzman, S. E. Francis, A. Oksman, C. E. Smith, K. L. Duffin, and D. E. Goldberg, "Order and Specificity of the Plasmodium falciparum Hemoglobin Degradation Pathway," vol. 93, pp. 1602–1608, 1994.

[25] M. B. Cassera *et al.*, "The methylerythritol phosphate pathway is functionally active in all intraerythrocytic stages of Plasmodium falciparum," *J. Biol. Chem.*, vol. 279, no. 50, pp. 51749–59, Dec. 2004.

[26] L. J. Nkrumah *et al.*, "Efficient site-specific integration in Plasmodium falciparum chromosomes mediated by mycobacteriophage Bxb1 integrase," *Nat. Methods*, vol. 3, no. 8, pp. 615–621, 2006.

[27] L. M. Coronado, N. M. Tayler, R. Correa, R. M. Giovani, and C. Spadafora, "Separation of Plasmodium falciparum late stage-infected erythrocytes by magnetic means," *J. Vis. Exp.*, no. 73, p. e50342, Mar. 2013.

[28] L. K. Basco, J. Le Bras, and O. Ramiliarisoa, "In Vitro Activity of Atovaquone Against the African Isolates and Clones of Plasmodium falciparum," *Am. J. Trop. Med. Hyg.*, vol. 53, no. 4, pp. 388–391, Oct. 1995.

CHAPTER 4: PyrKII and apicoplast maintenance

ABSTRACT

Pf harbors two isoforms of Pyruvate Kinase – PyrKI and PyrKII, which are localized to the cytosol and the apicoplast, respectively. While it has been shown that PyrKII is essential for the maintenance of the apicoplast, reasons for this requirement are yet to be determined. Within the apicoplast, PyrKII is thought to catalyze the conversion of PEP and ADP into pyruvate and ATP. Pyruvate can then either be converted into acetyl CoA, the precursor of the FAS-II pathway, or fed directly into the MEP pathway to generate isoprenoids. Using *Pf*Mev-based genetic knock-outs of various enzymes of the MEP pathway, we have empirically demonstrated that the MEP pathway, while essential to parasite survival during the ABS, is not required for maintaining the apicoplast. Furthermore, previous studies have shown that the deletion of certain components of the FAS-II pathway yielded no growth defect in the ABS. Taken together, these results indicate that maintenance of the apicoplast by PyrKII does not occur due to its pyruvate generation function. The alternative explanation, then, is that its ATP generation function is somehow required for maintaining the organelle. Given this, we have taken a twofold approach to help address the question – (1) we are testing the substrate specificity of various (d)NTPs against PyrKII *in vitro*, and (2) we aim to carry out a microarray analysis in order to examine the changes within the nuclear and apicoplast transcriptome in response to knocking down PyrKII during the ABS. Towards the second goal, we are testing two different knock-down methods. The first is a Tet-on system called the TetR-DOZI system and the second is a conditional localization system (CLD) that diverts PyrKII from the apicoplast and causes the protein to be secreted. Herein, we demonstrate the capability of the TetR-DOZI system and the CLD system to conditionally knock down PyrKII.

INTRODUCTION

PyrKII in *Plasmodium* spp.

Pf and the related apicomplexan parasite *Tg* both harbor two isoforms of PyrK – PyrKI and PyrKII. *Tg*PyrKI localizes to the cytosol, while *Tg*PyrKII localizes to both the mitochondrion and the apicoplast [1]. *Pf*PyrKII, unlike *Pf*PyrKI, contains a putative N-terminal apicoplast-targeting bipartite pre-sequence [2], and exclusively localizes to the apicoplast [3]. This exclusive localization, coupled with the fact that PyrKII is actively transcribed during the ABS [2], suggests that the protein likely carries out a function that is essential for the organelle. As shown in the putative metabolic pathways involving *Pf*PyrKII (**Figure 4.1**), cytosolic phosphoenolpyruvate (PEP) must first traverse the four membranes of the apicoplast in order to reach the apicoplast-localized PyrKII. This translocation is thought to be accomplished through the outer triose phosphate transporter (oTPT) and the inner triose phosphate transporter (iTPT), which are located across the outermost and innermost membranes, respectively, of the apicoplast [4]. Using PEP and ADP as substrates, PyrKII is thought to catalyze the generation of pyruvate and ATP. The resulting pyruvate can then serve as the starting material for either the MEP pathway or the FAS-II pathway.

Using *Pf*Mev as the parental line, we have generated ΔPyrKII parasites, and demonstrated, via a combination of fluorescence microscopy and organellar genome PCR, that PyrKII is required for the maintenance of the apicoplast. As shown in the **RESULTS AND DISCUSSION** section of **CHAPTER 2**, the MEP pathway, although essential for the survival of ABS *Pf*, is not required for maintaining the apicoplast itself. Furthermore, no growth defect in the ABS was observed upon knocking out certain components of either the PDH complex [5] or particular enzymes of the FAS-II pathway [6, 7]. Taken together, these results suggest that the generation of pyruvate by PyrKII is dispensable with respect to the maintenance of the apicoplast, which led to our hypothesis that the generation of ATP by PyrKII is required for maintaining the organelle. In that regard, preliminary

results from our lab have demonstrated that pure recombinant PyrKII exhibits catalytic activity against all NDPs and dNDPs *in vitro*, with the strongest activity against the purines ADP and GDP. While this indicates a lack of specificity for any single NDP substrate, we reasoned that a loss of various NTPs could inhibit certain apicoplast enzymes and functions, including translation (GTP) and transcription (all NTPs). Based on the hypothesis that transcription could be affected, we sought to compare the nuclear and apicoplast transcript levels upon knocking down PyrKII. To that end, we have applied the CLD system and the TetR-DOZI system [8] to our *Pf*Mev line to generate the PyrKII CLD and PyrKII TetR-DOZI lines, respectively. The results presented in this chapter demonstrate the capability of both systems to conditionally knock down PyrKII.

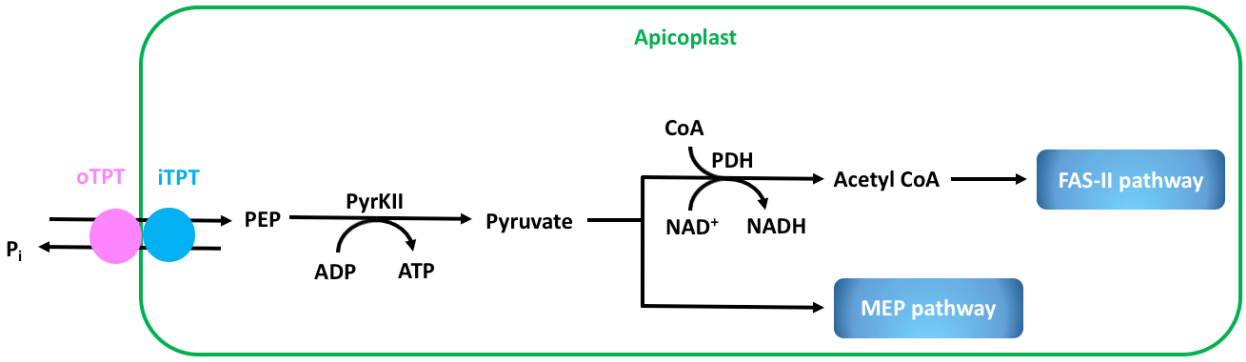

Figure 4.1. Putative metabolic pathways involving PyrKII in the *Plasmodium* apicoplast. In exchange for exporting an inorganic phosphate, PEP is imported into the apicoplast through the oTPT and iTPT. PyrKII catalyzes the conversion of ADP and PEP into pyruvate and ATP. Pyruvate can then undergo one of two fates: (1) it can be converted by the PDH complex into acetyl CoA, which is then fed into the FAS-II pathway to synthesize fatty acids, or (2) it can be directly fed into the MEP pathway to synthesize isoprenoids.

The CLD system for conditionally knocking down PyrKII

The design for the CLD system employed herein to conditionally knock down PyrKII was derived from a preexisting molecular tool for studying malaria parasites – the destabilization domain (DD) system. To implement the latter system, a mutated version of *Homo sapiens* (*Hs*) FK506 binding protein (FKBP) is fused to a protein of interest and serves as the so-called DD. Modulation of the protein level is achieved through the addition of Shield1, a synthetic cell-permeable ligand to which the DD binds. More specifically, when Shield1 is provided in the growth medium, it binds to the DD, stabilizing its structure and thus preventing degradation of the fusion protein. Under permissive conditions, however, the DD remains unstructured, and consequently targets the fusion protein for degradation by the proteasome of the parasite. Since the DD system relies on the cytosolic proteasome, it does not work well for organellar proteins. Nonetheless, for cytosolic proteins, the DD system has been shown to be capable of conditionally knocking down the expression of both episomally expressed [9] and endogenous [10–12] proteins in *Pf*. Given this, we adapted the DD system as a conditional localization system (see below) for the conditional knock-down of PyrKII in the parasite.

The CLD system relies on the N-terminal modification of a protein of interest to control its localization. In the phylum Apicomplexa, trafficking of a nuclear-encoded protein to the apicoplast is a two-step process that requires the presence, on the N-terminus of the protein, of a bipartite pre-sequence comprised of two domains – the signal peptide and the transit peptide [13] (**Figure 4.2A**). First, the signal peptide mediates co-translational import of the protein into the secretory pathway, i.e., the endoplasmic reticulum (ER). At some point during this process, perhaps shortly after import into the rough ER, the signal peptide gets cleaved off by the signal peptide peptidase (SgPP) [14]. The revealed transit peptide is thought to then mediate transfer of the protein into the lumen of the apicoplast [13]. Upon arrival at the apicoplast, the transit peptide is thought to be cleaved off by the stromal processing peptidase (SPP), thereby generating the functional mature protein [14] (**Figure**

4.2A). To generate the PyrKII CLD line, we genetically modified the natural bipartite pre-sequence of PyrKII – the original signal peptide was replaced with that of the acyl carrier protein (ACP), a nuclear-encoded apicoplast-localized protein [13, 15, 16] that functions in the FAS-II pathway, while the original transit peptide was replaced with what we named the CLD (**Figure 4.2B**). For the choice of CLD, we selected a variant of *Hs* FKBP containing specific mutations that enhance its binding with Shield1 [9]. We mutated this protein to introduce positively charged amino acid residues that are required for apicoplast transport. In addition, we introduced mutations that partially destabilize the FKBP domain so that the binding of Shield1 stabilizes the structure of the CLD. Importantly, a lack of transit peptide structure is required for the trafficking of proteins from the secretory pathway to the apicoplast, while the formation of structure in the transit peptide blocks apicoplast import [17]. Given this, the ability to control the structure of the CLD via the addition of Shield1 affords a molecular tool allowing the ligand-tunable mislocalization of a protein of interest. In particular, under permissive conditions (**Figure 4.2B**), the signal peptide$_{ACP}$ directs the protein to the ER. After cleavage of the signal peptide$_{ACP}$, the exposed CLD, with an unstable structure, directs the tagged protein to the apicoplast. By contrast, when Shield1 is provided in the growth medium (**Figure 4.2C**), the ligand binds to the CLD, stabilizing its structure and thereby causing the tagged protein to be secreted from the parasite into the parasitophorous vacuole.

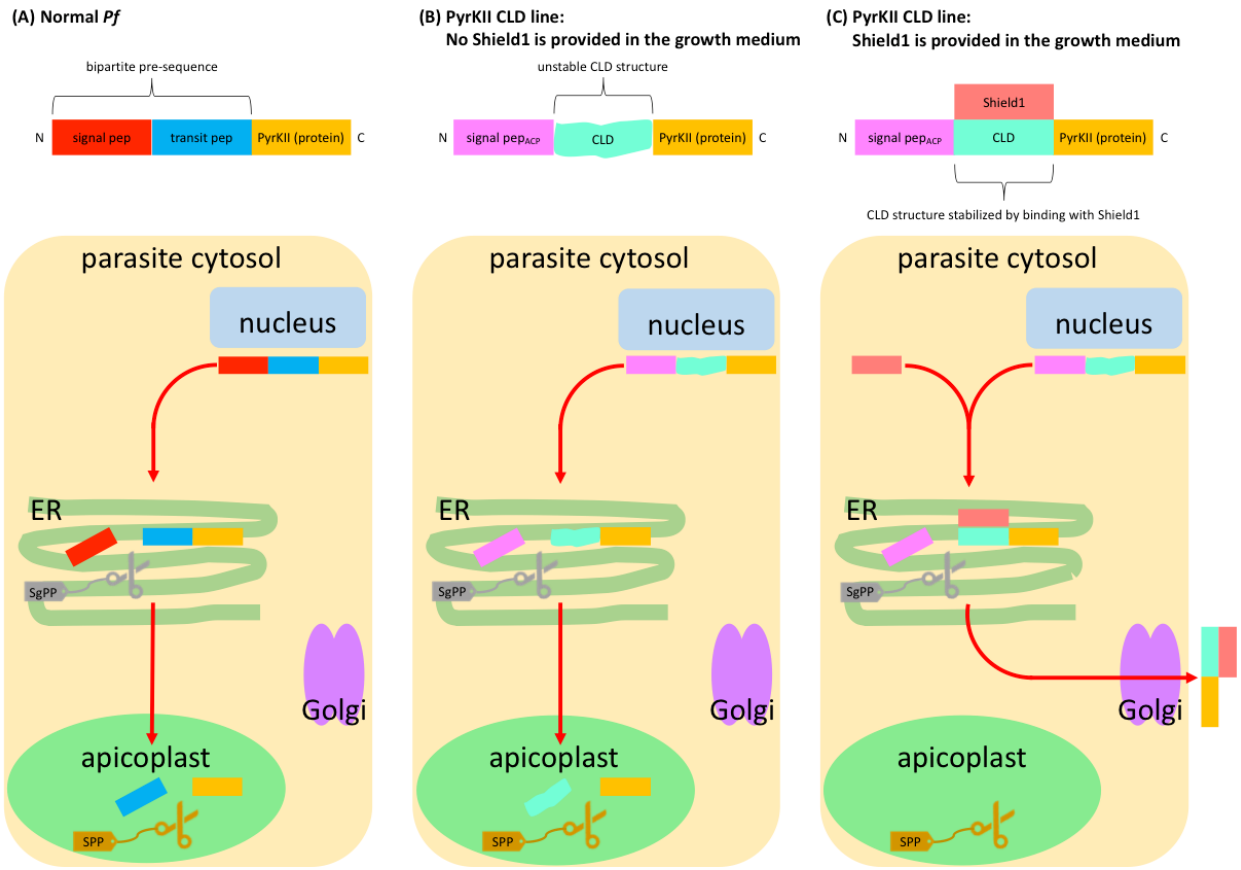

Figure 4.2. PyrKII translocation for normal *Pf vs.* the PyrKII CLD line. (A) Normal *Pf*. The signal peptide directs the protein to the secretory pathway, where the signal peptide gets cleaved off by the SgPP. The exposed transit peptide then directs the protein to the apicoplast, where the transit peptide gets cleaved off by the SPP, revealing the functional mature protein. **(B)** No Shield1 is provided in the growth medium for PyrKII CLD. The signal peptide$_{ACP}$ directs the protein to the secretory pathway, where the signal peptide$_{ACP}$ gets cleaved off. The exposed CLD then directs the protein to the apicoplast, where the CLD gets cleaved off by the SPP, revealing the functional mature protein. **(C)** Shield1 is provided in the growth medium for PyrKII CLD. The signal peptide$_{ACP}$ directs the protein to the secretory pathway, where the signal peptide$_{ACP}$ gets cleaved off. Shield1 binds to the CLD, stabilizing the structure of the CLD, and causing the tagged protein to be secreted from the parasite cytosol into the vacuolar space surrounding the parasite cell.

The TetR-DOZI system for conditionally knocking down PyrKII

Similar to the CLD system, the TetR-DOZI system also relies on the addition of a small molecule to conditionally modulate the expression of a protein of interest. The TetR-DOZI system was derived from its primitive variant, the TetR system. Under the latter system, Tet repressor protein (TetR)-binding RNA elements, or aptamers in short, are genetically encoded into the 5' untranslated region (5' UTR) of the mRNA of a protein of interest [18, 19]. These aptamer regions form stem loop structures, in the mRNA, to which TetR specifically binds [19]. Under this setup, therefore, exogenously introduced TetR binds to these aptamer regions, thereby inhibiting the translation of the open reading frame [8, 18, 19]. However, when tetracycline analogs such as anhydrotetracycline (aTc) and doxycycline (Dox) are provided, these small molecules bind to TetR, preventing the binding of TetR to the aptamer regions, and thus allowing translation to occur normally [8, 18, 19]. Initially, the capability of the system to control the expression of exogenously introduced reporter proteins was demonstrated in yeast [19]. However, when the system was implemented in *Pf* to successfully control the expression of both reporter and endogenous proteins, only aTc was used as the chemical inducer of translation [18], presumably to avoid the use of Dox, which possesses specific antimalarial properties [20].

Now, the TetR-DOZI system was optimized from its predecessor through two major changes: (1) the aptamer regions are genetically encoded within the 3' UTR (instead of the 5' UTR) of the mRNA of the protein of interest, and (2) a TetR-DOZI fusion protein (instead of TetR alone) is employed to achieve translational repression [8]. DOZI (development of zygote inhibited), an RNA helicase that belongs to the DDX6 family of RNA helicases, has been implicated in the translational repression of select mRNA transcripts in *Pb*, and its loss in female *Pb* gametocytes has been phenotypically linked to a failure of fertilized female gametes (zygotes) to develop normally [21]. In yeast, when non-optimal codons are encountered by the ribosome during the elongation process of

protein synthesis, Dhh1p targets the transcript for de-capping and degradation [22]. Being the *Pf* homologue of Dhh1p and having a role in translational repression in *Pb*, DOZI made for an apt choice as a TetR fusion protein for the enhancement of translational inhibition in *Pf*. Importantly, in *Pf*, the noted changes from the original TetR system have been shown to not only significantly (by nearly fourfold) enhance the aTc-inducible regulation of gene expression but also reduce leaky expression associated with the synthetic system [8].

Given the capability of the TetR-DOZI system to robustly and conditionally regulate gene expression in *Pf*, we have employed the system to knock down PyrKII, the protein of interest for our study. As depicted in the simplified schematic of our application of this system (**Figure 4.3A**), a 3' UTR containing aptamer regions along with a transgene encoding the TetR-DOZI fusion protein was site-specifically integrated at the 3' end of the PyrKII coding sequence. When no aTc is provided in the growth medium of the parasite (**Figure 4.3C**), TetR of the fusion protein binds to the aptamer regions within the 3' UTR, thereby leading to the translational inhibition of the mRNA transcript. On the other hand, when aTc is provided in the growth medium (**Figure 4.3B**), the molecule binds to TetR, preventing the binding of the fusion protein to the aptamer regions and thus allowing translation to proceed.

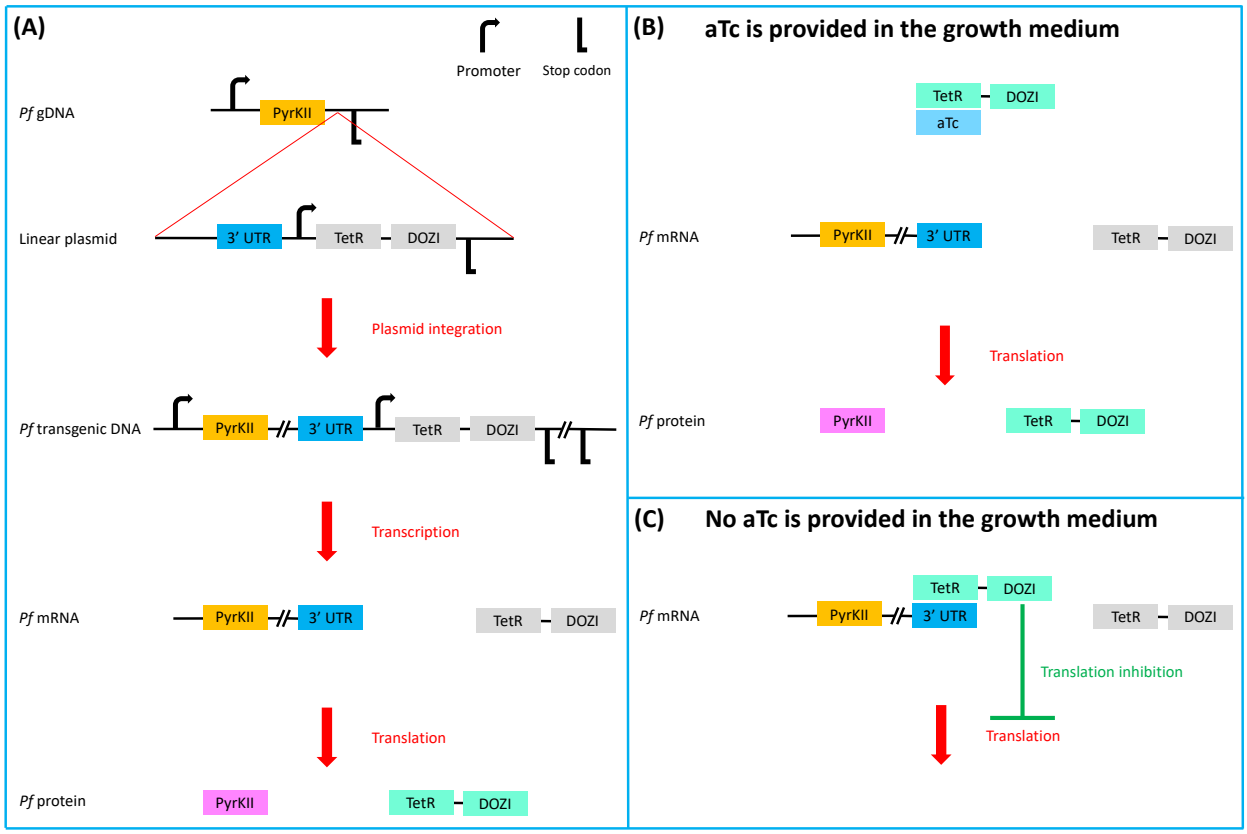

Figure 4.3. Conditional knock-down of PyrKII via the TetR-DOZI system. (A) A simplified schematic of our application of the TetR-DOZI system to conditionally knock down *Pf* PyrKII. A double-stranded cut is introduced at the 3' end of the PyrKII gene, followed by integration of the linear plasmid into the cut site. **(B)** When aTc is provided in the growth medium, the molecule binds to TetR of the TetR-DOZI fusion protein, preventing the binding of TetR to the aptamer region within the 3' UTR, thus allowing translation of the PyrKII mRNA. **(C)** When no aTc is provided in the growth medium, the TetR-DOZI fusion protein binds to the aptamer region within the 3' UTR, thereby inhibiting translation of the *Pf* PyrKII mRNA.

MATERIALS AND METHODS

Generation of growth curves

Growth curves were generated using a plate-based SYBR Green assay. As illustrated in the overall plan (per IC plate) used to generate growth curves for the PyrKII TetR-DOZI and PyrKII CLD parasite lines (**Table 4.1**), the IC plate was prepared 6 hours post synchronization. The parasites were allowed to grow up to day 4, at which time the parasitemia was cut by a factor of 10 to generate a cut IC plate in addition to the original uncut IC plate. The uncut version was allowed to grow for two additional days (up to day 6), while the cut version was allowed to grow for four additional days (up to day 8). For each curve, the parasitemia was measured using flow cytometry every other day, starting from day 0. This is different from the overall plan (per IC plate) given in **CHAPTER 2**, and is explained in the **RESULTS AND DISCUSSION** section of this chapter. The following subsections detail each step of the overall plan.

Table 4.1. The overall plan (per IC plate) for growth curve generation for the PyrKII lines. This plan was used for both the PyrKII TetR-DOZI and PyrKII CLD parasite lines.

day	0	1	2	3	4	5	6	7	8
IC plate	• MACS LS column (2:00 PM) • seed (8:00 PM)	• change media (~12:00 PM) • CR (~12:00 PM)	• change media (~12:00 PM)	• change media (~12:00 PM) • CR (~12:00 PM)	• 1:10 cut (after flow)	• change media (~12:00 PM) • CR (~12:00 PM)	• change media (~12:00 PM)	• change media (~12:00 PM) • CR (~12:00 PM)	
parasite life cycle #	1	1	1	2	2	3	3	4	4
eluate parasite stage	• schizonts • early rings	• rings	late stage: • trophs • schizonts	• rings	late stage: • trophs • schizonts	• rings	late stage: • trophs • schizonts	• rings	late stage: • trophs • schizonts
flow	run (8:00 PM)		run (~12:00 PM)		run (~12:00 PM)		run (~12:00 PM)		run (~12:00 PM)

Parasite culture maintenance

The culture was maintained using the same method as that detailed under the **MATERIALS AND METHODS** section from **CHAPTER 2**. The PyrKII CLD line was maintained on CMA medium;

the PyrKII TetR-DOZI line was maintained on CMA medium supplemented with 0.5 μM aTc (Sigma-Aldrich, cat. #37919).

Magnetic purification

The isolation of schizont-stage iRBCs from the mixed-stage culture employed the same method as that detailed under the **MATERIALS AND METHODS** section from **CHAPTER 3**, with the exception that, for the PyrKII TetR-DOZI line, CMA medium supplemented with 0.5 μM aTc was used.

Flow cytometry

The measurement of parasitemia employed the same flow cytometry-based method as that detailed under the **MATERIALS AND METHODS** section from **CHAPTER 2**, with the exception that the parasitemia was measured every other day. On each day of measurement, the measured samples included those that were collected on the day of measurement in addition to the CR plate samples that were collected from the previous day.

Sample collection and storage

The cold room (CR) storage conditions are the same as that detailed under the **MATERIALS AND METHODS** section from **CHAPTER 2**.

RESULTS AND DISCUSSION

Shield1 toxicity test

We have generated a *Pf*Mev-based ΔPyrKII line, and used a combination of organellar genome PCR and fluorescence microscopy to show that PyrKII is required for the maintenance of the apicoplast (**data not shown**), and thus the survival of ABS *Pf*. As mentioned in the **INTRODUCTION** section of this chapter, the addition of Shield1 to the PyrKII CLD line will result in the secretion of PyrKII from the parasite. Because of this, the knock down of PyrKII expression via the CLD system should result in a noticeable decrease in the parasitemia. Now, although one study has shown that the treatment of *Pf* with Shield1 at 500 nM for 48 h (i.e., spanning the entire first parasite life cycle) led to an 11% decrease in parasitemia [10], another study noted that treatment with the same concentration for 3 days did not inhibit parasite growth [9]. Regardless, we reasoned that it was imperative to first carry out a toxicity test in order to determine the maximum concentration of Shield1 at which no toxicity is elicited by the presence of the ligand itself. Presumably, this concentration would allow the maximum downregulation of protein expression while avoiding any potential inherent toxicity associated with the ligand. To that end, we used the *Pf*Mev parasite line for this test since it is the parent of the PyrKII CLD line. As for the concentration, we chose to test 0, 25, 100, and 500 nM. As evident from the resulting growth curve (**Figure 4.4**), there is an apparent decrease in growth for the 500 nM condition in comparison to the other three conditions, indicating that Shield1 at 500 nM might be slightly toxic. However, examination of the raw data shows that the precise mean ± SD starting parasitemia for the 0, 25, 100, and 500 nM Shield1 conditions were 0.47 ± 0.04%, 0.42 ± 0.06%, 0.45 ± 0.09%, and 0.40 ± 0.07%, respectively. Thus, given that the seeded parasitemia of the 500 nM condition is somewhat lower than of the other three media conditions, the apparent lower parasitemia for the 500 nM condition could be attributed, at least in part, to the lower starting parasitemia. Overall, given that Shield1 at 500 nM did not seem to confer any major growth defect

over the span of 7 days (the approximate duration of our growth curve experiment), this concentration of the ligand was used for subsequent experiments for the PyrKII CLD line.

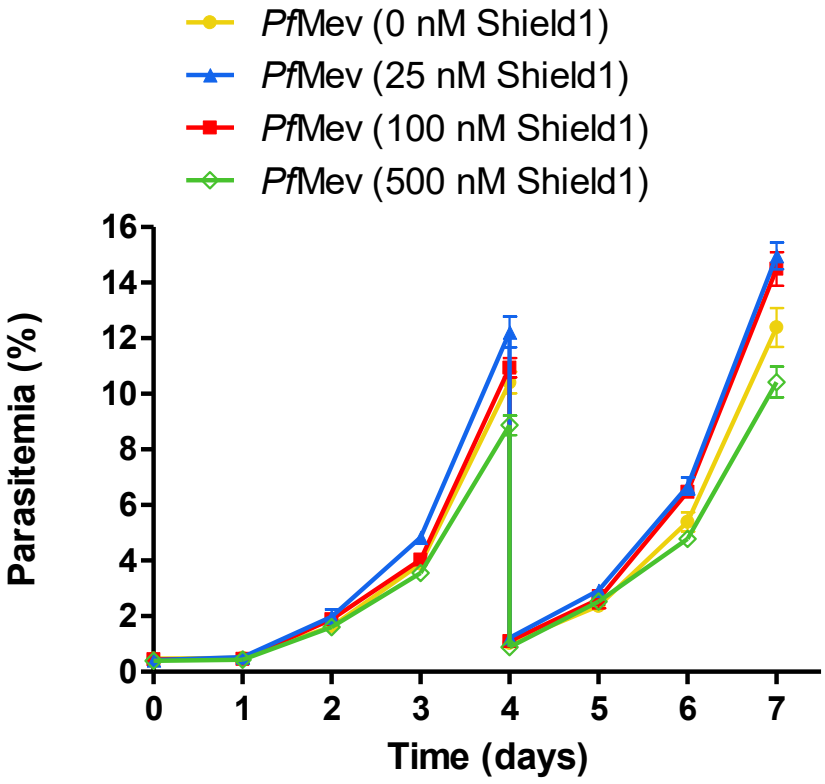

Figure 4.4. Shield1 toxicity test. Non-synchronous *Pf*Mev parasites were seeded on day 0 at ~0.5% parasitemia and allowed to grow up to day 4, at which time the parasitemia was cut down by a factor of 10. Thereafter, the parasites were allowed to grow up to day 7. As indicated, four different media conditions were used – CMA medium with 0, 25, 100, or 500 nM Shield1. Each data point (error bar) represents the mean (standard deviation) derived from four technical replicates. For any data point, the apparent absence of an error bar is due to its small size.

Optimization of the flow assay for the detection of synchronous parasites

Following the time scheme detailed under the **MATERIALS AND METHODS** section, the even-days (days 2, 4, 6, and 8) correspond to the late-stages of the parasite life cycle (**Table 4.1**). As we have

consistently observed under this time scheme, storage of parasite samples under 4°C and measuring the samples one or more days later yields an apparent dip in the parasitemia exclusively for the even-day samples (**data not shown**). On the other hand, measuring the parasitemia of the even-day samples on the day of sample collection eliminates the apparent dip (**Figure 4.4** and **Figure 4.5**). Our hypothesis for this phenomenon is that late-stage parasites either break down or release immature merozoites if left for one or more day period at 4°C. In particular, an examination of the flow cytometer gates (**data not shown**) revealed the presence, for the even-day samples exclusively, of a congregated group of SYBR Green-positive objects lying outside the R1 gate. The atypical scattering profile of these objects and the fact that they are SYBR Green-positive indicate that these objects are probably free merozoites. Furthermore, the invasion of RBCs by free merozoites is a complex process involving a slew of specific interactions between select parasitic and RBC surface proteins (reviewed in [23]), and it is possible that some of these proteins, of the RBC and/or the parasite, are only functional under a specific temperature range. Since the cytometer gates are set up to detect SYBR Green fluorescence that is derived exclusively from objects the size of RBCs (**Figure 2.5**), objects the size of merozoites, albeit SYBR Green-positive, would be excluded from the count, thus leading to an apparent dip in the parasitemia. Therefore, for all growth curve experiments involving synchronous parasites, the samples were analyzed every other day starting from day 0, following the time scheme given in **Table 4.1**. This method not only eliminates the problem with storing late-stage parasites for extended periods of time but also avoids the need to add additional steps and fixative reagents to preserve the cells.

The CLD system conditionally knocks down the expression of PyrKII

Synchronous early ring-stage PyrKII CLD parasites were seeded at 0.5% parasitemia on day 0 and allowed to grow under one of four media conditions (**Figure 4.5**). Based on the resulting growth

curves, three observations can be made regarding the conditional knock-down of PyrKII via the CLD system. (1) As expected, the addition of Shield1 to the growth medium led to a decrease in parasitemia compared to the other three media conditions (**Figure 4.5**, blue *vs.* yellow, red, and green), indicating that the expression of PyrKII is being knocked down via the CLD system; (2) starting from the early ring-stage of the first life cycle (day 0, 6:00 P.M.), the effect of the CLD system is observable starting from the beginning of the second life cycle (day 3, ~12:00 P.M.), indicating that the effect of the CLD system manifests in a phenotypically visible manner at some time point between day 2 and day 3; and (3) past day 2, Mevalonate supplementation only enables a partial restoration of growth, as evidenced by a parasitemia lying between that of the no-kill conditions (**Figure 4.5**, yellow and red) and that of the kill condition (**Figure 4.5**, blue).

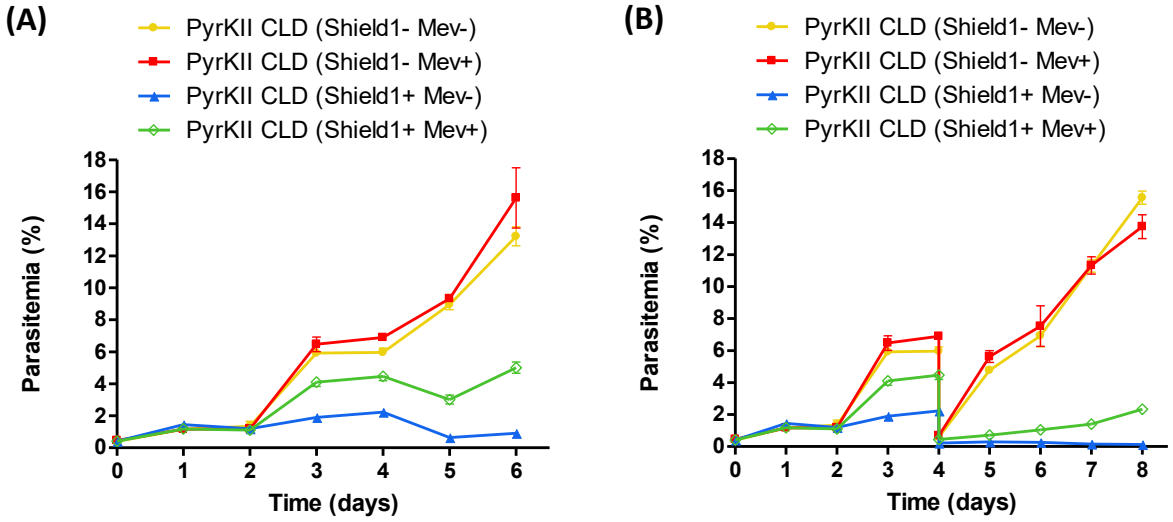

Figure 4.5. Growth curves for PyrKII CLD. On day 0, 6 hours post synchronization, the parasites were seeded at 0.5% parasitemia and either **(A)** allowed to grow up to day 6 without any cut down, or **(B)** cut down by a factor of 10 on day 4 and then allowed to grow up to day 8. Four different media conditions were used as indicated. Mevalonate was used at 50 μM, while Shield1 was used at 500 nM. Each data point (error bar) represents the mean (standard deviation) derived from four technical replicates. For any data point, the apparent absence of an error bar is due to its small size.

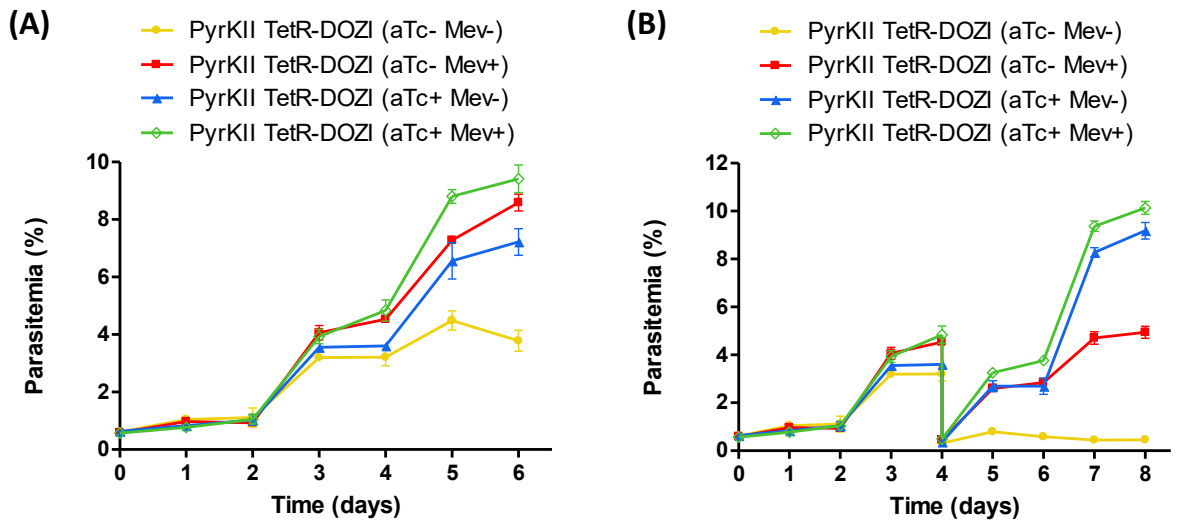

Figure 4.6. Growth curves for PyrKII TetR-DOZI. On day 0, 6 hours post synchronization, the parasites were seeded at 0.5% parasitemia and either **(A)** allowed to grow up to day 6 without any cut down, or **(B)** cut down by a factor of 10 on day 4 and then allowed to grow up to day 8. Four different media conditions were used as indicated. Mevalonate was used at 50 μM, while aTc was used at 0.5 μM. Each data point (error bar) represents the mean (standard deviation) derived from four technical replicates. For any data point, the apparent absence of an error bar is due to its small size.

The TetR-DOZI system conditionally knocks down the expression of PyrKII

As with the CLD system, synchronous early ring-stage PyrKII TetR-DOZI parasites were seeded at 0.5% parasitemia on day 0 and allowed to grow under one of four media conditions (**Figure 4.6**). Based on the resulting growth curves, three observations can be made regarding the conditional knock-down of PyrKII via the TetR-DOZI system. (1) As expected, the absence of aTc in the growth medium led to a decrease in parasitemia compared to the other three media conditions (**Figure 4.6**, yellow *vs.* red, blue, and green), indicating that the expression of PyrKII is being knocked down via the TetR-DOZI system; (2) starting from the early ring-stage of the first life cycle (day 0, 6:00 P.M.), the effect of the TetR-DOZI system is observable starting from the middle of the third life cycle (day

5, ~12:00 P.M.). Importantly, this timing has been consistently observed for the PyrKII TetR-DOZI line, and indicates that the effect of the system manifests in a phenotypically visible manner at some time point between day 4 and day 5; and (3) past day 6, Mevalonate supplementation only enables a partial restoration of growth (**Figure 4.6B**), as evidenced by a parasitemia lying between that of the no-kill conditions (**Figure 4.6B**, blue and green) and that of the kill condition (**Figure 4.6B**, yellow).

Comparison of the CLD system and the TetR-DOZI system

Two key observations can be made when the two conditional knock-down systems are compared. (1) For both parasite lines, the Mevalonate bypass system is only able to partially restore the growth of the parasites. Although this has been consistently observed for both lines, reasons for this are only a subject of speculation. Since the Mevalonate bypass condition allows PyrKII knock-out parasites to grow normally, it should work equally well for the knock-down lines. However, normal growth may require an adaptation period and we are still observing the transition to Mevalonate-dependence in our experiments. (2) Compared to the TetR-DOZI system, the CLD system seems to be more robust in that the growth phenotype on day 3 is more pronounced for the CLD system, at least under the present experimental conditions.

CONCLUDING REMARKS

The results presented in this chapter demonstrate that both the CLD system and the TetR-DOZI system are capable of conditionally knocking down PyrKII, our protein of interest for this study. Importantly, these systems allow us to scrutinize, using microarray analysis, the transcriptional changes within the nuclear as well as apicoplast genome that result from the knock-down of this essential protein. Based on such data, we hope to observe a disruption and loss of apicoplast gene transcription prior to any loss of nuclear gene expression. Those results will help shed light on why PyrKII is so important for the maintenance of this eccentric organelle.

REFERENCES

[1] T. Saito *et al.*, "A novel GDP-dependent pyruvate kinase isozyme from Toxoplasma gondii localizes to both the apicoplast and the mitochondrion," *J. Biol. Chem.*, vol. 283, no. 20, pp. 14041–52, May 2008.

[2] M. Chan and T. S. Sim, "Functional analysis, overexpression, and kinetic characterization of pyruvate kinase from Plasmodium falciparum," *Biochem. Biophys. Res. Commun.*, vol. 326, no. 1, pp. 188–196, 2004.

[3] T. Maeda *et al.*, "Pyruvate kinase type-II isozyme in Plasmodium falciparum localizes to the apicoplast," *Parasitol. Int.*, vol. 58, no. 1, pp. 101–105, 2009.

[4] L. Lim, M. Linka, K. A. Mullin, A. P. M. Weber, and G. I. McFadden, "The carbon and energy sources of the non-photosynthetic plastid in the malaria parasite," *FEBS Lett.*, vol. 584, no. 3, pp. 549–554, Feb. 2010.

[5] Y. Pei *et al.*, "*Plasmodium* pyruvate dehydrogenase activity is only essential for the parasite's progression from liver infection to blood infection," *Mol. Microbiol.*, vol. 75, no. 4, pp. 957–971, Feb. 2010.

[6] A. M. Vaughan *et al.*, "Type II fatty acid synthesis is essential only for malaria parasite late liver stage development," *Cell. Microbiol.*, vol. 11, no. 3, pp. 506–520, Mar. 2009.

[7] M. Yu *et al.*, "The Fatty Acid Biosynthesis Enzyme FabI Plays a Key Role in the Development of Liver-Stage Malarial Parasites," *Cell Host Microbe*, vol. 4, no. 6, pp. 567–578, 2008.

[8] S. M. Ganesan, A. Falla, S. J. Goldfless, A. S. Nasamu, and J. C. Niles, "Synthetic RNA-protein modules integrated with native translation mechanisms to control gene expression in malaria parasites," *Nat. Commun.*, vol. 7, pp. 1–10, 2016.

[9] C. M. Armstrong and D. E. Goldberg, "An FKBP destabilization domain modulates protein levels in Plasmodium falciparum," *Nat. Methods*, vol. 4, no. 12, pp. 1007–1009, 2007.

[10] M. F. de Azevedo *et al.*, "Systematic Analysis of FKBP Inducible Degradation Domain Tagging Strategies for the Human Malaria Parasite Plasmodium falciparum," *PLoS One*, vol. 7, no. 7, p. e40981, Jul. 2012.

[11] J. D. Dvorin *et al.*, "A Plant-Like Kinase in Plasmodium falciparum Regulates Parasite Egress from Erythrocytes," *Science*, vol. 328, no. 5980, pp. 910–912, 2010.

[12] I. Russo, A. Oksman, B. Vaupel, and D. E. Goldberg, "A calpain unique to alveolates is essential in Plasmodium falciparum and its knockdown reveals an involvement in pre-S-phase development," *Proc. Natl. Acad. Sci.*, vol. 106, no. 5, pp. 1554–1559, 2009.

[13] R. F. Waller, M. B. Reed, A. F. Cowman, and G. I. McFadden, "Protein trafficking to the plastid of Plasmodium falciparum is via the secretory pathway," *EMBO J.*, vol. 19, no. 8, pp. 1794–

802, Apr. 2000.

[14] G. G. Van Dooren, V. Su, M. C. D'Ombrain, and G. I. McFadden, "Processing of an apicoplast leader sequence in Plasmodium falciparum and the identification of a putative leader cleavage enzyme," *J. Biol. Chem.*, vol. 277, no. 26, pp. 23612–23619, Jun. 2002.

[15] B. J. Foth and G. I. McFadden, "The apicoplast: a plastid in Plasmodium falciparum and other Apicomplexan parasites," *Int. Rev. Cytol.*, vol. 224, pp. 57–110, 2003.

[16] R. F. Waller *et al.*, "Nuclear-encoded proteins target to the plastid in Toxoplasma gondii and Plasmodium falciparum," *Proc. Natl. Acad. Sci.*, 1998.

[17] J. R. Gallagher, K. A. Matthews, and S. T. Prigge, "Plasmodium falciparum apicoplast transit peptides are unstructured in vitro and during apicoplast import," *Traffic*, vol. 12, no. 9, pp. 1124–1138, 2011.

[18] S. J. Goldfless, J. C. Wagner, and J. C. Niles, "Versatile control of Plasmodium falciparum gene expression with an inducible protein-RNA interaction," *Nat. Commun.*, vol. 5, no. 5329, 2014.

[19] S. J. Goldfless, B. J. Belmont, A. M. De Paz, J. F. Liu, and J. C. Niles, "Direct and specific chemical control of eukaryotic translation with a synthetic RNA-protein interaction," *Nucleic Acids Res.*, vol. 40, no. 9, p. e64, 2012.

[20] E. L. Dahl, J. L. Shock, B. R. Shenai, J. Gut, J. L. Derisi, and P. J. Rosenthal, "Tetracyclines Specifically Target the Apicoplast of the Malaria Parasite Plasmodium falciparum," *Antimicrob. Agents Chemother.*, vol. 50, no. 9, pp. 3124–3131, 2006.

[21] G. R. Mair *et al.*, "Regulation of Sexual Development of Plasmodium by Translational Repression," *Source Sci. New Ser.*, vol. 313, no. 5787, pp. 667–669, 2006.

[22] A. Radhakrishnan, Y.-H. Chen, S. Martin, N. Alhusaini, R. Green, and J. Coller, "The DEAD-Box Protein Dhh1p Couples mRNA Decay and Translation by Monitoring Codon Optimality," *Cell*, vol. 167, no. 1, p. 122–132.e9, Sep. 2016.

[23] A. F. Cowman, J. Healer, D. Marapana, and K. Marsh, "Malaria: Biology and Disease," *Cell*, vol. 167, no. 3. pp. 610–624, 2016.

Curriculum Vitae

Hans B. Liu

Date of Birth: August 3, 1991 Cell: (612) 839-9803
Place of Birth: Minneapolis, Minnesota, USA E-mail: hliu82@jhmi.edu

EDUCATION

Johns Hopkins Bloomberg School of Public Health, Baltimore, MD 2016 – present

- Sc.M. candidate, Dept. of Biochemistry and Molecular Biology
- Sc.M. thesis: "The effect of apicoplast proteins and triclosan analogs on the growth of *Plasmodium falciparum*"
- M.H.S. thesis: "From a cellular perspective, an elucidation of the response of adult mammalian neural stem cells to traumatic brain injury"

Washington University in St. Louis, St. Louis, MO 2010 – 2014

- A.B. *cum laude* in Chemistry (Biochemistry concentration)
- Dean's list: Fall 2010, Spring 2012, Fall 2012, Fall 2013, and Spring 2014

RESEARCH EXPERIENCE

Lab of Dr. Sean T. Prigge Summer 2017 – present
Johns Hopkins Bloomberg School of Public Heath, Baltimore, MD
Sc.M. student

- Examined iron-sulfur cluster proteins with respect to their essentiality for the survival and apicoplast maintenance in asexual blood stage (ABS) *Plasmodium falciparum* (*Pf*) using genotyping PCR, organellar genome PCR, and flow cytometry
- Conducted single cloning of various *Pf* knock-out lines via limiting dilution
- Conducted drug screens on ABS *Pf* using various triclosan analogs
- Generated growth curves for the PyrKII conditional knock-down lines PyrKII CLD and PyrKII TetR-DOZI

Lab of Dr. Pierre A. Coulombe Spring 2017 – Summer 2017
Johns Hopkins Bloomberg School of Public Heath, Baltimore, MD
M.H.S. student

- Compared Krt6 -/- *vs.* WT keratinocytes with respect to collective migration using time lapse microscopy
- Compared Krt6 -/- *vs.* WT keratinocytes with respect to desmoplakin localization using fluorescence microscopy
- Compared Krt6 -/- *vs.* WT keratinocytes with respect to ROCK activity using the ROCK activity assay
- Conducted Krt6 rescue experiments in Krt6 -/- keratinocytes using nucleofection and time lapse microscopy

Lab of Dr. Sean X. Leng Spring – Summer 2016
Johns Hopkins School of Medicine, Baltimore, MD
Research Technologist

- Optimized a nested PCR method for detecting human cytomegalovirus (hCMV) from human peripheral blood mononuclear cells (PBMCs)

- Studied the *in vitro* effect of metformin on hCMV using quantitative PCR and Western blot analysis
- Analyzed longitudinal human immune cell profiling data using FlowJo

Lab of Dr. Nan-ping Weng Fall 2014 – Winter 2015
National Institute on Aging, Baltimore, MD
Post-baccalaureate Intramural Research Training Award program

- Measured the relative average telomere length (TL), using singleplex quantitative PCR, from the DNA samples of 923 Baltimore Longitudinal Study of Aging (BLSA) participants
- Measured the average Terminal Restriction Fragment length from BLSA DNA samples using Southern blot analysis
- Measured the average cellular TL using flow cytometry with Fluorescence In Situ Hybridization
- Isolated plasma, PBMCs, and $CD4^+$ and $CD8^+$ subsets from human whole blood

Lab of Dr. Shin-ichiro Imai Summer 2012
Washington University in St. Louis, St. Louis, MO
Undergraduate student

- Compared, using quantitative reverse transcription PCR, stearoyl-CoA desaturase-1, glycogen phosphorylase, glucose 6-phosphatase, phosphoenolpyruvate carboxylase kinase, and ACADM gene expression level in the liver of mice under different combinations of gender, genotype (Sirt1 +/+ *vs.* Sirt1 -/-), and diet (fed *vs.* fasted for 24 hrs)
- Genotyped mice (BRASTO and Sirt1 -/-)

Lab of Dr. Susana Gonzalo Summer 2011
Washington University in St. Louis, St. Louis, MO
Undergraduate student

- Assisted in Western blot analysis (determined protein concentration, changed solutions, and developed films)

POSTERS

Swift, R., Keutcha, C., **Liu, H.**, Rajaram, K., and Prigge, S. T. "Pyruvate Kinase II is Required for Apicoplast Maintenance." *Gordon Research Conference*, Newport, RI (Jun 13, 2018).

Liu, H. B., Swift, R., Rajaram, K., and Prigge, S. T. "Essentiality of Iron-sulfur Cluster Proteins for Blood Stage *Plasmodium falciparum* Survival and Apicoplast Maintenance." *JHSPH Dept. of Biochemistry and Molecular Biology retreat*, Baltimore, MD (Apr 13-14, 2018).

Lustig, A.*, **Liu, H. B.***, Metter, E. J., An, Y., Swaby, M. A., Elango, P., Luigi F., Richard J. H., and Weng, N. "Telomere Shortening, Inflammatory Cytokines, and Anti-cytomegalovirus Antibody Follow Distinct Age-Associated Trajectories in Humans." *Keystone Symposia on Molecular and Cellular Biology*, Austin, TX (Feb 25-Mar 1, 2018).

Shaked D., Leibel, D., Weng, N., **Liu, H. B.**, Evans, M. K., Zonderman, A. B., and Waldstein S. R. "Telomere Length and Cognitive Function: Differential Relations Across Sociodemographic Groups." *The International Neuropsychological Society 46th annual meeting*, Washington, DC (Feb 14-17, 2018).

Swift, R., Rajaram, K., Roberts, A., **Liu, H.**, and Prigge, S. T. "Iron-sulfur Cluster Formation is Required for Apicoplast Maintenance." *The American Society of Tropical Medicine and Hygiene*, Baltimore, MD (Nov 5-9, 2017).

Liu, H. B., Lustig, A., Najarro, K., Metter, J., Ferrucci, L., Hodes, R., and Weng, N. "Longitudinal Study of Telomere Length Changes of Over 900 BLSA Participants." *NIH Postbac Poster Day*, Bethesda, MD (Apr 30, 2015).

PUBLICATIONS

*indicates co-first authorship

Tang, J., **Liu, H. B.**, Yu, L., Meng, X., Leng, S. X., and Zhang, H. "Clinical-Pathological Characteristics and Prognostic Factors for Papillary Thyroid Microcarcinoma in the Elderly." *J Cancer* 9, no. 2 (Jan 2018): 256-62.

Zhao, M., **Liu, H.**, Tang, Y., Meng, X., Yu, J., Wang, Q., Zhou Q., Leng, S. X., and Zhang, H. "Clinicopathologic Features and Prognostic Factors for Patients with Colorectal Cancer Who are 75 Years and Older." *Oncotarget* 8, no. 45 (Sep 2017): 80002-11.

Lustig, A.*, **Liu, H. B.***, Metter, E. J., An, Y., Swaby, M. A., Elango, P., Ferrucci, L., Hodes, R. J., and Weng, N. "Telomere Shortening, Inflammatory Cytokines, and Anti-Cytomegalovirus Antibody Follow Distinct Age-Associated Trajectories in Humans." *Front Immunol* 8 (Aug 2017): 1027.

Li, H. F., Ning, X. X., **Liu, H.**, Chen, Y., Ding, X., Zhang, H., and Leng, S. X. "Metformin Suppressed Human Cytomegalovirus (hCMV) Replication and its Potential Molecular Mechanisms in Human Fibroblasts." *J Immunol* 198, no. 1 Supp. (May 2017): 158.23.

Jensen, S., Yu, Y., **Liu, H. B.**, and Liu, X. "Query-Centric Scientific Topic Evolution Extraction." *Am Soc Inform Sci Annu Meet Proc* 52, no. 1 (Feb 2016): 1-4.

MANUSCRIPTS UNDER REVIEW

Wang, F., Chen, S., **Liu, H. B.**, Parent, C. A., and Coulombe, P. A. "Keratins 6a/6b Regulate Keratinocyte Migration by Affecting Cell-Cell and Cell-Matrix Adhesion." *Under review for J Cell Biol* (2018).

Pantesco, E. J., Leibel, D. K., Ashe, J. J., Waldstein, S. R., Katzel, L. I., **Liu, H. B.**, Weng, N., Evans, M. K., Zonderman, A. B., and Beatty Moody, D. L. "Multiple Forms of Discrimination, Social Status, and Telomere Length: Interactions within Race." *Under review for Psychoneuroendocrinol* (2018).

Beatty Moody, D. L., Leibel, D. K., Darden, T. M., Ashe, J. J., Waldstein, S. R., Katzel, L. I., **Liu, H. B.**, Weng, N., Evans, M. K., and Zonderman, A. B. "Interpersonal-Level Discrimination Indices, Sociodemographic Factors, and Telomere Length in African-Americans and Whites." *Under review for Biol Psychol* (2018).

PERSONAL INTERESTS

Piano: Level 10, Minnesota Music Teachers Association

Drawing: Grand Prize, Art Competition, MN Dept. of Education, 2009

pencil1-HBL pencil2-HBL